INDOOR AIR QUALITY – COMBINING AIR HUMIDITY WITH CONSTRUCTION MOISTURE

Patrick Ken Amissah B.Sc.(Eng)Hons. M.Sc.(Eng)

A thesis submitted for the

Degree of Doctor of Philosophy

Department of Mechanical Engineering

Energy Systems Research Unit

University of Strathclyde

Glasgow, U.K.

April 2005

Indoor Air Quality: Combining Air Humidity with Construction Moisture

Acknowledgements

List of Symbols

Acknowledgements

In appreciation of the endless support and various forms of assistances given to me during the period of my studies within the Energy Systems Research Unit of the University of Strathclyde, Glasgow, acknowledgement is hereby given. I wish to express my sincere gratitude to Professor Joe Clarke for his expert guidance and encouragement throughout the study. My thanks go also to the government of Ghana for their support with the Scholarship grant for the programme. To my ESRU colleagues, Lori, Nick, John, Paul, Andy, Cameron, Ian and Kathleen, I am indebted for all forms of assistances. Finally, I am grateful to my wife and family for their support and help during the study.

Abstract

The project aims to improve the modelling of moisture transfers at internal surfaces by linking the finite volumes representing the Heat, Air and Moisture (HAM) and Computational Fluid Dynamics (CFD) domains. Conflation of both models facilitates the detailed study of moisture flow as it impacts on indoor air quality and occupant health. The thesis lays down the conceptual framework for the subsequent development of an indoor air quality analytical tool. The work thus improves the modelling of construction feature risk assessment, for example, moisture absorption and desorption at the internal fabric surfaces in as much as it relates to indoor air quality. Through such an improvement, an indoor air quality analytical tool for the prediction of time-varying temperature/humidity conditions at specific locations within the building is enabled and subsequently these conditions may be related to the likely occurrence of mould. Humidity in indoor spaces is one of the most important factors in the determination of indoor air quality. High indoor humidity is a major contributor to the accumulation of moisture in the building envelope. This often results in dampness within the building envelope and subsequent health-related problems for the occcupants. Moderation of the indoor relative humidity, temperature and moisture content of the indoor air amongst others is a pre-requisite for a healthy building because it affects the perception of indoor air quality, thermal comfort, occupant health (asthma, respiratory illness, etc), building durability, material emission and energy consumption. Excessively high relative humidity promotes the growth of moulds and mildew on building surfaces. The basis for the envisaged conflation evolves around the boundary layer theory as it pertains to the velocity, thermal and concentration profiles associated with flow parallel to a flat surface, a phenomenon which is recognised as being similar in nature to buoyancy-driven convective heat transfer within building enclosures (White 1988). Within the framework of modelling of indoor air flows, the conflated modelling approach is very much dependent upon the treatment of the internal surface convection, for example, in the

conflation of HAM and CFD models. This is referred to as the pivot point for the handshaking between HAM and CFD modelling domains. Within the framework of this project, the pivot point refers to the treatment of surface convection mass transfer at the internal surface to facilitate the hand shaking between HAM and CFD modelling domains. The two-time step coupling approach based on the loose coupling algorithm is adapted for the conflation. The technique involves a process whereby the HAM and CFD models are processed independently but exchange information at the interface at every time-step. The numerical method for the solution of the Navier-Stokes equations is based on the co-located grid arrangement, whereby all flow variables are defined in the centre of the grid cells. The transport equations are integrated for each grid cell and the Gauss Theorem applied to yield an integral over the cell face. These cell face integrals are then approximated using interpolation of the cell centred data. For the resolution of flow in the near-wall regime, the Low-Reynolds number k-ε turbulence model is used. A configuration mechanism with a rules-based moisture control algorithm to facilitate the handshaking of the HAM and CFD domains is presented. Methods for the solution of problems due to moisture migration across the interface, which are effected through variation of the convective mass transfer coefficient, h_m, through variation of the standard k-ε turbulence model, namely the low-Reynolds number model with its embedded wall damping functions and through adjustment of the source terms of governing transport equations of the CFD and HAM models are also discussed.

List of Symbols

A   area

a   dry air

C   vapour concentration in the air

$C_{A,\infty}$ species molar concentration

C_f local friction factor

C_p specific heat at constant pressure

C_s vapour concentration at the surface

C_w concentration of water vapour

c   specific heat capacity, specific mass concentration

D   diffusion coefficent

D_{AB} mass diffusivity of species, e.g. A and B

D_w moisture diffusivity of water vapour with respect to moisture content, w

(moisture content mass by volume, kg/m^3)

D_u moisture diffusivity of water vapour with respect to moisture content, u

(moisture content mass by mass, kg/kg)

E   total energy

f   friction factor

f_μ, f_1,wall damping functions

g_v vapour flux

H_i^{in} shorthand notation for the sum of the advective and viscous terms

h   average convective heat transfer coefficient

h_c local convective heat transfer coefficient

h_f enthalpy of liquid, fluid enthalpy

h_{fg} enthalpy of evaporation

h_m convective mass transfer coefficient

h_s enthalpy of moisture flux source

h_v enthalpy of vapour

J vapour mass flux

$J_{j'}$ diffusion flux of species, j'

J_H Colburn j-factor for heat transfer

J_M Colburn j-factor for mass transfer

$J_{v,}$ vapour flux

K hydraulic conductivity

K_θ thermal moisture permeability

k thermal conductivity, kinetic energy of turbulence

k_a air permeance

$k_{eff,}$ effective thermal conductivity

k_f fluid phase thermal conductivity

k_m moisture permeability

k_s solid medium thermal conductivity

Le Lewis number

l_m mixing length

M molecular weight

$m_{j'}$ mass fraction of species j'

m mass flux, mass flow rate

N total molar transfer

Nu Nusselt number

n_A'' molar flux of species A

n thickness of porous medium

n_{vent} air change rate

Pr   Prandtl number

Pr_t turbulent Prandtl number

P_{suc} suction pressure

p   absolute pressure

p_A, p_o ambient pressure

p_s saturated vapour pressure

p_L partial pressure of dry air

p_w, p_v partial pressure of water vapour

p_{air} partial water vapour pressure of the zone air

p_{in} logarithmic mean air partial pressure

Q   quantity of heat gain or loss

Q^P_n sum of pressure forces in the X-direction over all control volume faces

q   heat flux

q "   local heat flux

R   gas constant

Ř   universal gas constant

Re   Reynolds number

R_v vapour resistance

S   source term

Sc   Schmidt number

Sh   Sherwood number

St   Stanton number

T   temperature

T_o absolute temperature

T_P temperature at near-wall point, y_P

T_q heat flux temperature

T_{ref}, T_∞ reference temperature

t fluctuating temperature or time

U internal energy, mean velocity of flow

u_p velocity at grid node P

u_τ friction velocity

u, v, w velocities in spatial directions x, y, z

V volume of zone

w humidity ratio

X,Y,Z body forces in the spatial directions, x, y, z

x mass fraction

x, y, z spatial coordinates

Greek symbols

λ thermal conductivity

μ vapour resistance factor, molecular viscosity

μ_t turbulent dynamic viscosity, eddy viscosity

ν kinematic viscosity

ρ density

ε emissivity, dissipation of turbulence kinetic energy

ζ moisture capacity

Δ incremental change

ϕ mass fraction of water vapour, relative humidity, porosity, general variable

Ω volume of cel

τ_w wall shear stress

σ_c turbulent Schmidt number

Γ_{Cw} diffusion coefficient for water vapour

σ_{pw} turbulent Schmidt number of water vapour

δ boundary layer thickness

δ_p water vapour permeability

κ von Karman's constant

σ_k, σ_t turbulent Prandtl number

Subscript

in   inlet

b, B   bottom

c   concentration boundary layer

max   maximum

min   minimum

e, E   east

n, N   north

out   outlet

s, S   south

surf   surface

w   wall

Superscript

h   enthalpy

n   exponent

T   thermal

*   normalised quantities

1.1 Introduction

Indoor air quality is determined by a constantly changing interaction of complex factors that affect the types, levels and importance of pollutants in the indoor environment. It is a major concern to businesses, building managers, tenants and employees because it affects the health, comfort and productivity of building occupants. The quality of the indoor air is expressed as the extent to which human requirements are met. By definition, an *acceptable indoor air quality* is defined as air in which there are no known contaminants at harmful levels and to which a substantial majority of the people are not dissastified. The quality of the indoor air depends on both the quality of the outdoor air and on the strength of emissions from indoor sources. To satisfy comfort needs, indoor spaces must receive a quantity of tempered outdoor air and a sufficient quantity of clean air to create an acceptable indoor air quality. Similarly, to satisfy health ventilation needs, indoor spaces must receive air that is free from hazardous chemical or microbiological contaminants. Indoor air quality is influenced by changes in building operation, occupant activity and outdoor climate.

Perceived air quality may be expressed as the percentage of dissatisfied persons, that is, those persons who perceive the air to be unacceptable just after entering a space. The pollution generated by standard person is referred to as one olf. Standard person refers to the average sedentary adult office worker, who feels thermally neutral, that is, such person is not influenced thermally (Fanger et al 1988). The strength of most pollution sources indoors may be expressed as persons equivalents. For example, one decipol is the perceived air quality in a space with a pollution source strength of one olf, ventilated by 10 l/s of clean air (Fanger et al 1988). The next sub-section is a discussion on factors influencing indoor air quality and their classification.

1

1.2 Factors affecting indoor air quality

The following four elements are involved in the development of indoor air quality problems: *source; HVAC systems; pollutant pathways and building occupants.*

Source

Air pollution sources can be described as fitting into one or a combination of the following categories: contamination from indoors, outdoors, faulty HVAC systems, through human activities (metabolism, cooking, washing, etc), and building components and furnishings. These pollution sources contribute to the deterioration of the indoor air quality.

HVAC - systems

It is anticipated that a properly designed and an efficient HVAC system will perform the following activities within the framework of indoor air quality satisfactorily:

- provide thermal comfort;

- distribute an adequate amount of outdoor air to meet the ventilation needs of occupants; and

- isolate and remove odours/contaminants through pressure control, filtration and exhaust fans.

HVAC systems includes all heating, cooking, humidification, dehumidification and ventilation equipment serving a building.

Pollutant pathways

One or more pollutant pathways connect the pollutant source to the occupants and a driving force exists, for example, buoyancy force, to move pollutants along these pathways. The air flow patterns in buildings results from the combined action of mechanical and natural

2

ventilation systems (e.g. through infiltration) as well as from human activities. Pressure differentials created by these forces move airborne contaminants from areas of relatively high pressure to areas of relatively low pressure through any available opening. All components of the building (walls, ceilings, floors, penetrations, HVAC equipment and occupants) interact to effect the distribution of contaminants. Natural ventilation exert an influence on air movement between zones and between the building's interior and exterior areas. For leaky buildings, there is the tendency for the disruption of the indoor air circulation by the stack effect and wind pressure. Air movement from higher to lower pressure can produce many patterns of contaminant distribution, including local circulation in the room containing the pollutant source:

- air movement into adjacent spaces that are under lower pressure;

- movement from lower to upper levels of the building; e.g as in thermally-driven flows , using thermal plumes; and

- air movement into the building through either infiltration or re-entry of exhaust air.

Building occupants

Building occupants are considered as source of contaminants by virtue of their metabolism and activities (e.g. cooking, washing, etc). Groups that may be particularly susceptible to the effects of indoor contaminants include, but are not limited to;

- allergic or asthmatic individuals;

- people with respiratory diseases;

- people with suppressed immune systems, due to disease or other causes; and

- susceptible persons, e.g. children and the elderly.

1.3 Impact of humidity on building performance and health

Humidity in indoor spaces is one of the most important factors in the determination of

indoor air quality. High indoor humidity is a major contributor to the accumulation of moisture in the building envelope. This often results in dampness within the building envelope and subsequent health-related problems for the occupants. Moderation of the indoor relative humidity is a pre-requisite for a healthy building because it affects the perception of indoor air quality, thermal comfort, occupant health (asthma, respiratory illness, etc), building durability, material emissions and energy consumption. Humidity extremes can also create other indoor air quality problems. Excessively high or low relative humidities can produce discomfort. High relative humidities can promote the growth of mould and mildew on building surfaces. Normally few problems occur when the relative humidity is between 30% and 70%, assuming that no condensation occurs (Oldengarn et al 1990). Similarly, low relative humidity causes irritation of the skin and the eyes of the occupants.

From the designer's perspective, application of appropriate building materials, which are vapour permeable and highly hygroscopic, can provide good indoor air quality. To minimise the effects of humidity on occupants' health, due consideration must be given to organisms of biological agents and their life cycles in the context of the building's surface materials, mechanical systems, operational schedules and surrounding climate (that is, the entire ecosystem of the organism).

1.4 Health aspects of indoor air quality

A number of pollutants including building materials are of much concern for human health. Exposure to such pollutants in the air may provide a certain health risk (e.g. respiratory illness). As a measure of awareness and to limit the health risk to a low level, an extensive list of maximum permissible concentration and the coresponding exposure times to individual chemicals in the air has been published. (Air Quality Guidelines for Europe

1987). For example, the Threshold Limit Values (TLV) exist for individual premises. These are applicable to work places where chemicals are used routinely in the production process. In offices and similar work places, exposure to any individual pollutant is typically much lower than the situation in the industry.The exposure is characterised by a wide spectrum of compounds at low concentration levels from building materials, furniture, office equipment, human metabolism and outdoor air. Other pollutants within the health risk category are: radon gas, gases from landfill or waste sites, combustion products, formaldehyde, volatile organic compounds (VOC), metabolic gases, micro-organisms and humidity. These pollutants are discussed in the next sub-section.

Radon

Radon is a radioactive gas which occurs in the indoor air. The major source of indoor radon is usually soil gas under the building. Radon occurs in high concentrations in soil gas with large variations due to local geology (the type of soil). Soil gas with radon may enter a building by infiltration through cracks and other openings in floors and walls seperating the building from the soil. Indoor radon level can be controlled by sealing the building against the entry of soil gas or where possible, by venting the air in sub floor spaces to the atmosphere. Alternatively, radon sumps under the floor may be used, where no sub-floor space exists. Radon control, for example, requires an airtight floor and/or basement system. Ventilation of living areas does aid radon control. Radon increases the risk of lung cancer. Risk estimates for radon are provided in 'Air Quality Guidelines for Europe' (World Health Organisation 1967).

Gases from landfill and waste sites

Within areas of waste disposal a broad range of potentially toxic chemicals may be present. Landfill gas is produced by the action of micro-organisms on organic waste material

deposited in landfill sites. The gas principally consists of methane, (CH_4) and carbon dioxide, (CO_2) but other gases such as hydrogen and hydrogen-sulphide may be present. Other traces of volatile-organic compounds (VOC) detected in landfill gas include alphatic and aromatic hydrocarbons, alcohols, esters, ethers and organosulphur compounds. The major hazard that landfill gas represents is that of explosions; methane is inflammable when mixed with air in the concentration range of 5 to 15%. Buildings constructed on or near sites where there are high levels of these hazarduos gases need to be sealed to prevent gas ingress and a means to disperse the gases must be provided.

Combustion products

Carbon monoxide (CO) is generated by incomplete combustion. Sources of carbon monoxide are coal and kerosene heaters, wood stoves, amongst others. Nitrogen dioxide, (NO_2), is.another toxic gas generated by the combustion of fossil fuels at higher temperatures. Major indoor sources are appliances for cooking with gas and unvented domestic water heaters. An effective means to control indoor combustion products is to avoid or reduce the pollution sources. Leakages from garages etc. to occupied spaces should be sealed. It is recommended that gas appliances for cooking be provided with a proper hood for local exhaust of the combustion products (Commission of the European Communities 1989).

Formaldehyde

Formaldehyde is a colourless and a very reactive gas with a pungent smell. The main area of application is the fabrication of synthetic resins. Formaldehyde may occur in indoor air as an emission from particle boards containing adhesives based on urea-formaldehyde foam insulation. Possible adverse health effects due to formaldehyde exposure in indoor environments depend on the concentration and the duration of the exposure. Formaldehyde

can cause watery eyes, burning sensations in the eyes and throat, nausea, and difficulty in breathing in some humans exposed at elevated levels (above 0.1 parts per million).

Volatile organic compounds

Volatile organic compounds (VOC), other than formaldehyde, are emitted by humans, by many natural materials and most importantly by a large number of building materials, furnishings and equipment used in buildings. The VOC are defined by the World Health Organisation (WHO) as having melting points below room temperature and boiling points ranging from 50 to 260^0C. Human response to VOC in indoor air is classified as acutely perceived deterioration of the environment.

Metabolic gases

The metabolic processes of the occupants in a space require oxygen and produce carbon monoxide, moisture, aldehydes, esters and alcohols. To avoid adverse health effects, an acceptable long-term exposure range for CO_2 in the residential indoor air of a value less than 0.3 g/m^3 (or less than 3500 ppm) has been recommended (Environment Health Directorate 1989). The ventilation rate required to maintain this safe level is very low. Other metabolic gases (bioeffluents) never reach harmful concentrations in practice but have an unpleasant odour which requires much more ventilation than the carbon dioxide production.

Micro-organism

The micro-organisms of most concern in indoor air are bacteria, viruses and fungi. Many bacteria and viruses originate from humans and can cause infectious diseases. Other sources are poorly maintained humidifiers which can cause the spread of legionella disease. Abnormal levels of fungal spores originate from moist surfaces and building materials and may induce allergic and hypersensitive reactions to humans. Micro-organisms can be

7

controlled by controlling the surface moisture levels and bioeffluents.

Impact of building materials on indoor air quality

From designers perspective, application of appropriate building materials, which are vapour permeable and highly hygroscopic, can provide good indoor air quality. To minimise the effects of humidity on occupants' health, due consideration must be given to organisms of biological agents and their life cycles in the context of the building's surface materials, mechanical systems, operational schedules and surrounding climate (that is, the entire ecosystem of the organism).

In summary, this Chapter is a presentation on indoor air quality and its influencing factors in relation to safeguarding a healthy-built environment. Avoidance of materials which offgas is a useful and necessary approach to mitigate the effects of such pollution sources. Similarly, the effects of high indoor humidity, a major contributor to the accumulation of moisture in the building envelope, is highlighted. Such effects often results in dampness within the building envelope, occurrence of moulds on building surfaces and subsequent health-related problems for the building occupants.

1.5 Research objectives and thesis outline

The objectives of this research are to advance the modelling of indoor air quality through the development of a conceptual framework for the development of an indoor air quality analytical tool for the resolution of health-related problems within the context of whole building simulation and accurately treating the impact of construction moisture transfer on the indoor air humidity. These objectives are realised through the convergence of moisture and air flow modelling techniques. Specifically, the project aims to improve the modelling of moisture transfer at internal surfaces by linking the finite volumes representing the two domains. Conflation of both models, HAM and CFD, facilitates the detailed study of

moisture flow as it impacts on indoor air quality and occupant health. Generally, the work improves modelling of construction feature risk assessment as much as it does indoor air quality. The research is based on the integrated modelling approach presented in Chapters 2, 3 and 5, whereby CFD techniques are combined with HAM model. Within this approach, the HAM model supplies realistic boundary conditions to the CFD model, enabling high resolution air flow simulatios for specific spaces within the building. The CFD's air flow predictions are then used to enhance the construction moisture flow by supporting the direct modelling of convection mass transfers at internal fabric surfaces.

An introduction to indoor air quality and its influencing factors is presented in Chapter 1. A review of the underlying theories supporting this research, namely moisture transfer through porous media and through the airspace within the enclosure are presented in Chapters 2 and 3 respectively. This review is necessary since the conflation activity can either be effected at the wall's internal surface or at an adjacent air point node within the indoor enclosure. The former option is chosen for this project as a contribution towards the improvement of the versality of the ESP-r (Environmental Systems Performance; r for 'research') system through the establishment of a 'handshaking' facility between construction moisture flow and the indoor air humidity.

ESP-r is a transient energy and environmental performance analysis tool having the capabilities of modelling the energy and fluid flows within combined building and plant systems when costrained to conform to control actions. It has been in a constant state of evolution and renewal since its development over two decades ago (Clarke 1977). The scope of ESP-r has since its inception broadened to embrace the simulation of non-energy domains, more resolved and embedded with advanced modelling approaches (ESRU 1999 and Hensen 1991). It is actively developed and supported and has been successfully applied

to a host of building design, analysis, techniques and research activities. ESP-r considers heat transfer, inter-zone air flow, water flow (in hydronic plant system), electric power flow, moisture transfer and illumination (via the Radiance modelling tool). It is capable of modelling these physical processes in an integrated and rigorous fashion (Clarke 1999). All aspects of model creation. simulation and results analysis within ESP-r are controlled by the *Project Manager*, which also provides a graphical interface between the user and the underlying data model. In effect, the *Project Manager* controls the simulator and the results analyser.

ESP-r employs a partitioned solution approach and applies customized solvers to each model domain (thermal, inter-zone air flow, intra-zone air flow, moisture flow, electric power flow, etc.) to facilitate optimized treatment of each of the equation sets. Inter-dependencies are safeguarded by passing information between the solution domains on a time-step basis to enable global solution to evolve in a coupled manner. Handshaking (or information exchange) between the soluton domains, for example between HAM and CFD models is central to the current research. An overview of ESP-r's simulation methodology in relation to the characterisation of the energy transfer mechanism through the internal fabric surfaces is provided in Appendix F.

A review of indoor air flow modelling with CFD including turbulence models for flow within the building enclosure and the near-wall flow region as well as discussions on co-located grid arrangement and its application for the solution of the Navier-Stokes equations are presented in Chapter 3. In Chapter 4 is a presentation on the boundary layer theory as it pertains to the velocity, thermal and concentration profiles associated with flow parallel to a flat surface. A discussion on the heat and mass transfer analogy is also presented as well as a suite of correlations for the convection mass transfer coefficient to support the conflation.

A two-time step coupling approach is adopted for the project and is presented in Chapter 5. Resolution enhancement methods, as well as the configuration of the CFD model to support the surface conflation, are also presented. An illustration of the conflation process, including a moisture control algorithm for the solution of moisture absorption and desorption problems at the interface (internal wall surface), is also discussed. Finally, conclusions and recommendations for future work are presented in Chapter 6.

CHAPTER TWO   REVIEW OF HEAT AIR AND MOISTURE TRANSFER MODELLING

2.1 Porous medium heat and mass transfer

This section presents a review of heat and mass transfer through the building construction within the framework of building energy simulation. The conceptual basis and the capabilities and limitations of HAM models are discussed. The aim of an integrated HAM model is to predict the thermal and humidity conditions of an indoor space when taking into account the thermal and moisture conditions throughout the adjacent building constructions. Humidity is exchanged by convective transfer between the zone air and the adjacent construction surfaces, a process by which moisture is either released or absorbed by the construction. Several influences on the air humidity are considered in the HAM model through its boundary conditions and source terms:

- humidity transfer to and from adjoining constructions;

- contribution of humidity from various sources and activities, e.g. occupants

  (metabolism), washing and drying, cooking, HVAC systems, building materials;

- penetration of humidity from outdoor air (by infiltration and ventilation);

- supply of humid or dry air from ventilation systems; and

 humid air transferred from other zones.

Since the hygrothermal behaviour of buildings is the result of a complex interaction between the heat balance and the mass balance of air and moisture, a computer model with coupling capabilities is required:

- to facilitate the quantification of the impact of the hygrothermal process on the building envelope and the occupants; and

- to enhance the overall performance evaluation process.

The next sub section presents theories of moisture migration in solids

2.1.1 Moisture flow model

Moisture flow through solids plays a major role in the surface conflation of the construction moisture and the indoor air humidity through the solid/surface interface. In building physics, moisture is defined as 'water that is physically bound in the pores of a material that is able to evaporate at high temperatures' (Marit Stoere Valen et al 1998). In order for the building envelope to perform its role of separating the interior and exterior environments, it must have structural integrity and durability. Of all environmental conditions, moisture poses the biggest threat to integrity and durability, accounting for up to 80% of damage in building envelopes (Bomberg and Brown et al 1993). More recently recognised are the serious hazards of mould and other organisms which fluorish on surfaces with excessive moisture. The study of moisture transfer between the building envelope and the room air is often focused on the moisture transfer due to the difference in water vapour pressure on the exterior and the interior sides of the building envelope. Many construction materials contain moisture, most notably masonry or concrete. Excessive moisture, however, jeopardises both the material and its ability to function. Building materials can then be broadly classified into two major categories; porous and non-porous as per the discussion below.

Classification of building materials

Many building materials have a large number of interstices and pores that may or may not be inter-connected. Moisture transfer can be classified into three types (Wong and Wang et al 1990):

Capillary-porous media

There is a clearly recognizable pore space. The amount of physically bound water is negligible, that is, the medium is non-hygroscopic. The medium does not shrink when moisture is being driven from it. The enthalpy of wetting, often refered to a unit mass of a

13

solid, is defined as the difference (at constant temperature) between the enthalpy of a solid completely immersed in a wetting liquid, and that of the solid and liquid taken separately (Nikos Drakos et al 1996). Examples of this group are packings of sand, crushed minerals, polymer particles, bricks and concrete.

Hygroscopic-porous media

There is also clearly recognizable pore space. This type of medium has a significant amount of physically bound liquid. When moisture is being driven from the surface of large pores, shrinkage often occurs. Enthalpy of wetting is significantly higher. Example of this group are clay, wood or timber, and natural textile fibres.

Coloidal (non-porous) media

There is no pore space with such medium. Evaporation of liquid water can take place only at the surface. All liquid water is physically bound. Examples of this group are nylon, glue, etc.

In practice, consideration must be given to the influence of transient heat, air infiltration or ventilation, and moisture transfer between the building envelope and the room air during the period. Many theories have been proposed to predict moisture migration within solids. Luikov et al 1934 proposed the phenomenon of moisture thermal diffusion and claimed that the temperature gradient is also a factor influencing moisture transfer in solids. Luikov assumed that the fluxes due to vapour and liquid diffusion consisted of two parts: one due to the concentration gradient and the other due to the temperature gradient. Philip and deVries also developed equations describing moisture and heat transfer in porous materials under combined moisture and temperature gradients (Webb et al 1991). Their approach was a mechanistic one that assumed that moisture moves in solids by both vapour diffusion and

capillary action. Hedenblad et al 1993, referred to a model suggested by Kohonen et al (1984) that illustrated the moisture flow in a porous material as a combination of three different kinds of flow which make up the total moisture flow in a complex manner:

- water vapour diffusion taking place in the pore space;

- adsorptive surface flow, where a multi-layer of water molecules is built up at the pore walls; and

- capillary flow in the narrow pores (capillaries).

Vapour transfer through porous media

Vapour transfer in and through porous materials is caused by vapour diffusion and the convective flow of moist air in and through the pores. Water vapour diffusion is a continuos random motion of the vapour molecules in the air that takes place in the pores of the material. Fick's law defines vapour flux, (g_v), for one-dimensional flow system as

$$g_v = -\delta_p \cdot \partial p_v / \partial x \qquad (\text{kg/s.m}^2) \qquad (2.1)$$

where δ_p is the water vapour permeability, which is a function of the relative humidity. Generally, for a given permeable structure, the greater the vapour pressure difference across the assembly, the greater will be the rate of diffusion. Fick's law for vapour flux can be stated in different forms with different potentials, e.g. related to moisture content, u or w, as follows.

$$g_v = -D_w \frac{\partial w}{\partial x} = -D_u \, \rho \, \frac{\partial u}{\partial x} \qquad (2.2)$$

where D_w or D_u (m^2/s) is the water vapour diffusivity coefficients with regard to the moisture content, w (kg/m^3) is mass per volume of the dry material, or moisture content, and u (kg/kg) is mass per mass of the dry material, respectively. Figure 2.1 shows a typical water vapour permeability curve for a porous material (Hedenblad 1993).

Sorption Isotherm

A sorption isotherm is the graphic representation of the sorptive behaviour of a material. It

represents the relationship between the moisture content of the product and the relative humidity of the ambient air (equilibrium conditions) at a particular temperature. The profile of a sorption isotherm is characteristic of the hygroscopicity of a product. Highly hygroscopic products exhibit a steep isotherm, while sparingly hygroscopic products exhibit flat sorption isotherms. For example, a porous material absorbs moisture from the surrounding air, for which the moisture sorption region is characterised by accumulation of water from the surrounding moist air until a state of equilibrium is reached. The moisture content of the material at this point is the equilibrium moisture content. A typical moisture isotherm is shown in Figure 2.2 with its characteristic S-shaped curve. The slope of the curve defines the moisture capacity (x) of the material. Beyond the hygroscopic range,
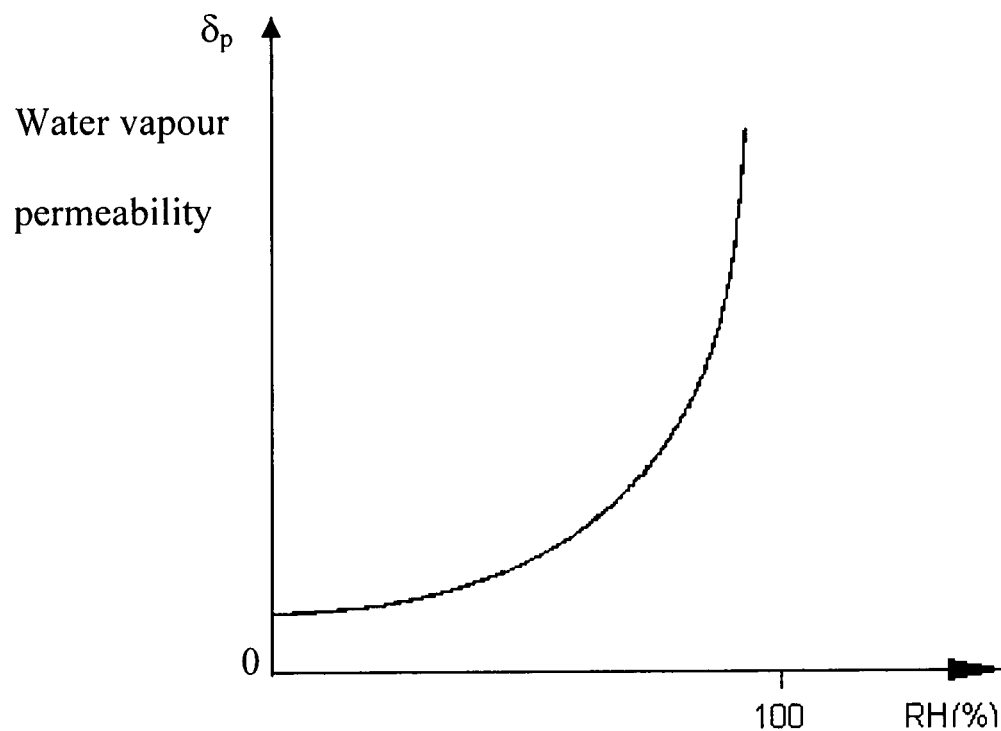
Figure 2.1: Water vapour permeability curve of a porous material.

when the RH is higher than 98%, capillary condensation occurs. At this stage there is no continuity of the liquid in the capillaries. The process continues until a critical moisture content, w_{cr}, is established. The critical moisture content is defined as the lowest content that is necessary to initiate moisture transport in the liquid phase. Due to hysteresis, many building materials show different adsorption and desorption isotherms. Hysteresis effects

16

in building materials are due to the difference in energy levels in terms of moisture content values during the wetting process (absorption) and the drying process (desorption). The gap between the two curves depicts the vapour loss, for example, through cavity flows, infiltration, etc. Most often the hysteresis effect on the sorption isotherm is neglected in the model (Figure 2.2). The correlations used for the diffusion coefficient are based on the average of the adsorption and desorption data (Thomas and Burch 1990).
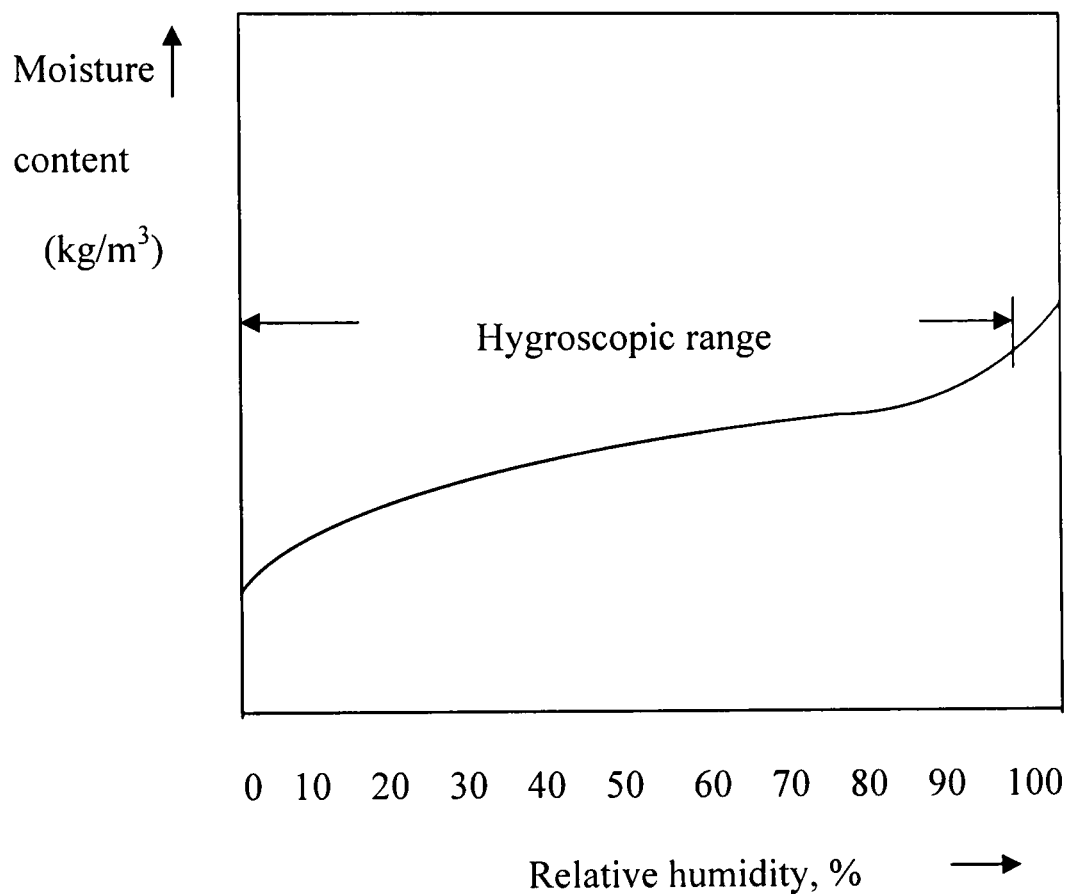
Figure 2.2:The Sorption Isotherm for a porous material.

Combined Vapour and Liquid Transport

In the hygroscopic region, the moisture flow is dominated by water vapour diffusion and moisture is mainly adsorbed to the pore walls. As the moisture content increases, islands form within the small capillaries. According to Anderson (1985), this combined transport of water and liquid occurs in series, as shown in Figure 2.3. As mentioned earlier, the moisture flow in the whole moisture area can be described by equation (2.2), with the moisture content as potential and D_w or D_u as transport properties.
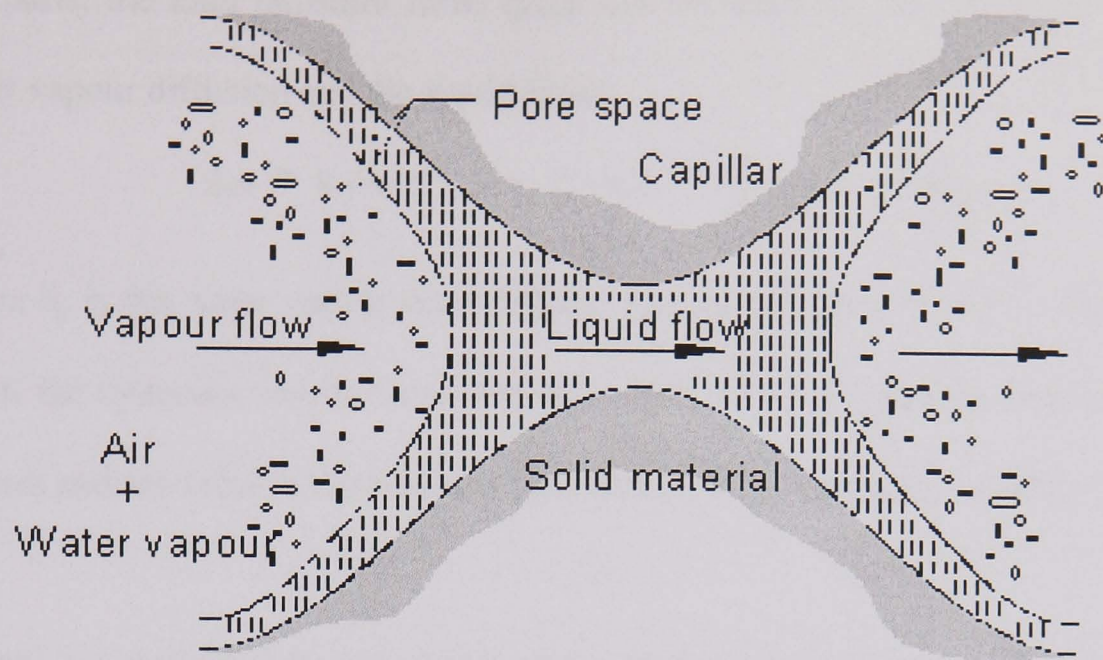
Figure 2.3: Combined moisture transport in a porous material (Anderson 1985).
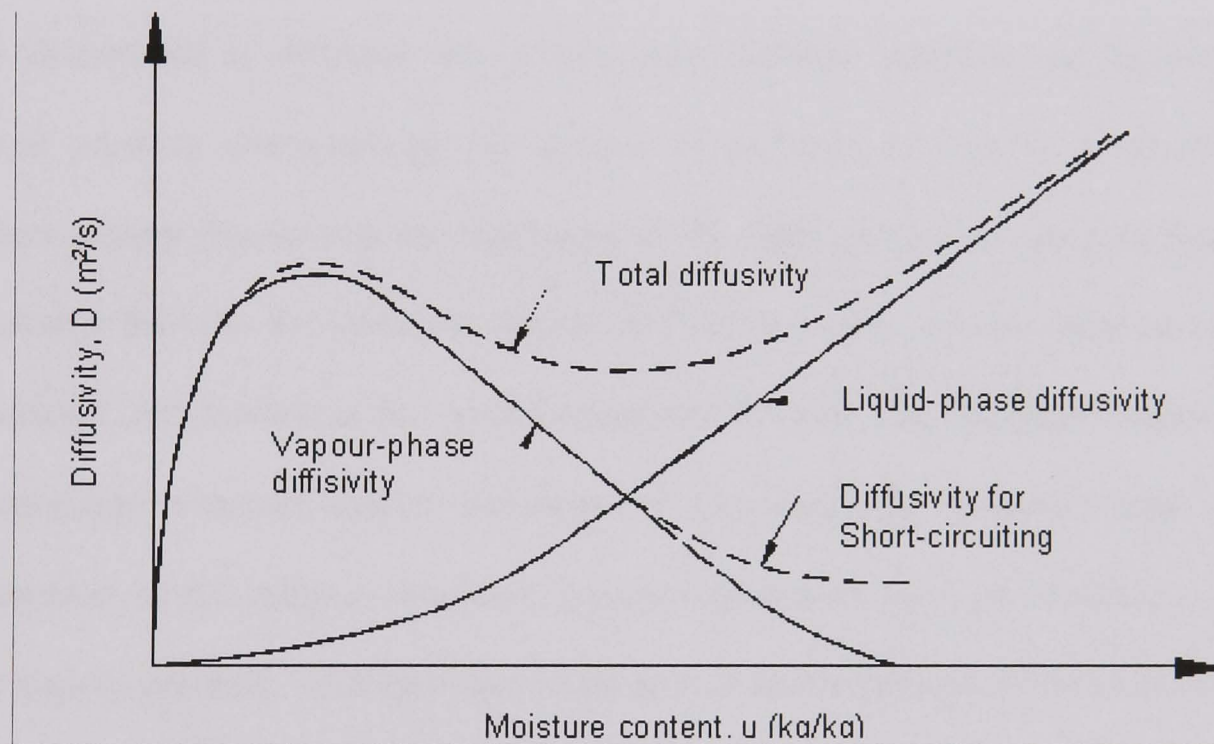
Figure 2.4: Moisture diffusivity curves (Philips & de Vries 1957).

The transport property is the moisture diffusivity that is dependent upon the moisture

content. This property is valid in the whole moisture region, from vapour to capillary flow.

Figure 2.4 shows the total moisture diffusivity curve as a function of moisture content and

as the sum of the water vapour diffusivity and water liquid diffusivity, taken from Philip &

de Vries (1957). On the other hand, separating the water vapour and the capillary flow into

18

two parts, the total moisture flow, (g_{tot}), can be found by combining the equations of the water vapour diffusion and the liquid flow:

$$g_{tot} = g_{v+w} = g_{diff} + g_{cap} = \delta_p \frac{\partial p_v}{\partial x} + K \frac{\partial p_{suc}}{\partial x} \qquad (2.3)$$

where δ_p is the water vapour permeability, p_{suc} the suction pressure, p_v the vapour pressure and K the hydraulic conductivity. Moisture diffusivity of materials depends on the moisture content and are valid in the whole moisture area, from vapour to capillary flow.

Several researchers have reported moisture diffusivity measurements. It was observed that, there are large discrepancies in the data found in the literature. Kumaran in (1992) showed experimentally that there are differences in the moisture diffusivity for the same material when determined at different laboratories with different methods and techniques. The material property characterising the amount of moisture retained in a structure is the moisture content (Karagiozis and Salonvara 1994). Each material has its own characteristic relationship between the moisture content and the maximum vapour pressure at a certain temperature, represented as the sorption isotherm (Figure 2.2). Moisture content, being a discontinuous potential across interfaces of constructional materials adds additional complexities in the analysis. Moisture transport potentials used are moisture content and water vapour pressure, with the latter being more popular because of lesser problems with discontinuous functions, which often leads to inaccurate results. In a composite construction, for example, the moisture content of the material is not well suited as a choice for the driving potential for moisture transport since it does change in a continuos manner over the material interfaces. Further, the moisture diffusivity may show some sign of hysteresis emanating from traces of hysteresis in the moisture retention properties (Carsten Rode 1990).

2.1.2 Heat, air and moisture transport through a porous medium

A 1-D HAM model facilitates the simulation of coupled heat, air and moisture transfer within porous media in order to analyse the hygrothermal performance of building elements under transient conditions. The model is capable of predicting the material moisture content, relative humidity distribution and temperature distribution within the building enclosure and the likelihood of the occurrence of mould growth on building internal surfaces. Typically, the model comprises a 1-dimensional conduction model coupled to a zonal air flow network and constructional moisture transport model (Kerestecioglu et al 1990). The model for moisture transport within a multi- layered construction considers moisture transport in the form of vapour diffusion, with the driving potential being the vapour pressure gradient. Application of mass and energy conservation principles to a stationary, homogeneous, isotropic, constructional control volume, gives following differential equation system for combined heat, air and moisture transfer.

For the *moisture balance term* (in one dimension):

$$\rho_0 \xi \frac{\partial}{\partial t}(p/p_s) + \frac{dp_1}{dt} = \frac{\partial}{\partial x}\left\{\delta^T_P \frac{\partial p}{\partial x} + D^P_T \frac{\partial T}{\partial x}\right\} + S_g \qquad (2.4)$$

where ρ is density (kg/m^3; 0 and 1 denote porous media and liquid respectively), ξ the moisture storage (kg/kg), p the partial water vapour pressure (Pa), p_s the saturated vapour pressure (Pa), δ^T_p the water vapour permeability due to vapour pressure gradient when the second driving potential is the temperature gradient (kg/Pa.m.s), D^P_T the moisture diffusion coefficient when the second driving potential is the vapour pressure gradient, S_g the moisture source term. For moisture transport by vapour diffusion, the driving potential is the partial water vapour pressure gradient.

For the *energy balance term* (in one dimension):

$$\left[\rho_0\left\{c_0 + c_v u_v\right\} + c_1\rho_1\right]\frac{\partial T}{\partial t} + h_v\frac{\partial \rho_v}{\partial t} + h_1\frac{\partial \rho_1}{\partial t} = \frac{\partial}{\partial x}\left\{\lambda\frac{\partial T}{\partial x}\right\} - \frac{\partial}{\partial x}h_s J_v + g \qquad (2.5)$$

where J_v is the vapour mass flux (kg/m^{2}s due to phase change, J_v is negative for adsorption

and condensation and positive for desorption and evaporation phenomena); h_v, h_l and h_s the enthalpies (J/kg) of vapour, liquid and moisture flux source respectively and g a source of heat. The driving potential for the energy term is the temperature gradient. The derivation of the transport equations, boundary conditions and the solution technique are provided in Appendix A.

2.1.3 The IEA Annex XIV enquiry on HAM codes

The scope of the Annex XIV project of the International Energy Agency (IEA) was to explore the capabilities of HAM codes in relation to the assessment of the impact of constructional moisture flow on building envelopes and to analyse the consequences of the energetic and hygric performances on the durability of the building envelope. Within the project 29 HAM codes were initially vetted and finally reduced to 9 types. These types vary from steady-state heat conduction and vapour diffusion models to transient heat, air and moisture transfer models. Common to all the codes were the conservation law and the assumption of linear relations between the densities of flow rates and the gradients of the driving forces. The observed differences were related to the level of simplifying assumptions concerning material properties, boundary conditions and the flow of air in cavities. A classification in order of complexity of the implemented models appeared possible, and resulted in 9 types ranging from the very simple to the most complete as shown in Table 2.1. Enhanced modelling from Type 4 onwards facilitates a realistic evaluation of the hygrothermal behaviour of constructional elements. An overview of the classification of these codes as a result of the IEA Annex XIV enquiry is presented in Appendix B. With reference to Table 2.1, K_a is the permeance (s/m), K_m the moisture permeability (s), K_θ the thermal moisture permeability (W/msK), λ the thermal conductivity (W/mK) and μ the vapour resistance factor. It became clear during the IEA study that several HAM phenomena led to moisture problems in buildings. With respect to the

21

moisture behaviour, four different type of problems were identified: heat, air and moisture transport through building structures; interaction between the indoor climate and the building structure, in particular with respect to the thermal and hygric inertia, air infiltration and inter-zonal air transport phenomena, and the accompanying airborne moisture transport.

Table 2.1: Classification of HAM codes (IEA Annex XIV)

Type	Short Description	Material Properties
1	steady-state heat conduction and vapour diffusion	λ and μ constant
2.	steady-state heat conduction and vapour diffusion, corrected for capillary flow	λ and μ constant
3.	transient heat and vapour transfer	λ, function of moisture content μ, function of relative humidity
4.	transient heat and moisture transfer	λ, k_m and K_θ function of moisture content
5.	transient heat and air transfer	λ and k_a constant
6.	steady-state forced air, heat and vapour transfer	λ, k_a or K_a and μ constant
7	steady-state air and heat transfer, transient vapour transfer	λ, k_a or K_a and μ constant
8	transient air, heat and vapour transfer	λ, k_a and μ function of moisture content and temperature
9.	transient air, heat and moisture transfer	λ, k_a, k_m and K_θ function of moisture content and temperature.

22

Based on the problems mentioned above, HAM models have been classified into four categories (IEA Annex XIV 1986) as follows:

- building structure HAM models;

- HAM building simulation models;

- ventilation /air infiltration models, and

- air flow models.

It became apparent that the way forward for a successful modelling exercise is through the integration of two categories of HAM models, namely, the HAM building simulation model and the CFD air flow model.

2.2 Zone moisture transfer

The zone air is represented in the building description at a nodal point within the enclosure for which the air temperature and water vapour are calculated. An air humidity and energy balance for the zone is set up as described in the next section

2.2.1 Air humidity and energy balance for zone air

A humidity balance equation is established for each zone. These equations represent the humidity that is exchanged by infiltration, ventilation and air change with adjacent zones. Humidity is also exchanged by convective mass transfer between the zone air and the building envelope as a result of which moisture is either released or absorbed from or to the porous medium. Information is retained for each zone about the temperature and the humidity ratio. The air in the zone is considered to be fully mixed. The following influences on the air's humidity condition are considered:

- humidity transfer from adjoining construction(s);

- contribution of humidity from various sources and activities;

- penetration of humidity from the outdoor air;

23
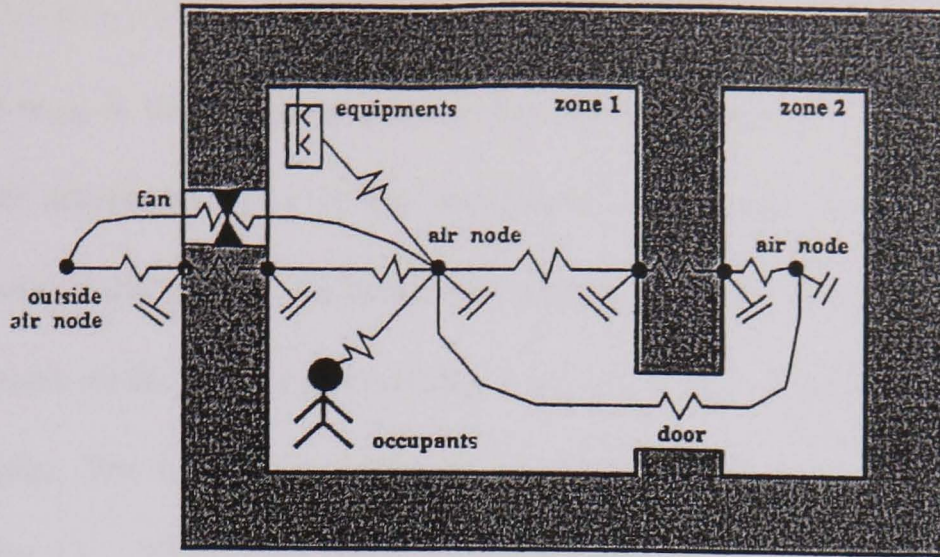
Moisture transport model

Figure 2.5: Integration of moisture transport model with ESP-r (Nakhi 1995).

- supply of humid air from the ventilation system; and

- humid air transferred from other zones.

The time dependency of changing the moisture content of the air is taken into account. Figure 2.5 shows the integration of the moisture transport model within ESP-r and shows also the constituent elements of the humidity balance for the zone. The moisture balance equation is given by

$$V. \rho_{air} \ w \frac{w^{new} - w^{old}}{\Delta t} = \Sigma G \qquad (2.6)$$

where V is the volume of the zone, w the air humidity ratio, G the summation of the moisture flux into the zone from all available sources and ρ_{air} the density of the zone air. The humidity transferred between the construction surfaces and the zone air is governed by the convective mass transfer coefficient, which may be calculated from

$$G_{constr} = \sum_{constr} A_{surf} h_m (p_{surf} - p_{air}) \qquad (2.6a)$$

where G_{constr} is the vapour flux through the porous medium, A_{surf} the wall surface area, h_m, the convective mass transfer coefficient, p_{surf} the partial pressure of the water vapour at the inside wall surface and p_{air} the partial water vapour pressure of the zone air. The moisture contributed to the zone air by ventilation is calculated by summation of all air sources:

24

$$G_{vent} = \sum_{\text{Air sources}} n_{vent} \cdot V \rho \left(w_{vent} - w_{air} \right) \qquad (2.6b)$$

where w_{vent} is the humidity ratio of the air as it enters the zone (from the outside or from another zone) and n_{vent} is the associated air change rate. Moisture contributions may originate from people (metabolism) and from other moisture loads in the zone. Such influences on the indoor air humidity vary according to defined schedules or various control strategies. The humidity contribution from these sources may be combined into a single quantity, G_{sys}. This parameter indicates the mass of vapour induced to the air per unit time (kg/h). The total humidity balance for the zone is obtained by inserting the different moisture constituents in equation (2.6c):

$$\Sigma G = G_{constr} + G_{vent} + G_{sys}. \qquad (2.6c)$$

Thermal energy balance

The thermal energy balance equation for the zone air is expressed as

$$\sum_{i=1}^{N} q_{i,c} A_i + Q_{other} - Q_{heat,extraction} = \frac{1}{\Delta t} \left(\rho V_{zone} Cp \, \Delta T \right) \qquad (2.7)$$

where $\sum_{i=1}^{N} q_{i,c} A_i$ is the convective heat transfer from the enclosure surfaces to the room air, N the number of enclosure surfaces, A_i the area of surface i, and Q_{other} the heat gains from lights, people, appliances and infiltration. Similarly, $\left(\rho V_{zone} C_p \, \Delta T \right)/\Delta t$ is the zone air energy change and Δt the sampling time interval. Figure 2.6 shows the thermal energy flow acting at a surface within a zone. The heat extraction rate is the same as the cooling/heating load when the room air temperature is maintained constant ($\Delta T = 0$). The convective heat fluxes are determined from the energy equation for the corresponding surfaces as shown in Figure 2.6. The surface energy balance equation can be written as

$$q_i + q_{i,r} = \sum_{k=1}^{N} q_{i,k} + q_{i,c} \qquad (2.7a)$$

where q_i is the conductive heat flux at surface i, $q_{i,r}$ the radiative heat flux from heat sources (such as solar radiation), $q_{i,k}$ the radiative heat source from surface i to k, with the radiative

25

heat flux given by

$$q_{i,k} = h_{ik,r} (T_i - T_k) \qquad (2.7b)$$

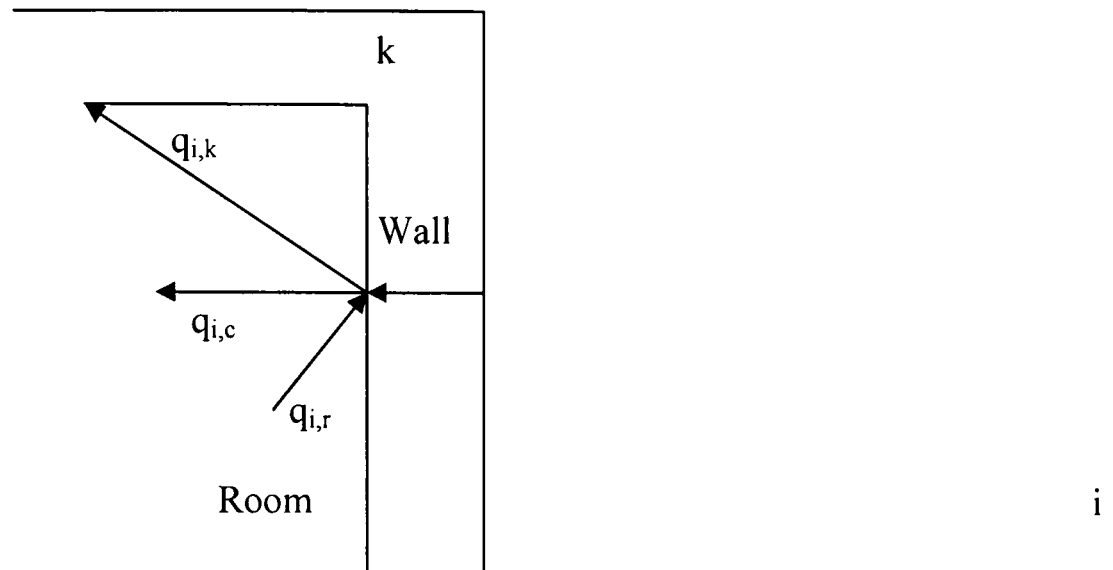where $h_{ik,r}$ is the linearized radiative heat transfer coefficient between surfaces i and k.

Figure 2.6 Energy balance on the interior surface of a wall, ceiling, floor and roof.

The convection heat flux is given by

$$q_{i,c} = h_c (T_i - T_{zone}) \qquad (2.7c)$$

where h_c is the convective heat transfer coefficient and T_{zone} the room air temperature. The next chapter is a review of indoor air flow modelling with CFD.

26

CHAPTER 3   REVIEW OF INDOOR AIR FLOW MODELLING WITH CFD

3.1 Introduction

Air transport within buildings underscores virtually all facets of environmental control as it moves both heat and moisture from place to place. In buildings and the HVAC systems which service them, air flow phenomena are encountered in three areas:

- air flow through cracks and openings in the building structure, primarily through infiltration and natural ventilation;

- the flow of air through the mechanical ventilation network; and

- the movement of air within the interior building spaces and plant components.

Air flow simulation has been focused on two approaches:

- Zonal Networks (ZN); and

- Computational Fluid Dynamics (CFD).

Although the ZN method is well adapted for air flow simulation with the HAM model, it is limited in application when it comes to consideration of the details of indoor air quality. Since momentum effects are neglected, intra-room air movement cannot be studied and local surface convective heat and mass transfer is poorly represented as a result of the low resolution. To overcome the limitations with the nodal approach, the CFD method is often employed. The method permits the analysis of systems involving fluid flow, heat and mass transfer and associated phenomena such as indoor air quality assessment. The conceptual basis of the CFD method is presented with the focus on those parts that act as pivot points with other models for building performance assessment within the integrated simulation approach.

Conceptual basis of CFD

CFD involves the solution of a set of non-linear partial differential equations using numerical methods. These equations express the fundamental physical laws that govern fluid flow and related phenomenon, namely, the conservation of mass, momentum and energy. The equations are discretised and linearised and the computational domain is enclosed with the relevant boundary conditions (e.g. inlet, outlet, solid surfaces, etc). The resultant set of algebraic relations are solved iteratively to predict (at discrete points) the distribution of pressure, temperature and velocity amongst other relevant physical quantities. The pertinent aspects of CFD are presented in the following order within this sub-section: transport equations; discretisation and linearisation; characteristics of turbulent flows; boundary conditions and their implementation, and solution procedures.

Transport equations

All variants of CFD methods are based on the governing equations for fluid flow, which are derived from the laws of conservation of mass, momentum and energy as well as the conservation of chemical species. The conservation of a general flow variable, ϕ, within a finite control volume can be expressed as a balance of the affecting processes. In words, the conservation principle states that:

$$
\left\{\begin{array}{l}\text{Rate of change of } \phi \\ \text{in the control volume} \\ \text{with respet to time}\end{array}\right\} = \left\{\begin{array}{l}\text{Net flux of } \phi \text{ due to} \\ \text{convection into the} \\ \text{control volume}\end{array}\right\} + \left\{\begin{array}{l}\text{Net flux of } \phi \text{ due to} \\ \text{diffusion into the} \\ \text{control volume}\end{array}\right\} + \left\{\begin{array}{l}\text{Net rate of creation} \\ \text{of } \phi \text{ inside the} \\ \text{control volume}\end{array}\right\}
$$

$$
+ \left\{\begin{array}{l}\text{Net rate of destruction} \\ \text{of } \phi \text{ inside the control} \\ \text{volume}\end{array}\right\}
$$

The governing equations are characterised as a set of transient, non-linear, elliptic, partial differential equations of second order. For a transient incompressible flow, the standard differential equation, which invariably serves as the control equation for CFD is given as

$$\frac{\partial(\rho\phi)}{\partial t} + \text{div}\,(\rho V\phi - \Gamma_\phi \nabla\phi) = S_\phi \qquad (3.1)$$

where ϕ is a general variable that can stand for any mean scalar variable or velocity component u, v, and w are the velocity components in the x, y and z directions; k represents the turbulent kinetic energy; ϵ represents the energy dissipation; while C and T represent the concentration and temperature respectively. The diffusion coefficient, Γ_ϕ, and the source terms, S_ϕ, are provided in standard text books. Substitution of the general variable, $\phi = 1$ in the CFD equation (3.1) yields the continuity equation as stated below by equation 3.2.

Continuity equation (3D)

$$\frac{\partial(\rho u)}{\partial t} + \frac{\partial(\rho v)}{\partial t} + \frac{\partial(\rho w)}{\partial t} = 0 \qquad (3.2)$$

Equation 3.1 ensures that the mass is conserved for a small volume of the flow, the difference between incoming and outgoing air flow being zero.

Momentum (Navier-Stokes) equation (3D)

<u>x-direction</u>

$$\frac{\partial(\rho u)}{\partial t} + \frac{\partial(\rho uu)}{\partial x} + \frac{\partial(\rho vu)}{\partial y} + \frac{\partial(\rho wu)}{\partial z} = \frac{-\partial P}{\partial x} + \frac{\partial}{\partial x}\left[\mu\left\{\frac{\partial u}{\partial x} + \frac{\partial u}{\partial x}\right\}\right]$$

$$+ \frac{\partial}{\partial y}\left[\mu\left\{\frac{\partial u}{\partial y} + \frac{\partial v}{\partial x}\right\}\right] + \frac{\partial}{\partial z}\left[\mu\left\{\frac{\partial u}{\partial z} + \frac{\partial w}{\partial x}\right\}\right] \qquad (3.3a)$$

<u>y-direction</u>

$$\frac{\partial(\rho v)}{\partial t} + \frac{\partial(\rho uv)}{\partial x} + \frac{\partial(\rho vv)}{\partial y} + \frac{\partial(\rho wv)}{\partial z} = \frac{-\partial P}{\partial y} + \frac{\partial}{\partial x}\left[\mu\left\{\frac{\partial v}{\partial x} + \frac{\partial u}{\partial y}\right\}\right] \qquad (3.3b)$$

$$+ \frac{\partial}{\partial y}\left[\mu\left\{\frac{\partial v}{\partial y} + \frac{\partial v}{\partial y}\right\}\right] + \frac{\partial}{\partial z}\left[\mu\left\{\frac{\partial v}{\partial z} + \frac{\partial w}{\partial y}\right\}\right]$$

z-direction

$$\frac{\partial(\rho w)}{\partial t} + \frac{\partial(\rho u w)}{\partial x} + \frac{\partial(\rho v w)}{\partial y} + \frac{\partial(\rho w w)}{\partial z} = \frac{-\partial P}{\partial z} + \left[\frac{\partial}{\partial x} \left\{ \mu \left\{ \frac{\partial w}{\partial x} + \frac{\partial u}{\partial z} \right\} \right\} \right.$$

$$\left. + \frac{\partial}{\partial y} \left[\mu \left\{ \frac{\partial w}{\partial y} + \frac{\partial v}{\partial z} \right\} \right] + \frac{\partial}{\partial z} \left[\mu \left\{ \frac{\partial w}{\partial z} + \frac{\partial w}{\partial z} \right\} \right] \right] - \rho g \beta (T_\infty - T) \qquad (3.3c)$$

Energy equation (3 D)

$$\frac{\partial}{\partial t}(\rho C_p T) + \frac{\partial(\rho C_p u T)}{\partial x} + \frac{\partial(\rho C_p v T)}{\partial y} + \frac{\partial(\rho C_p w T)}{\partial z} = \frac{\partial}{\partial x}\left[k\frac{\partial T}{\partial x} \right] + \frac{\partial}{\partial y}\left[k\frac{\partial T}{\partial y} \right] \qquad (3.4)$$

$$+ \frac{\partial}{\partial z}\left[k\frac{\partial T}{\partial z} \right] + S_c$$

The following scalar variables in the above equations are defined: ρ is the density (kg/m^3), μ the viscosity (Pa s), β the thermal expansion coefficient of air (K^{-1}), P the pressure (Pa), and T the temperature (^{0}C). The dependent variable in each momentum equation is a velocity component. The most significant simplification in the transport equation is the Boussinesq approximation, which assumes that the fluid is incompressible. Although the variation in density resulting in buoyancy effects is accounted for, the effects of pressure on density is neglected. The equation of state thus approximates to

$$\rho_0 - \rho = \rho \beta (T - T_\infty) \qquad (3.5)$$

which substitutes into equation (3.3c) for the z-direction momentum expression This approximation is only valid for small temperature variations, which is reasonable in room air flow. Equations (3.2) to (3.3c) characterize the fluid flow, but not the heat transfer. Although temperature appears in equation (3.3c), it is an independent variable. Equation (3.4) represents the conservation of energy and it is introduced to characterise the heat transfer and to predict the temperature distribution. The energy conservation equation is considered as a balance of the energy flows that affect the temperature. The last term (S_c) is the generation of heat within the control volume as a result of a heat source located within part of the the room.

The energy equation has a structural similarity with the momentum equations. Each equation contains transient, convection, diffusion and source terms. Equations (3.2) to (3.4) fully characterize the transient fluid motion and heat transfer throughout the air volume of a zone. The initial step involved in the solution of the Navier-Stokes equations, which includes the discretisation and linearization of these equations, is presented in the next section, where pertinent features of the CFD technique for the conflation are described.

Discretisation and Linearisation

The discretisation procedure is the transformation of the partial differential equations into a system of linear algebraic equations. In fluid flow with heat and mass transfer calculations, this represents the conservation equations for the three directions. Although all numerical methods can be viewed as being derived from the Weighted Residual Method, differing only in the weighting function used in the integration procedure, the finite volume method is preferred due to its conservative properties even for coarse grids. There are two major reasons for requiring conservation at discrete level for any grid size. First, the partial differential equations satisfying conservation require to be solved at point level. Second, the finite volume procedure of obtaining the approximate equations also produces linear systems with positive coefficients and diagonal dominance. With the finite volume method, this is achieved by subdividing the zone into finite volumes using a gridding system. Rather than solving over the continuum, temperature, pressures and velocities are predicted only at discrete points located at the centres of the finite volumes. The individual terms of the conservation equation (transient, convection, diffusion and source) are approximated by algebraic relations in terms of quantities discrete points as

$$a_P \phi_P = a_E \phi_E + a_W \phi_W + a_N \phi_N + a_S \phi_S + a_H \phi_H \; a_L \phi_L + b$$

31

$$= \Sigma a_{nb}\phi_{nb} + b \qquad\qquad (3.6)$$

where ϕ is the relevant dependent variable, P the domain cell of interest and E, W, N, S, H and L are the neighbouring points; b results from source terms as well as from terms that do not include the dependent variable, e.g. the $(-\partial P/\partial x)$ term in the x-momentum equation. It is observed from the equations deduced through the discretisation and linearisation process, that the fluxes (advective and diffusive) are the natural information to be given at the finite volume interfaces. The next sub section is an introduction to the matrix solution technique employed by ESP-r for the solution of the resultant algebraic equations for the nodal scheme through the application of equation 3.6.

The matrix solution technique as used by the ESP-r in the solution of zonal heat balance equations is described briefly within this sub section. From the algebraic relations of (Eq. 3.6), the resultant nodal equation set for the zonal heat balance equations, for example, can be represented in matrix form as shown in Figures 3.2, which emanates from the nodal scheme for the referenced zone shown in Figure 3.1. In matrix notation, the system of equations representing the discretised state of the building over some relatively small interval, can be given as

$$AT_{n+1} = BT_n + C = Z \qquad\qquad (3.7)$$

where A is a sparse matrix of future time-row coefficients of the nodal temperature or heat injection terms of the energy conservation equations, B the corresponding matrix established at the present time-row, C a column matrix of known boundary excitations in relation to the present and future time-rows, T a column matrix of nodal temperature and heat injections, n+1 relates to the future time-row, n the present time-row, and Z a column matrix. The initial

conditions are given by T(0) = T₀. Since the system of equations usually contain both present and future time-row terms, they must be solved simultaneously. Similarly, to minimise the computational effort, a specially adapted solver is often required because the entire system is sparse and populated by clusters of equations relating to componenets with different time constants (Clarke 2001). ESP-r employs a simultaneous direct solution approach based on the matrix partitioning and Gauss elimination methods.

Matrix of zone heat balance equations

To highlight on the matrix processing technique of the ESP-r, a windowless rectangular box, enclosed, for example by six fabric components to represent a zone is considered. Each fabric component is constructed of a single material layer. The default nodal scheme is illustrated in Figure 3.1, in which case four of the fabric components are shown. The zone's air point is represented by node, T_a. Each of the six fabric components is represented by three nodes, one at the internal surface, one at the external surface and one within the construction. It is assumed that a constant room air temperature is maintained through heat injection via an in-floor heating system at node F,2. Application of the general heat balance equations as presented in Appendix F and its subsequent arrangement in the form of equation 3.7 results in a sytem of 19 equations with 20 unknowns (that is, 19 nodal equations and that for the plant injection) as shown in Figure 3.2. The zone matrix of the heat balance equations as shown in Figure 3.2 can be interpreted as follows. While the equations of the external surface nodes are placed in rows 1, 4, 7, 10, 13, and 16 those for the intra-constructional nodes are located in rows 2, 5, 8, 11, 14 and 17. Also located in rows 3, 6, 9,12, 15 and 18 are the heat balances for the internal – surface nodes while row 19 contains the heat balance for the air-point node.
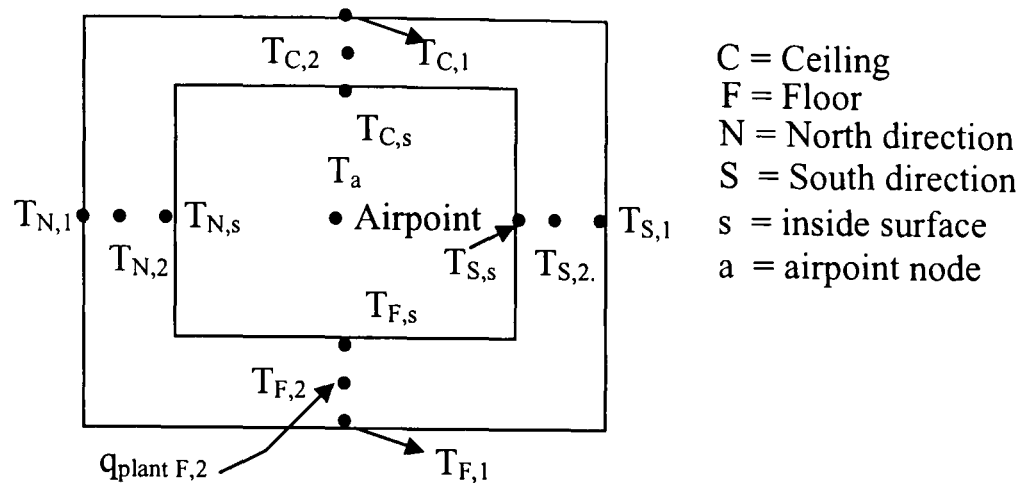
C = Ceiling
F = Floor
N = North direction
S = South direction
s = inside surface
a = airpoint node

Figure 3.1: Nodal Scheme for a zone.

Figure 3.2: Zone matrix of heat balance equations

34

The momentum coefficients appear in 26 of the 105 coefficients. As illustrated in Figure 3.2, each italised coefficient includes a convection coefficient. The internal surface node's self coupling coefficients ($a_{3,3}$, $a_{6,6}$, $a_{12,12}$, $a_{15,15}$, $a_{18,18}$), known boundary excitations (z_3, z_6, z_9, z_{12}, z_{15}, z_{18}), as well as the cross-coupling coefficients to the air-point ($a_{3,19}$, $a_{6,19}$, $a_{9,19}$, $a_{12,19}$, $a_{15,19}$ and $a_{18,19}$) include heat transfer coefficients, h_c values. The heat transfer coefficient also appears in every coefficient of the air-point balance ($a_{19,3}$, $a_{19,6}$, $a_{19,9}$, $a_{19,12}$, $a_{19,15}$, $a_{19,18}$, $a_{19,19}$, and z_{19}). The air-point balance normally includes terms that do not involve h_c, for example, inter-zone air flow and infiltration. It is quite apparent from the above discussion that, erroneous convection heat transfer coefficient can distort the zone matrix. This would cause inaccuracies in for example, nodal temperatures, plant injections, and inter-nodal energy flows.

The procedure for discretisation and linearisation of the transport equations based on the finite-volume approach is provided in standard literature on computational fluid dynamics (Malalasekera 1995). The next section is a discussion on the type of grid arrangement available for the discretisation process.

Grid arrangement

Conventional numerical algorithms based on a structured computational grid mostly fall into three classes: *regular*, *staggered* and *co-located* grid systems. In the *regular* grid system, the velocity components, u_i, (i =1,2,3), and pressures, p, are stored at the same points. The discretisation of the continuity and momentum equation are centred at these points. An example of a regular grid system in a two dimensional plane is shown in Figure 3.3.

Discussion within this sub section relates more to the two most popular grid arrangement, namely, the staggered and the co-located grid types.

In the staggered grid system the velocity components, U_i (i = 1,2,3), are distributed around the pressure points. The continuity equation is centred at these pressure points. The momentum equation corresponding to each velocity component is centred at the respective velocity point. An example of a staggered grid system in a two-dimensional plane is shown in Figure 3.4. The idea for the staggered grid approach is to evaluate scalar variables, such as pressure, density, temperature, etc, at nodal points but to calculate velocity components on staggered grids centred around the cell faces as shown. The distinction comes through the definition of an auxilliary *flux velocity*, F_i (i = 1,2,3), which is obtained via interpolation. The flux velocity is distributed in the staggered grid system. Figure 3.5 shows an example of a co-located grid system in a two-dimensional plane. With the co-located grid arrangement, the coupling of equations is achieved by the global iteration algorithm, which employs a solution procedure similar to the SIMPLE and Rhie Chow interpolattion (Ferziger and Peric 1996).
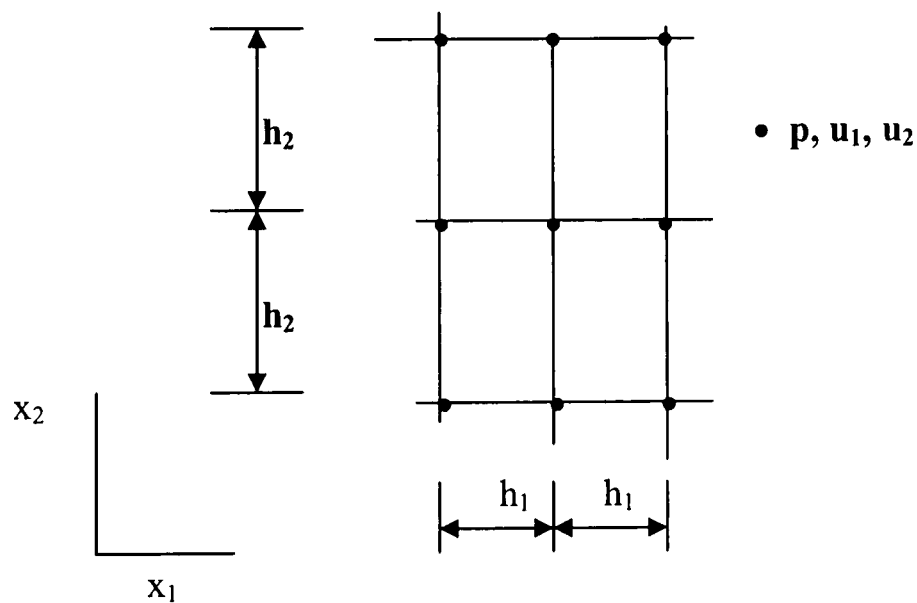
Figure 3.3: Regular grid system.

For a user, this means that the cell-centred velocity projections are solved for the variables. The face-centred velocity projections are aligned with the grid lines. With the co-located grid system, these are calculated using interpolation. As illustrated in Figure 3.5, the fluxes are defined on the cell-bounding surfaces.
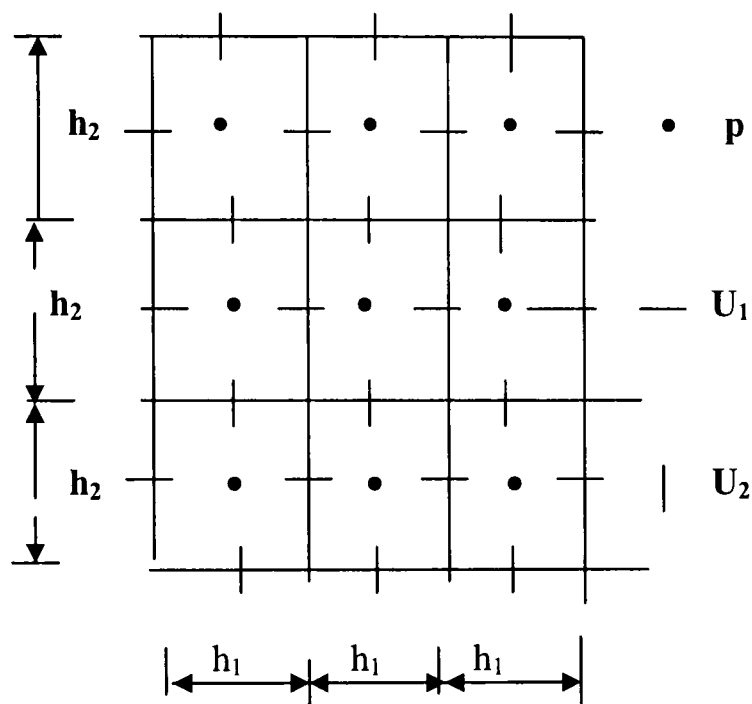
Figure 3.4: Staggered grid system.
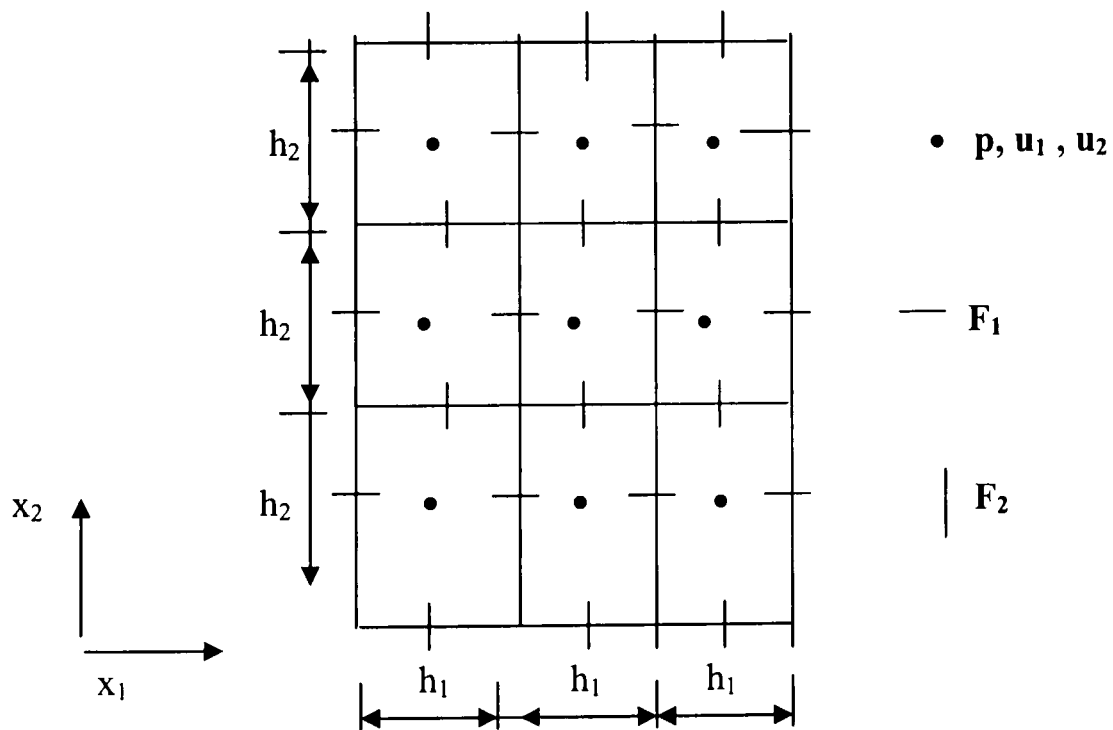
Figure 3.5: Co-located grid system.
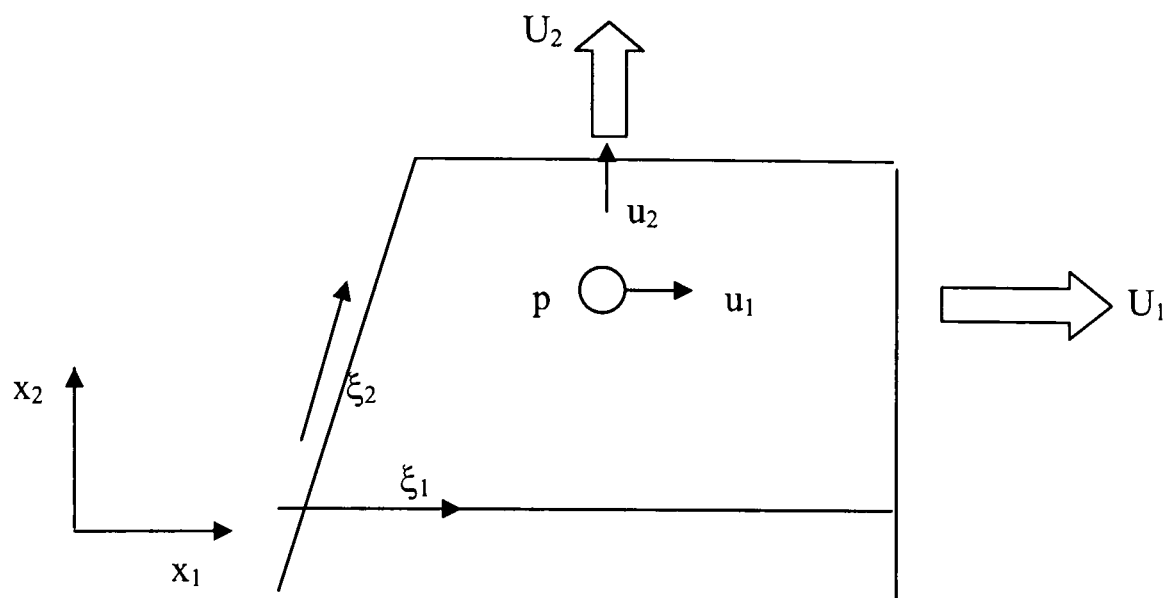
Figure 3.6: Variable arrangement in a co-located grid system.

The fluxes have the capabilities to control the oscillatory behaviour of the numerical system, for example, the suppresion of pressure oscillations. Pressure oscillations lead to instabilities in the numerical solution and subsequently lead to inaccurate simulation results.The differencing of the conservation equation of momentum follows similar procedure as done with the regular grid arrangement. Similarly, the diifferencing of the conservation of mass is carried out via the volume flux, U_1 (Figure 3.6).

With reference to the two popular grid arrangement, the advantages and disadvantages associated with their respective application are presented.

Advantages with the co-located grid type are:

- It provides the choice to store all the variables at the same set of grid points and to use the same control volumes for all the variables,

- It results to savings in computational time,

- Since many of the terms in each of the equations to be solved are essentially identical, the number of coefficients that must be computed and stored is minimised and the programming is simplified, and

- It offers additional advantage of simpler coding.

A major disadvantage is that, for incompressible flow computation, the co-located grid arrangement is not favoured due to difficulties with the pressure-velocity coupling and the occurrence of oscillations in the pressure.

In Cartesian coordinates, the staggered grid arrangement offers some advantages over the co-located arrangement. For example, several terms that require interpolation with the co-located grid arrangement can be calculated (to a second order approximation) without interpolation. Other advantages are:

- The evaluation of mass fluxes in the continuity equation on the faces of a pressure control volume is often carried out without much difficulty, and

- A major advantage of the staggered grid arrangement is the strong coupling between the velocities and the pressure.

A major disadvantage of the staggered grid approach is that, the different variables have different control volumes used in their solution and hence demands a much computational efforts and time.

Figure 3.7 shows a control volume for a two-dimensional, co-located grid arrangement and the notation used. The solution procedure adopted for the staggered and the co-located grid arrangements is the SIMPLE method (and variants thereof), which has the capability of coupling the solution for pressure and that for the velocities. Details of the SIMPLE algorithm

as an analytical tool for the solution of the Navier-Stokes equations for the co-located variable arrangement is presented in section 3.2. The next section is a presentation on boundary conditions associated with CFD problems.

Boundary conditions

CFD problems are defined in terms of initial and boundary conditions. In transient and steady state problems the initial values of all the flow variables are specified at all solution points in the flow domain. The finite volume method requires that the boundary fluxes are either known or expressed in terms of known quantities. The number of equations must match the number of unknowns. The pressures are set at fixed values and sources and sinks of mass are placed on the
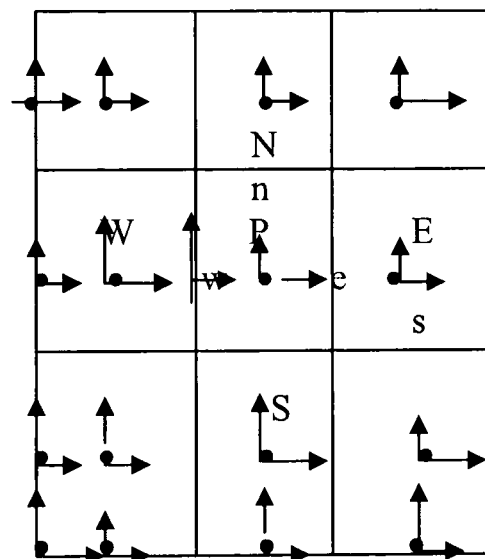
Figure 3.7: Co-located arrangement of velocity components
and pressure on a finite volume grid.

boundaries to carry the correct mass flow into and out of the solution zone across the constant pressure boundaries. The most common boundary conditions in the discretised equations of the finite volume method are as follows: inlet, outlet, wall, prescribed pressure and symmetry.

For illustration purposes, the staggered grid arrangement is again considered. Additional nodes surrounding the physical boundary are provided as shown in Figure 3.8 (Malalasekera 1995). The calculations are performed at internal nodes only (I = 2 and J = 2 onwards). Two notable features of the arrangement are:

(i) the physical boundaries coincide with the scalar control volume boundaries; and

(ii) the nodes just outside the inlet of the domain (along I=1 in Figure 3.8) are available to store the inlet conditions.

This facilitates the introduction of boundary conditions with only small modifications to the discretised equations for near-boundary internal nodes. Normally, the boundary conditions enter the discretised equations by suppression of the link to the boundary side and modification of the source terms. The appropriate coefficient of the discretised equation is set to zero and the boundary flux is introduced through the source terms.
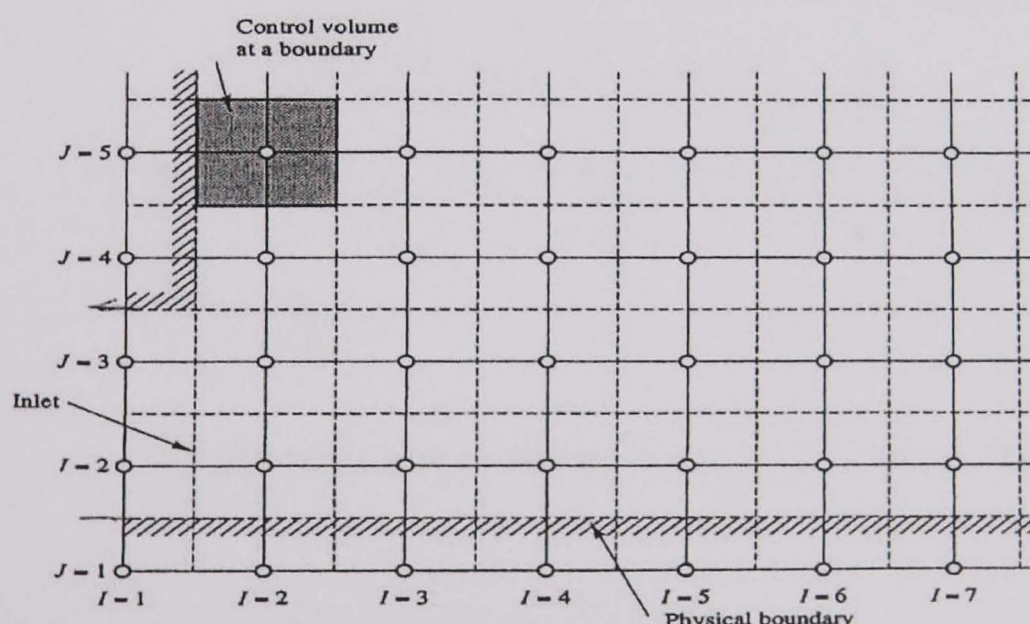
Figure 3.8: The grid arrangement at boundaries (Malalasekera 1995).

Boundary condition treatments at solid surfaces

Figure 3.9 shows a 2-D staggered grid arrangement, which is used to illustrate the methods

used to absorb the boundary conditions into the algebraic form of the governing equations

41

(Eq. 3.6). An (i,j) indexing system is used to identify the discrete points, where i represents the grid number in the x-direction and j represents the grid in the y-direction. It is common practice to number the first solution grids as (2,1), this grid poiint being reserved for 'fictitious' cells located outside the solution domain. A consequence of the staggered grid arrangement is that, for a given i and j, T(i,j), u(i,j) and v(i,j) are located at different points in space.
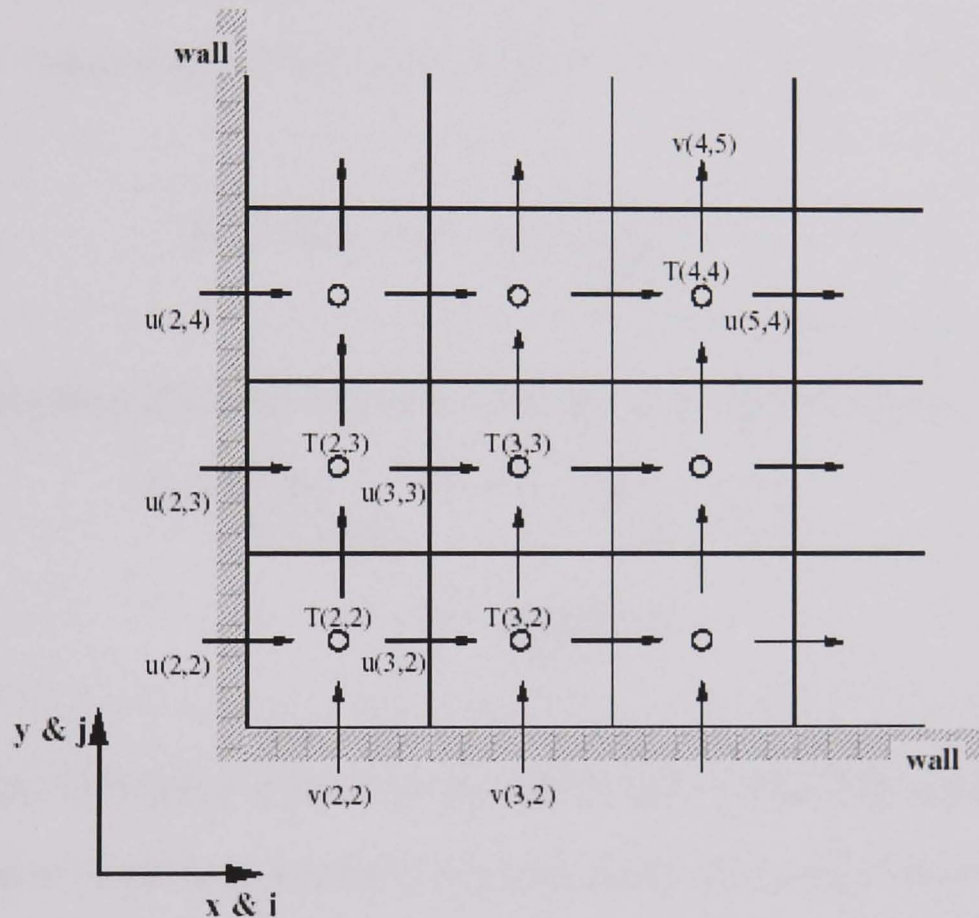
Figure 3.9: Two-dimensional staggered grid arrangement.

Air flow boundary conditions at solid surfaces

In considering air flow boundary conditions at solid surfaces, the no-slip condtion is applied for the velocity components ,

$$u = v = w = 0 \tag{3.8}$$

This is represented in the algebraic form of the momentum equations for the velocity components normal to the solid surfaces by considering, for example, the left wall in Figure 3.9. the no-slip condition is applied simply by putting u(2,j) to zero over the range of j covering the solid surface. The equation for the next-to-wall u-points (i = 3) and all other u-points are unaffected by the application of this boundary condition. From the velocity components parallel to the surfaces, the no-slip condition manifests itself in the diffusion term representing wall shear. Consideration of the x-momentum shear along the lower wall, gives the wall shear, F_{wall}, as

$$F_{wall} = A_{wall} \cdot \tau_{wall} = A_{wall} \cdot \mu \left\{ \frac{\partial u}{\partial y} \right\}_{wall} \quad . \tag{3.10}$$

This is approximated by assuming a piecewise-linear variation of u in y,

$$A_{wall} \cdot \mu \left\{ \frac{\partial u}{\partial y} \right\}_{wall} = A_{wall} \cdot \mu \left\{ \frac{u(i,2) - u|_{wall}}{\Delta y_P} \right\} \tag{3.11}$$

$$= \frac{A_{wall} \cdot \mu \cdot u(i,2)}{\Delta y_P} \quad .$$

Since $u|_{wall} = 0$ by Eq. 3.9, Δy_P is the distance from the wall to the next-to-wall u-points (m). This boundary condition is absorbed into the algebraic relations for the next-to-wall u-points (j =2) in two steps. As a first step, the next-to-wall u-points are disconnected from the wall by setting the appropriate coefficient to zero. Secondly, the self-coupling coefficient (a_P) for each next-to-wall u-point is incremented by $A_{wall} \mu/\Delta y_P$ to account for the retarding influence of the wall shear. Similarly, the other u-points are unaffected.

Thermal boundary conditions at solid surfaces

Characterisation of the thermal influence of solid surfaces is commonly effected by either prescribing the surface temperature (Dirichlet condition) or the convective heat transfer at the

43

surface (Neumann condition). Considering the left wall in Figure 3.9, a Dirichlet condition imposes the following boundary condition on the energy equation,

$$q_{wall} = -kA_{wall}\frac{\partial T}{\partial x}\bigg|_{wall} . \qquad (3.12)$$

where q_{wall} is the heat transfer from the wall to the air. Upon assumption of a piecewise-linear variation of T in x, this can be represented by

$$-kA_{wall}\frac{\partial T}{\partial x}\bigg|_{wall} = -kA_{wall}\left\{\frac{T(2, j) - T_{wall}}{\Delta x_P}\right\} \qquad (3.13)$$

where Δx_P is the distance from the wall to the next-to-wall T-points and T_{wall} is the known wall surface temperature. This boundary conditions is absorbed into the algebraic relations for the next-to-wall grid points (i =2) in three steps. As a first step, the points are disconnected from the wall by setting the neighbour coefficient to zero (a_W in this case). Secondly, the self-coupling coefficients (a_P) are incremented by $kA_{wall}/\Delta x_P$. Finally, the source terms (b) in equation (3.6) are incremented by $kA_{wall}.T_{wall}/\Delta x_P$. With q_{wall} being known, the application of the Neumann condition becomes trivial. Considering the left wall again (Figure 3.9), the Neumann condition is absorbed by disconnecting the next-to-wall T-points from the wall by setting the a_W coefficients to zero. The b-coefficients for the next-to-wall points are then incremented by q_{wall}.

The constant pressure boundary condition

The constant pressure boundary condition is used in situations where exact details of the flow distribution are unknown but the boundary values of pressure are known. Typical problems where this boundary condition is appropriate include external flows around objects, free surface flows, buoyancy-driven flows such as natural ventilation and fires, and also internal flows with

multiple outlets. For incompressible flows, however, the density of the fluid is by definition not linked to the pressure. Coupling between pressure and velocity introduces a constraint on the solution of the flow fields. Problems associated with the pressure-velocity linkage are resolved through the application of the SIMPLE algoerithm (Patankar and Spalding 1974). The convective fluxes per unit mass, F, through the respective cell faces are determined from guessed velocity components using this algorithm.

Within the SIMPLE algorithm, a guessed pressure field is used to solve the momentum equations. The pressure correction equivalent, determined from the continuity equation is solved to obtain a pressure correction field, which is in turn used to update the velocity and pressure fields (Appendix C). Due to the anticipated inaccuracies contained in the guessed pressure field a pressure-correction term, (p') is introduced. It is given by the difference between the correct pressure, whose solution is required (p) and the guessed pressure p*. The pressure-correction term (p') is defined as (Malalasekera 1995)

$$p' = p - p^* \qquad\qquad (C.1)$$

In applying the fixed pressure boundary condition, the pressure correction is set to zero at the nodes. The grid arrangement of the p'-cells near a flow inlet and outlet is shown in Figures 3.10 and 3.11. A convenient way of dealing with a constant pressure boundary condition is to fix the pressure at the nodes just inside the physical boundary as indicated in the diagrams by solid squares. The u-momentum equation is solved from i = 3 and the v-momentum and other equations are solved from I = 2 onwards. The main outstanding problem is the unknown flow direction, which is governed by the conditions inside the calculation domain. The u-velocity component across the domain boundary is generated as part of the solution process by ensuring

that continuity is satisfied at every cell. For example, in Figure 3.10 the values of u_e, v_s and v_n

emerge from solving the discretised u- and v- momentum equations inside the domain. Given

these values, u_w is computed by ensuring that mass is conserved for the p'-cell. This yields

$$u_w = \frac{(\rho vA)_n - (\rho vA)_s + (\rho uA)_e}{(\rho A)_w} . \qquad (3.14)$$

The implementation of the boundary condition causes the p'-cell nearest to the boundaries to

act as a source or sink of mass. The process is repeated for each pressure boundary cell. Other

variables such as v, T, k and ε are assigned values where the flow direction is into the domain.

Where the flow is outwards, their values just outside the domain are obtained by means of

extrapolation.
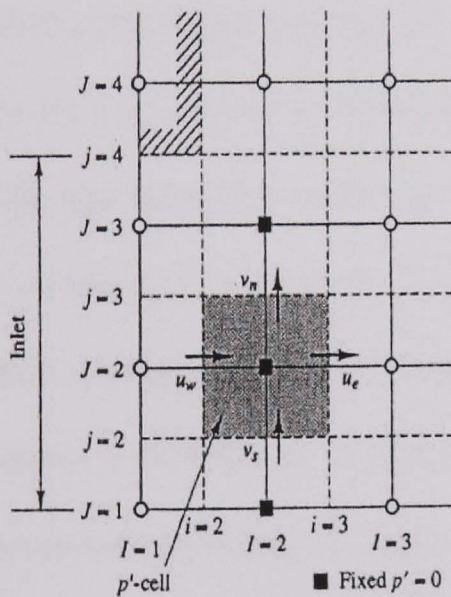
Figure 3.10: p'-cell at an inlet boundary (from Malalasekera 1995).
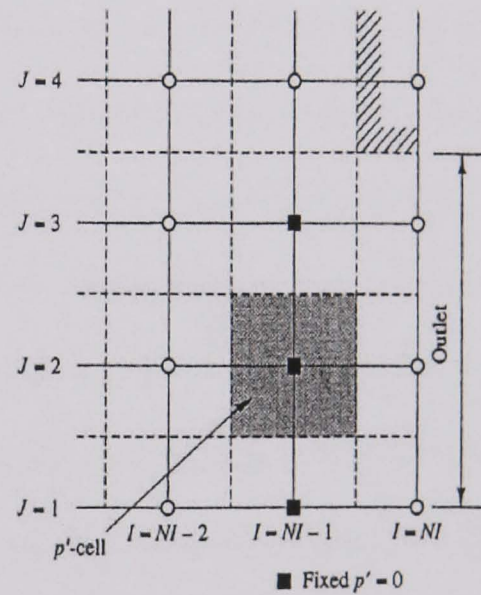
Figure 3.11: p'-cell at an outlet boundary (from Malalasekera 1995).

Symmetry boundary condition

The condition at a symmetrical boundary are: (i) no flow across the boundary and (ii) no scalar

flux across the boundary. In the implementation of the boundary conditions, normal velocities

are set to zero at a symmetry boundary and the values of all other properties just outside the solution domain (say I or i =1) are equated to their values at the nearest node just inside the domain (I or i = 2):

$$\phi_{1,J} = \phi_{2,J} \, . \tag{3.15}$$

In the discretised p'-equations the link with the symmetry boundary is cut by setting the appropriate coefficient to zero. The next section is a discussion on the co-located grid system as they relate to the present work.

3.2 Co-located grid system

3.2.1 Numerical solutions and algorithms

This section presents an overview of numerical techniques available to solve the Navier-Stokes equations for a co-located grid arrangement. This summary focuses on techniques for coupling of pressure and velocities, coupling of the equations for conservation of mass and momentum, and the co-location of volumes at the interfaces. Mathematically, this system constitutes a mixed type problem, because the equation of conservation of mass is elliptic and that for the conservation of momentum is parabolic. The numerical procedures for solving each class of equation are incompatible. Physically, by the approximation of incompressibility, any change in pressure is communicated instantaneously to the rest of the flow, while the changes in velocity need to march in time. The combination of instantaneous and sequential exchange of information causes numerical instabilities. Many techniques have been developed to circumvent this problem (Kwak 1989; Hirsch 1989). This method has been used successfully in many two-dimensional computations. The other reported technique for solving the incompressible Navier-Stokes equations uses a primitive-variable formulation (which implies that the pressure and the velocities are the dependent variables) and focuses on coupling the

conservation of mass equations and the pressure by special means, e.g. via the pressure correction method. Primitive variable formulations are generally more convenient to extend to equation for the auxilliary velocity. These expressions are discretised implicitly and then substituted into the equations for the conservation of mass. Discussions on the solution of the Navier-Stokes equations for co-located variables including the treatment of pressure and the use of the SIMPLE algorithm is presented in the next sub-section. Conservation properties of the mass, momentum and kinetic energy equations for incompressible flows are regarded as analytical requirements for a proper set of discrete equations.

Solution of the Navier–Stokes equation for co-located variables

The solution procedure usually adopted is the SIMPLE approach (or variants thereof) to couple the solution of the pressure to the solution of velocities (Ferziger 1996). A major disadvantage of the staggered grid approach is that, the different variables have different control volumes used in their solution. An alternative choice is the co-located grid arrangement in which all variables are stored at the same location, usually at the cell centre in a finite-volume scheme. With this arrangement the mass flux through any control volume face is calculated by interpolating the velocities at two nodes on either side of the face.

The interpolation function is a key tool of the numerical technique. It tries to represent the behaviour of the exact solution between grid points. The interpolation function is therefore responsible for the truncation error embodied in the numerical solution. It also influences the stability of the numerical scheme. The discusssion on the solution of the Navier-Stokes equations is included to facilitate future modifications to an existing computer code which

employs the staggered grid arrangement based on the Phoenix computer programm. An example of CFD program that uses both the co-located and the staggered grid arrangement is the FLUENT 5 CFD simulation program.

Treatment of pressure for co-located variables

Considering the semi- discretised momentum equations, symbolically written as

$$\frac{\partial}{\partial t}(\rho u_i) = -\frac{\delta}{\delta x_j}(\rho u_i u_j) - \left\{\frac{\delta p}{\delta x_j}\right\} + \left\{\frac{\delta \tau_{ij}}{\delta x_j}\right\} = H_i - \left\{\frac{\delta p}{\delta x_i}\right\} \qquad (3.16)$$

where $\delta/\delta x$ represents a discretized patial derivative and H_i is shorthand notation for the advective and viscous terms (Ferziger and Peric 1996). The solution of equation 3.16 with the Euler method for time advancement gives

$$(\rho u_i)^{n+1} - (\rho u_i)^n = \Delta t \left\{ H_i^n - \frac{\delta p^n}{\delta x_i} \right\}. \qquad (3.17)$$

With this application, the velocity at time step n is used to compute H_i^n and, if the pressure is available, $\delta p^n/\delta x_i$ may also be computed. This gives an estimate of ρu_i at the new time step n+1. In general, the velocity field does not satisfy the continuity equation:

$$\frac{\delta(\rho u_i)^{n+1}}{\delta x_I} = 0. \qquad (3.18)$$

To enforce continuity, the numerical divergence of equation 3.17 is taken. The result is

$$\frac{\delta(\rho u_i)^{n+1}}{\delta x_i} - \frac{\delta(\rho u_i)^n}{\delta x_i} = \Delta t \left[\frac{\delta}{\delta x_i} \left\{ H_i^n - \frac{\delta p^n}{\delta x_i} \right\} \right]. \qquad (3.19)$$

The first term is the divergence of the new velocity field, which must be zero. The second term is zero if continuity was enforced at time step n; it is assumed that this is the case. Retaining this term is necessary when an iterative method is used to solve the Poisson equation. Similarly, the divergence of the viscous component of H_i should be zero for constant ρ, but a non-zero value is easily accounted for. The resultant discrete Poisson equation for the pressure p^n is

$$\frac{\delta}{\delta x_i}\left\{\frac{\delta p^n}{\delta x_i}\right\} = \left\{\frac{\delta H_i^n}{\delta x_i}\right\} \tag{3.20}$$

where H_i^n is the shorthand notation for the sum of the advective and viscous terms. The operator $\delta/\delta x_i$ is the divergence operator inherited from the continuity equation. $\delta p/\delta x_i$ in equation (3.20) is the pressure gradient from the momentum equation. If the pressure p^n satisfies this discrete Poisson equation, then the velocity field at time step n+1 will be divergence free (in terms of the discrete divergence operator). Equation 3.20, however, is not specific to any grid arrangement. H_i^n is given by

$$H_i^n = -\frac{\delta(\rho u_j u_j)^n}{\delta x_j} + \frac{\delta \tau_{ij}^n}{\delta x_j} \quad . \tag{3.21}$$

Summation on j is implied here. Figure 3.12 shows a control volume in a co-located grid arrangement. Various difference schemes for the pressure gradient terms in the momentum equations and for the divergence in the continuity equation are considered. In this regard, a forward difference scheme is used for the pressure terms and a backward difference scheme for the continuity equation. For simplicity it is assumed that the grid is uniform with spacings
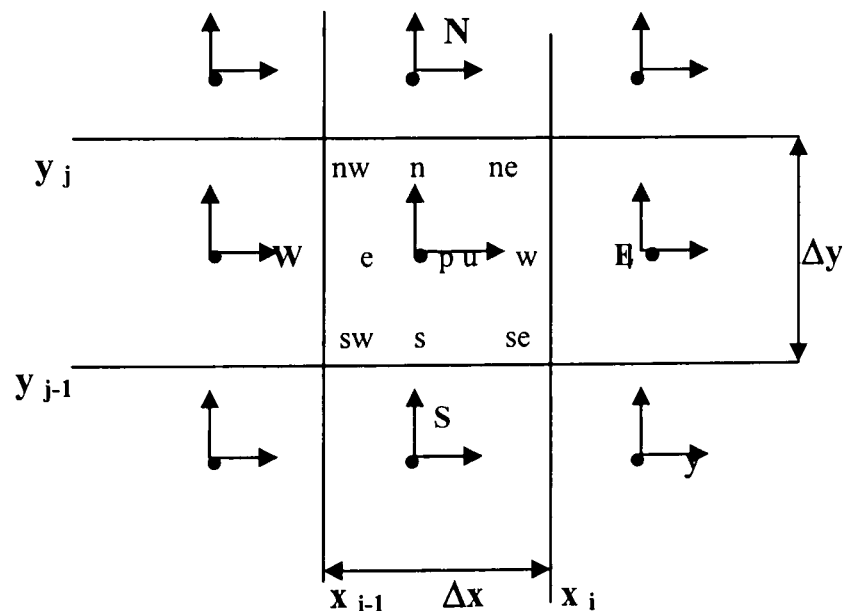
Figure 3.12: Control volume in a co-located grid and the notation used.

Δy and Δx as shown in Figure 3.12. An approximation of the outer difference operator, $\delta/\delta x_i$, in the pressure equation with the backward scheme gives

$$\frac{\left\{\frac{\delta p^n}{\delta x}\right\}_P - \left\{\frac{\delta p^n}{\delta x}\right\}_W}{\Delta x} + \frac{\left\{\frac{\delta p^n}{\delta y}\right\}_P - \left\{\frac{\delta p^n}{\delta y}\right\}_S}{\Delta y} =$$

$$\left\{\frac{H^n_{x,P} - H^n_{y,W}}{\Delta x}\right\} + \left\{\frac{H^n_{y,P} - H^n_{y,S}}{\Delta y}\right\} . \tag{3.22}$$

Denoting the right-hand-side as Q_P^H and using the forward difference approximations for the pressure derivatives, yields

$$\frac{\left\{\frac{p_E^n - p_P^n}{\Delta x}\right\} - \left\{\frac{p_P^n - p_W^n}{\Delta x}\right\}}{\Delta x} + \frac{\left\{\frac{p_N^n - p_P^n}{\Delta y}\right\} - \left\{\frac{p_P^n - p_S^n}{\Delta y}\right\}}{\Delta y} = Q_P^H . \tag{3.23}$$

The system of algebraic equations for the pressure then takes the form

$$A^P_P p^n_P + \sum_l A^P_l p^n_l = -Q^H_P , \quad l = E, W, N, S, \tag{3.24}$$

where the coefficients are

$$A_E^P = A_W^P = -\left\{\frac{1}{(\Delta x)^2}\right\}, \quad A_N^P = A_S^P = -\left\{\frac{1}{(\Delta y)^2}\right\}, \quad A_P^P = -\sum_l A^P_l . \tag{3.25}$$

It can thus be shown that the finite volume approach reproduces equation (3.18) if the control volume shown in Figure 3.10 is used for both the momentum equations and the continuity equation. Similarly, the following approximations are relevant: $u_e = u_P$, $p_e = p_E$, $v_n = v_P$, $p_n = p_N$; $u_w = u_W$, $p_w = p_P$; $v_s = v_S$ and $p_s = p_P$. Consider the case that the central difference approximations is chosen for both the pressure gradient in the momentum equations and the divergence in the continuity equation. An approximation of the outer difference operator in equation 3.20 by central differences yields

$$\frac{\left\{\frac{\delta p^n}{\delta x}\right\}_E - \left\{\frac{\delta p^n}{\delta x}\right\}_W}{2\Delta x} + \frac{\left\{\frac{\delta p^n}{\delta y}\right\}_N - \left\{\frac{\delta p^n}{\delta y}\right\}_S}{2\Delta y} =$$

$$\left\{\frac{H^n_{x,E} - H^n_{x,W}}{2\Delta x}\right\} + \left\{\frac{H^n_{y,N} - H^n_{y,S}}{2\Delta y}\right\} . \tag{3.26}$$

Again, the right hand side is denoted as Q_P^H. Insertion of the central difference approximations for the pressure derivatives gives

$$\frac{\left\{\frac{P^n_{EE}-P^n_P}{2\Delta x}\right\} - \left\{\frac{P^n_P-P^n_{WW}}{2\,\Delta x}\right\}}{2\Delta x} + \frac{\left\{\frac{P^n_{NN}-P^n_P}{2\Delta y}\right\} - \left\{\frac{P^n_P-P^n_{SS}}{2\Delta y}\right\}}{2\Delta y} = Q_P^H \qquad (3.27)$$

The system of algebraic equations for the pressure takes the form

$$A^P_P P^n_P + \sum_l A^P_l Pn_l = -Q^H_P, \qquad l = EE, WW, NN, SS \qquad (3.28)$$

where the coefficients are

$$A^P_{EE} = A^P_{WW} = -1/(2\,\Delta x)^2, \quad A^P_{NN} = A^P_{SS} = -1/(2\Delta y)^2, \quad A^P_P = -\Sigma_l A^P_l \qquad (3.29)$$

One approach to dealing with the pressure-velocity coupling on co-located grids that has found widespread use in complicated geometries, follows. On staggered grids, central difference approximations are based on Δx differences. With reference to the pressure equation (3.20), a Δx approximation of its outer derivative has the form

$$\frac{\left\{\frac{\delta p^n}{\delta x}\right\}_e - \left\{\frac{\delta p^n}{\delta x}\right\}_w}{\Delta x} + \frac{\left\{\frac{\delta p^{n+}}{\delta y}\right\}_n - \left\{\frac{\delta p^n}{\delta y}\right\}_s}{\Delta y} = \left\{\frac{H^n_{x,e}-H^n_{x,w}}{\Delta x}\right\} + \left\{\frac{H^n_{y,n}-H^n_{y,s}}{\Delta y}\right\} \qquad (3.30)$$

For co-located grids, unlike the staggered grid arrangement, interpolation is used since the values of pressure derivatives and quantities H are not available at cell face locations. A linear interpolation method, which has the same accuracy as the central difference scheme is chosen for the approximation of the derivatives. Also, the inner derivatives of the pressure in equation (Eq.3.20) is approximated using the central difference scheme. Linear interpolation of cell centre derivatives gives

$$\left\{\frac{\delta p^n}{\delta x}\right\}_e \cong \frac{1}{2}\left[\left\{\frac{p_E - p_W}{2\,\Delta x}\right\} + \left\{\frac{p_{EE} - p_P}{2\,\Delta x}\right\}\right] . \qquad (3.31)$$

With this interpolation the pressure equation (3.22) is recovered. The pressure derivatives at cell faces are evaluated using central differences and Δx spacings:

$$\left\{\frac{\delta p^n}{\delta x}\right\}_e \approx \left\{\frac{p_E - p_P}{\Delta x}\right\}. \qquad (3.32)$$

An application of this approximation at all cell faces results in the following pressure

equation (which is also valid on non-uniform grids). That is

$$\left\{\frac{\delta p^n}{\delta x}\right\} = \frac{\left\{\frac{p^n_E - p^n_P}{\Delta x}\right\} - \left\{\frac{p^n_P - p^n_W}{\Delta x}\right\}}{\Delta x} + \frac{\left\{\frac{p^n_N - p^n_P}{\Delta y}\right\} - \left\{\frac{p^n_P - p^n_S}{\Delta y}\right\}}{\Delta y} = Q^H_P. \qquad (3.33)$$

This is the same as equation (3.24), except that the right-hand side is now obtained by

interpolation:

$$Q^H_P = \frac{\overline{(H^n_x)}e - \overline{(H^n_x)}w}{\Delta x} + \frac{\overline{(H^n_y)}n - \overline{(H^n_y)}s}{\Delta y} \qquad (3.34)$$

The next sub-section describes SIMPLE algorithm for the co-located variable arrangement.

3.2.2 SIMPLE algorithm for a co-located grid arrangement

The success of an algorithm of this type is mainly judged by three qualities: consistency,

accuracy and stability (Hirsch 1989). Implicit solution of the momentum equations discretised

with the co-located finite volume method follows the line of approach for the staggered

arrangement. The control volume for all variables with the co-located arrangement are the

the same. The pressures at the cell face centres, which are not nodal locations are obtained by

interpolation. The gradients at the control volume centre, which are needed for the calculation

of cell face velocities are obtained using Gauss' theorem (Ferziger 1996). The pressure forces

in the x and y directions are summed over all faces and divided by the cell volume to yield the

mean pressure derivative. For example:

$$\{\delta p / \delta x\}_P = \{Q^P_u / \Delta\Omega\} \qquad (3.35)$$

where Q^P_u stands for the sum of pressure forces in the x-direction over all control volume faces

and $\Delta\Omega$ is the volume of the cell. On Cartesian grids this reduces to the standard central

difference scheme approximation. For the discretised continuity equation, the cell face velocities needed are determined by linear interpolation. Similarly, the pressure correction equation of the SIMPLE algorithm is derived following the line of approach for the staggered grid arrangement. The interpolated cell face velocities required in the continuity equation involve interpolated pressure gradients, so their correction is proportional to the interpolated pressure gradient:

$$u'_e = \overline{\left[\frac{-\Delta\Omega}{A^u_P} \frac{\delta p'}{\delta x} \right]}_e \quad . \tag{3.36}$$

Here, the overbar denotes interpolation. The volume centred around a cell face is defined by $\Delta\Omega_e = (x_E - x_P)\,\Delta y$. Thus, the cell face velocity in the SIMPLE method is given by

$$u'_e = -\Delta\Omega_e \overline{\left\{ \frac{1}{A^u_P} \right\}}_e \left\{ \frac{\delta p'}{\delta x} \right\}_e = -S_e \overline{\left\{ \frac{1}{A^u_P} \right\}}_e (p'_E - p'_P) \tag{3.37}$$

with corresponding expressions at other faces. When these expressions are inserted into the discretised continuity equation, the pressure-correction equation as given by the staggered grid arrangement is obtained. The only difference is that the coefficients $1/A^u_P$ and $1/A^v_P$ at the cell faces are not the nodal values as with staggered grids. They are the interpolated cell centre values.

Boundary conditions for the Navier-Stokes equations

For the co-located grid arrangement all control volumes extend to the boundary and hence a boundary pressure is required to calculate the pressure forces in the momentum equations in comparison with the staggered grid arrangement. Extrapolation is used to obtain the pressure at the boundaries and in most cases linear extrapolation is sufficiently accurate for a second order

method.

For the purpose of illustrating the finite volume method and to demonstrate some of the properties of the discretization method presented, an example is considered. Consider the problem illustrated in Figure 3.13, which involves the transport of a scalar quantity in a known velocity field. The latter is given by $u_x = x$ and $u_y = -y$, which represents the flow near a stagnation point. The streamlines are lines of xy = constant and change in direction with respect to the Cartesian grid. It is assumed that on any cell face the normal velocity component is constant so the error in the approximation of the convective flux depends only on the approximation used for ϕ_e. The scalar transport equation to be solved is given as

$$\int_S \rho \phi \upsilon \cdot \mathbf{n} \, dS = \int_S \Gamma \mathrm{grad}\, \phi \cdot \mathbf{n} \, dS \ . \qquad (3.38)$$

The following conditions are applicable to the example:

- $\phi = 0$ along the north (inlet) boundary;

- linear variations of ϕ from $\phi = 0$ at $y = 1$ to $\phi = 1$ at $y = 0$ along the west boundary ;

- symmetry condition (zero gradient normal to boundary) on the south boundary and

- Zero gradient in the flow direction at outlet (east) boundary.

Figure 3.13 shows a sketch of the geometry and the flow field. Details of discretisation for the 'e' face is considered. The convective flux is evaluated using the mid-point rule and either the upwind differencing scheme or the central differencing scheme interpolation. Since the normal velocity is constant along cell faces, the *convective flux* is expressed as a product of the mass flux and the mean value of ϕ:

$$F^c_e = \int_{Se} \rho \phi v \cdot \mathbf{n} dS \ \approx m_e \phi_e \ , \qquad (3.39)$$

where m_e is the *mass flux* through the 'e' face:

$$m_e = \int_{Se} \rho v.ndS = (\rho u_x)_e \, \Delta y \; . \tag{3.40}$$

Equation 3.40 is exact on any grid, since the velocity $u_{x,e}$ is constant along the face. The flux approximation is then

$$F^c_e = \begin{cases} \max(m_e, 0)\, \phi_P + \min(m_e, 0.)\phi_E & \text{for upward differencing} \\ m_e(1-\lambda_e)\phi_P + m_e\lambda_e\phi_E & \text{for central differencing} \end{cases} \tag{3.41}$$

where the linear interpolation coefficient, λ_e, is defined as $\lambda_e = (x_e - x_P)/(x_E - x_P)$.

Consider the equation at a location 'e' on a Cartesian grid, which is given by

$$\phi e = \phi_E\lambda_e + \phi_P(1 - \lambda_e) \; . \tag{3.42}$$
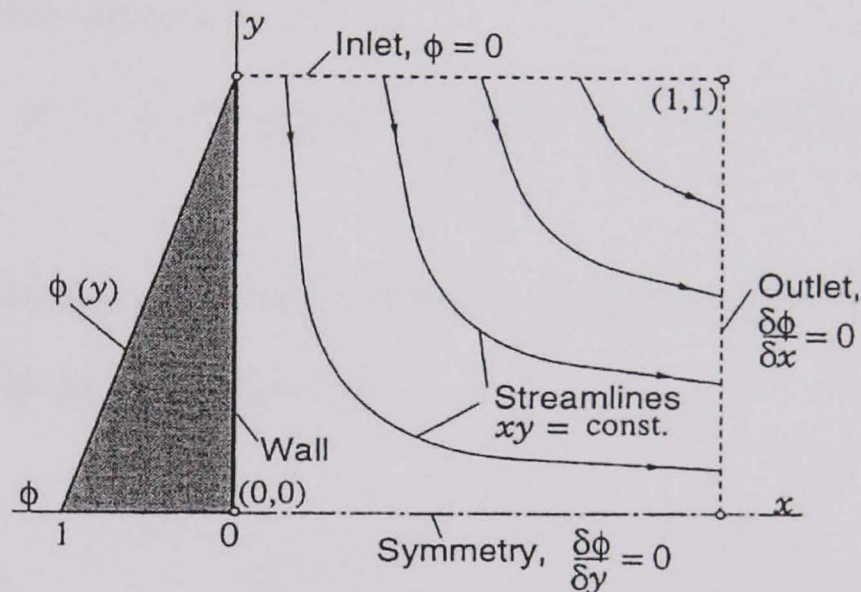
Figure 3.13: Geometry and boundary conditions for the scalar transport

in a stagnation point flow (Ferziger, 1996).

Analogous expressions for the fluxes through the other CV faces produce the following

coefficients in the algebraic equations for the case of an upward differencing scheme:

$$A^c_E = \min(m_e, 0.) \; ; \qquad A^c_W = \min(m_w, 0.);$$

$$A^c_N = \min(m_n, 0.) \; ; \qquad A^c_S = \min(m_s, 0.), \tag{3.43}$$

$$A^c_P = -(A^c_E + A^c_W + A^c_N + A^c_S) \; .$$

For the central differencing scheme, the coefficients

$$A^c_E = m_e\lambda_e \;\; ; \;\;\;\; A^c_W = m_w\lambda_w \; ,$$

$$A^c_N = m_n\lambda_n \;\; ; \;\;\;\; A^c_S = m_s\lambda_s \; , \tag{3.44}$$

$$A^c_P = -(A^c_E + A^c_W + A^c_N + A^c_S)$$

The expression for $A_P{}^c$ follows from the continuity condition:

$$m_e + m_w + m_n + m_s = 0$$

which is satisfied by the velocity field, noting that m_w and λ_w for the CV centred around node P are equal to $-m_e$ and $1 - \lambda_e$ for the CV centred around node W. In a computer code the mass fluxes and interpolation factors are calculated once and stored as m_e, λ_e and λ_n for each CV. The diffusive flux integral is evaluated using the mid-point rule and central differencing approximation of the normal derivative:

$$F^d_e = \int_{Se} \Gamma \; grad\phi.ndS \approx \left[\Gamma\frac{\partial\phi}{\partial x}\right]_e \Delta y = \left\{\frac{\Gamma\Delta y}{x_E - x_P}\right\} (\phi_E - \phi_P). \tag{3.45}$$

The diffusion coefficient is assumed constant. The contribution of the diffusion term to the coefficient of the algebraic equation are:

$$A^d_E = -\left\{\frac{\Gamma\Delta y}{x_E - x_P}\right\}; \;\;\;\;\; A^d_W = -\left\{\frac{\Gamma\Delta y}{x_P - x_W}\right\},$$

$$A^d_N = -\left\{\frac{\Gamma\Delta x}{y_N - y_P}\right\} \;\; ; \;\;\;\;\; A^d_S = -\left\{\frac{\Gamma\Delta x}{y_P - y_S}\right\} \tag{3.46}$$

$$A^d_P = -(A^d_E + A^d_W + A^d_N + A^d_S) \; .$$

With the same approximations applied to other CV faces, the integral equation becomes:

$$A_W\phi_W + A_S\phi_S + A_P\phi_P + A_E\phi_E = Q_P \tag{3.47}$$

which represents the equation for a generic node, P. The coefficients, A, are obtained by summing the convective and diffusive contributions, (equations 3.43, 3.44, and 3.45):

$$A_l = A^c_l + A^d_l \tag{3.48}$$

57

where l represents any of the indices P, E, W, N and S. A_P being equal to the negative sum of all neighbour coefficients is a feature of all conservative schemes and ensures that a uniform field is a solution of the discretised equations. The above expressions are valid at all internal CVs. For CVs next to a boundary, the boundary conditions are modified accordingly. At north and west boundaries, where ϕ is prescribed, the gradient in the normal direction is approximated using one-sided differences, e.g. at the west boundary:

$$\left\{ \frac{\partial \phi}{\partial x} \right\} \approx \left\{ \frac{\phi_P - \phi_W}{x_P - x_W} \right\} \tag{3.49}$$

where W denotes the boundary node whose location coincides with the cell face centre 'w'. This approximation is of first order accuracy, but it is applied on a half width CV. The product of the coefficient and the boundary value is added to the source term. For example, along the west boundary (CVs with index i = 2), $A_W \phi_W$ is added to Q_P (in equation 3.44) and the coefficient A_W is set to zero. The same applies to the coefficient A_N at the north boundary. At the south boundary, the normal gradient of ϕ is zero. This implies that, when the above approximation is applied , the boundary values are equal to the values at CV centres. Thus, for cells with index j = 2, $\phi_S = \phi_P$, the algebraic equation for those CVs is modified to

$$(A_P + A_S)\phi_P + A_N\phi_N + A_W\phi_W + A_E\phi_E = Q_P \tag{3.50}$$

which requires adding A_S to A_P and then setting $A_S = 0$. The zero-gradient condition at the outlet (east) boundary is implemented in a similar manner.

Further discussion with regards to the boundary conditions at a wall and a symmetry plane for the solution of the Navier-Stokes equations is presented.

At a *wall*, the no-slip boundary condition applies, that is, the velocity of the fluid is equal to the wall velocity, a Dirichlet boundary condition. Another condition, that the normal viscous stress is zero at a wall can be directly imposed in a finite volume method. This follows from the continuity equation, e.g. for a wall at y = 0 (Figure 3.14):

$$\left\{\frac{\partial u}{\partial x}\right\}_{wall} = 0 \Rightarrow \left\{\frac{\partial v}{\partial y}\right\}_{wall} = 0 \Rightarrow \tau_{yy}= 2\mu\left\{\frac{\partial v}{\partial y}\right\}_{wall} = 0 \qquad (3.51)$$

Therefore, the diffusive flux in the velocity-equation at the south boundary is

$$F^d_{\ s} = \int_{Ss}\tau_{yy}\, dS = 0 \, . \qquad (3.52)$$

This is implemented directly, rather than using only the condition that v = 0 at the wall. A non-zero derivative in the discretised flux expression would be obtained if this was not done; v = 0 is used as a boundary condition in the continuity equation. The shear stress is calculated by using a one-sided approximation of the derivative $\partial u/\partial y$.

$$F^d_{\ s} = \int_{Ss}\tau_{xy}\, dS = \int_{Ss} \mu \frac{\partial u}{\partial y}\, dS \approx \mu_s S_s \cdot \frac{u_P - u_S}{y_P - y_S} \, . \qquad (3.53)$$

At a *symmetry plane* the opposite situation is the case: the shear stress is zero, but the normal stress is not, since

$$\left\{\frac{\partial u}{\partial y}\right\}_{sym} = 0 \; ; \quad \left\{\frac{\partial v}{\partial y}\right\}_{sym} \neq 0 \, . \qquad (3.54)$$

The diffusive flux in the u-equation is zero, and that in the v-equation is estimated as

$$F^d_{\ s} = \int_{Ss}\tau_{yy}\, dS = \int_{Ss} 2\mu \frac{\partial u}{\partial y}\, dS \approx \mu_s S_s \frac{v_P - v_S}{y_P - y_S} \qquad (3.55)$$

where $v_s = 0$ applies.

Figure 3.14 shows the velocity profiles asssociated with boundary conditions at a wall, a symmetry plane and a near-boundary control volume.
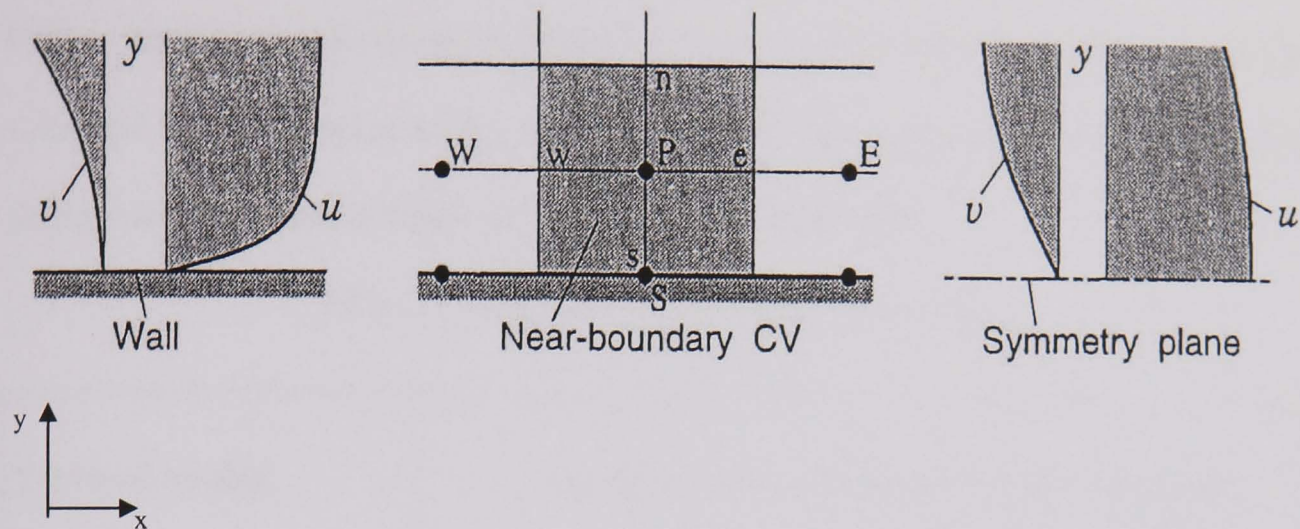
Figure 3.14: Boundary conditions at a wall and a symmetry plane (Ferziger 1996).

The next section describes the turbulence models in relation to the modelling of buoyancy-induced room air flow with CFD.

.

3.3 Turbulence modelling

Issues regarding CFD's suitability for predicting zone air flow are further expanded through the presentation of turbulence models with the emphasis on the standard k-ε model. This model, however, is valid for only the fully-developed turbulence case (notwithstanding near-wall regions for which adjustments are made to account for viscous effects). Consequently, the application of the standard k-ε model (Malalasekera 1995) implies an important assumption: that the flow is fully turbulent or at least behaves like a fully turbulent flow. The most common turbulence models are classified as shown in Table 3.1.

Classical models use the Reynolds equations and form the basis of turbulence calculations currently available in CFD codes (Malalasekera 1995). Most zero-, one-, and two-

equation models represent the Reynolds shear stresses by way of a turbulent viscosity concept. Of the classical models the mixing length and k-ε models are by far the most widely used and validated. They are based on the presumption that there exists an analogy between the viscous stresses and Reynolds stresses on the mean flow (Rodi 1980).

Table 3.1: Classification of turbulence models.

Classical models	based on (time-averaged) Reynolds equations
	1. zero-equation model–mixing length model
	2. two–equation model– k-ε model
	3. Reynolds stress equation model
	4. algebraic stress model
Large eddy simulation	based on space-filtered equations

The criteria for the choice of a turbulence model include economy of computations, degree of universality and accuracy. As shown in Table 3.1, turbulence models can conveniently be classified according to the number of additional differential equations which they contain.

Zero–equation model

Zero-equation models use only partial differential equations for the mean fields and no differential equation for the turbulence quantities.The models in this group relate the turbulent shear stress uniquely to the mean-flow conditions at each point and require only algebraic expressions. The zero-equation model employs the mixing length hypothesis (Prandtl 1975) in which the length scale is specified by a 'mixing length, l_m'; the velocity scale is of the form

($l_m \partial U_i/\partial x_j$); and the velocity gradient ($\partial U_i/\partial x_j$) is calculated from the local mean flow conditions. The mixing length hypothesis implies that generation and dissipation of turbulence energy are in balance everywhere, so the convection and diffusion of turbulence energy are ignored. Rather than solving the k- ε equations to determine μ_t, zero-equation models use a fixed value for the eddy-viscosity or relate it to the mean-velocity distribution. This substantially reduces computational requirements compared with the k-ε model and other approaches. Like the k-ε model, the zero-equation turbulence model characterises the turbulent diffusion of heat and momentum with an eddy viscosity. Chen and Xu et al (1980) presented a zero-equation model specifically developed for modelling air flow and heat transfer in buildings. They relate the local eddy-viscosity to the local mean velocity and a length scale, through the expression

$$\mu_t = 0.03874 \, \rho v \, l . \tag{3.56}$$

The length scale (l) varies from solution-point to solution point and equals the distance to the nearest solid surface (Xu 1998). Although the constant 0.03874 has a semi-empirical basis it is treated as universal for zone air flows.

One–equation model

In one-equation models, the turbulent viscosity is related to the kinetic energy of turbulence and a length scale (l) by the expression

$$\mu_t = C_\mu \rho k^{\frac{1}{2}} l \tag{3.57}$$

where C_μ is an empirical coefficient, which is assigned a value of 0.5478 (Malin and Qin 1985) in accordance with experimental data. One-equation models require the input of a length-scale distribution based on experimental information and experience. Due to lack of data on the flow

distribution pattern, two or even more equation models are more popular.

Two-equation model

Two-equation models are the simplest available means of calculating turbulent stresses in recirculating or separated flow where the length scale distribution cannot be prescribed algebraically. The turbulence effects are accounted for by use of the k-ε model, which requires the solution of two differential equations for the kinetic energy of turbulence, k, and the dissipatiion of turbulent kinetic energy, ε. The variables are related by the equation (Launder and Spalding 1974)

$$\varepsilon = C_D \, k^{3/2} / l \qquad (3.58)$$

where the constant C_D is assigned a value of 0.1643.

Standard k-ε model

Launder and Spalding (1974) proposed a modified version of the k-ε model. The eddy viscosity, μ_t, at each point is related to local values of the turbulence kinetic energy, k, and the dissipation rate of turbulence energy, ε:

$$\mu_t = C_\mu \rho k^2 / \varepsilon \qquad (3.59)$$

where C_μ is an empirical constant and ρ the fluid density. The turbulent kinetic energy, k, is determined from the following velocities: $k = \frac{1}{2} \left(\overline{u'^2} + \overline{v'^2} + \overline{w'^2} \right)$.

The local distributions of k and ε require the solution of two additional transport equations, which are defined from the Navier-Stokes equations. The k-ε transport equations have the same general structure as the momentum and energy equations. They comprise transient, convection, diffusion, and source terms. In the k and ε equations, Prandtl numbers, σ_k and σ_ε connect the diffusivities of k and ε to the eddy viscosity, μ_t.

The **k–transport equation** is given by

$$\frac{\partial}{\partial t}(\rho k) + \frac{\partial}{\partial x}(\rho u k) + \frac{\partial}{\partial y}(\rho v k) + \frac{\partial}{\partial z}(\rho w k) = \frac{\partial}{\partial x}\left[\frac{\mu_t}{\sigma_k}\frac{\partial k}{\partial x}\right] + \frac{\partial}{\partial y}\left\{\frac{\mu_t}{\sigma_k}\frac{\partial k}{\partial y}\right\} + \frac{\partial}{\partial z}\left\{\frac{\mu_t}{\sigma_k}\frac{\partial k}{\partial z}\right\}$$

$$+ \mu_t\left\{\frac{\partial u}{\partial x} + \frac{\partial u}{\partial x}\right\}\frac{\partial u}{\partial x} + \mu_t\left\{\frac{\partial v}{\partial y} + \frac{\partial v}{\partial y}\right\}\frac{\partial v}{\partial y}$$

$$+ \mu_t\left\{\frac{\partial w}{\partial z} + \frac{\partial w}{\partial z}\right\}\frac{\partial w}{\partial z} - \rho\varepsilon - g\beta\frac{\mu_t}{\sigma_t}\frac{\partial T}{\partial z} \qquad (3.60)$$

where σ_k is an empirical constant and μ_t the eddy viscosity. Similarly, the

ε-transport equation is given by

$$\frac{\partial}{\partial t}(\rho\varepsilon) + \frac{\partial}{\partial x}(\rho u \varepsilon) + \frac{\partial}{\partial y}(\rho v \varepsilon) + \frac{\partial}{\partial z}(\rho w \varepsilon) = \frac{\partial}{\partial x}\left\{\frac{\mu_t}{\sigma_\varepsilon}\frac{\partial\varepsilon}{\partial x}\right\} + \frac{\partial}{\partial y}\left\{\frac{\mu_t}{\sigma_\varepsilon}\frac{\partial\varepsilon}{\partial y}\right\}$$

$$+ \frac{\partial}{\partial z}\left\{\frac{\mu_t}{\sigma_\varepsilon}\frac{\partial\varepsilon}{\partial z}\right\} + \frac{C_1\varepsilon\mu_t}{k}\left\{\frac{\partial u}{\partial x} + \frac{\partial u}{\partial x}\right\}\frac{\partial u}{\partial x}$$

$$+ \frac{C_1\varepsilon\mu_t}{k}\left\{\frac{\partial v}{\partial y} + \frac{\partial v}{\partial y}\right\}\frac{\partial v}{\partial y} + \frac{C_1\varepsilon\mu_t}{k}\left\{\frac{\partial w}{\partial z} + \frac{\partial w}{\partial z}\right\}\frac{\partial w}{\partial z}$$

$$- \frac{C_2\rho\varepsilon^2}{k} - \frac{C_1\varepsilon g\beta\mu_t}{k}\frac{\partial T}{\sigma_t\partial z} . \qquad (3.61)$$

The last terms in equations (3.60) and (3.61) represent the production of turbulence energy by

buoyancy as given by Rodi et al (1980). Empiricism is introduced into the model through the

five constants C_μ, σ_k, σ_ε, C_1 and C_2. Launder and Spalding (1974) recommended values for

these constants, as obtained from data-fitting for a wide range of turbulent flows:

$$C_\mu = 0.09; \quad \sigma_k = 1.00; \quad \sigma_\varepsilon = 1.30; \quad C_1 = 1.44; \quad C_2 = 1.92.$$

Production and destruction of turbulent kinetic energy are always closely linked. The factor ε/k

in the reproduction and destruction terms makes these terms dimensionally correct in the ε-

equation. When the discretisation, linearisation and boundary condition techniques described

earlier are applied, further reduction yields the algebraic form of equation 3.6. This implies that

the k and ε equations can be solved in the same manner as the other governing equations. The

solution process illustrated in Figure (C1.1) of Appendix C remains unaltered, except by the

addition of the k and ε equations. These are solved just before or after the energy equation in the sequential process. Following each iteration the local values of μ_t are calculated with equation (3.59), using the k and ε solutions. The eddy viscosity, μ_t, is then used to update the diffusion coefficients in the momentum and energy equations for the next iteration.

Boundary conditions for the k-ε model

The k-ε model calls for further consideration of boundary conditions and near-wall treatments especially in flows with low Reynolds number. The model equation for k and ε are elliptic by virtue of the gradient diffusion term. Their behaviour is similar to other elliptic flow equations and thus gives rise to the need for the following boundary conditions:

- inlet - distributions of k and ε must be given;

- outlet or symmetry axis - $\partial k/\partial n = 0$ and $\partial \varepsilon / \partial n = 0$;

- free stream - k = 0 and ε = 0; and

- solid walls - approach depends on Reynolds number.

Limitations of the k-ε model

The main weakness of the k-ε model is its inability to model near-laminar flows, due to the fact that it was originally developed for the analysis of fully turbulent isothermal flow. To improve upon its capabilities, the traditional k-ε model is extended through an appropriate wall treatment approach to analyse low-Reynolds number flows. Inclusion of buoyancy source terms in both equations is necessary to facilitate the surface conflation of the construction moisture and the zone air humidity.

Large eddy simulations (LES) are turbulence models where the time-dependent flow equations are solved for the mean flow and the largest eddies and also where the effects of the

smaller eddies are modelled. Wall boundary conditions as they relate to CFD applicaions and some near-wall treatments are presented in the next sub-section.

3.3.1 Near-wall treatments

Wall boundary conditions

The wall is the most common boundary encountered in confined fluid flow problems. Fluid flow near a solid wall parallel to the x-direction as well as the characteristics of turbulent flow near such structures is considered. Owing to the presence of the solid boundary, the flow behaviour and turbulence structure are considerably different from free turbulent flows. For example, if a Reynolds number is formed based on a distance y away from the wall ($Re_y = Uy/v$), it is noted that if the value of y is on the order of L, then the inertia forces dominate in the flow far away from the wall. As y is decreased to zero, however, a Reynolds number based on y also decreases to zero. Just before y reaches zero, there are values of y for which Re_y is on the order of 1. At this distance from the wall and closer, the viscous forces will be equal in order of magnitude to the inertia forces or layer. Thus, in flows along solid boundaries there is usually a region of substantially inertia-dominated flow far away from the wall and a thin layer within which viscous effects are important.

Close to the wall, the flow is influenced by viscous effects. The mean velocity flow depends on the distance y from the wall, fluid density, ρ, viscosity, μ, and the wall shear stress, τ_w.

$$U = f (y, \rho, \mu, \tau_w) \, . \qquad (3.62)$$

Dimensional analysis shows that

$$u^+ = \frac{U}{u_\tau} = f \left\{ (\rho u_\tau y)/\mu \right\} = f (y^+) \, . \qquad (3.63)$$

Equation 3.63 is the *law of the wall* (Malalasekera et al 1995) and contains the definitions of two important dimensionless groups u^+ and y^+. The appropriate velocity scale, u_τ, which represents the friction velocity, is given as $u_\tau = (\tau_w/\rho)$.

Far away from the wall the velocity at a point is expected to be influenced by the retarding effect of the wall through the value of the wall shear stress, but not by the viscosity itself. The length scale appropriate to this region is the boundary layer thickness, δ. In this region

$$U = g(y, \delta, \rho, \tau_w). \tag{3.64}$$

Dimensional analysis yields

$$u^+ = \frac{U}{u_\tau} = g(y/\delta). \tag{3.65}$$

The most useful form of expression (3.65) emerges if the wall shear stress is viewed as the cause of a velocity deficit, $U_{max} - U$, which decreases the closer the edge of the boundary layer is approached. Thus,

$$\frac{U_{max} - U}{u_\tau} = g(y/\delta) . \tag{3.66}$$

Equation 3.66 is the *velocity-defect law*. The next sub-section presents a discussion on the velocity distribution near a solid wall within the framework of near wall treatments.

Figure 3.15 illustrates the velocity distribution near a solid wall in relation to the regions and zones associated with the near wall flow phenomenon. It also shows the applicable corresponding zones and regions and their related laws, namely, the linear sub layer, the buffer layer and the log-law layer within the inner region and the law of the wake within the outer region. This description highlights the significance of the resolution enhacement of the internal fabric surfaces which is vital for a successful handshaking of the CFD and HAM models.

The turbulent boundary layer adjacent to a solid surface is composed of two regions as shown in Figure 3.15 (Malalasekera et al 1995):

- The *inner region*: within 10% to 20% of the total thickness of the wall layer, the shear stress is (almost) constant and equal to the wall shear stress τ_w. Within this region there are three zones, in order of increasing distance from the wall: the *linear sub-layer*, where the viscous stresses dominate the flow adjacent to the surface; the *buffer sub-layer*, where viscous turbulent stresses are of similar magnitudes; and the *log-law layer*, where turbulent (Reynolds) stresses dominate.

- The *outer region* or law-of-the-wake layer: inertia–dominated core flow from the wall; free from direct viscous effects.

Linear sub-layer

Here the fluid layer is in contact with a smooth wall. At the solid surface the fluid is stationary. Turbulent eddying motions also stop very close to the wall. In the absence of turbulent (Reynolds) shear stress effects the fluid closest to the wall is dominated by viscous shear. This layer is in practice extremely thin. For a near-wall flow, for example, this implies that, the dimensionless distance between the wall and the next-to-wall grid point is far less than the critical value for a laminar flow. It is assumed that the shear stress is approximately constant and equal to the wall shear stress, τ_w, throughout the layer. That is

$$\tau(y) = \mu \frac{\partial U}{\partial y} \cong \tau_w .$$

After integration with respect to y and the application of the boundary condition, U = 0 if y =0. a linear relationship between the mean velocity and the distance from the wall is obtained.

$$U = \tau_w y/\mu$$
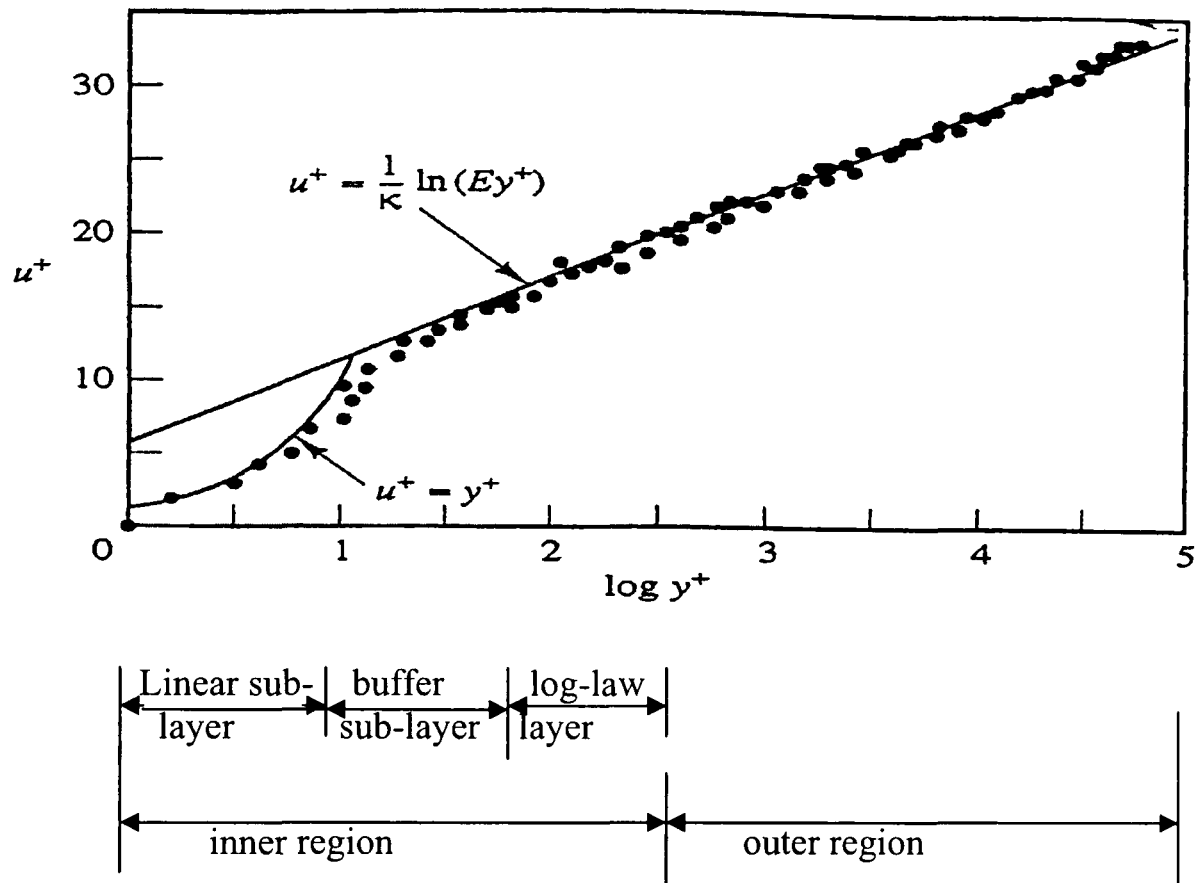
Figure 3.15: Velocity distribution near a solid wall (Malalasekera 1995).

After some algebraic simplifications and use of the definitions of u^+ and y^+, the following relationship is obtained:

$$u^+ = y^+ \qquad (3.67)$$

The fluid layer adjacent to the wall represents the linear sub-layer. It is so called because of the linear relationship between the velocity and the distance from the wall. As can be observed from Figure 3.16, there exists a linear relation between the thermal boundary layer thickness, δ_t and the temperature gradient, dT/dx, for the flow along the horizontal plate. It illustrates the development of the thermal boundary thickness δ_t for a flow in the x-direction parallel to a flat plate.
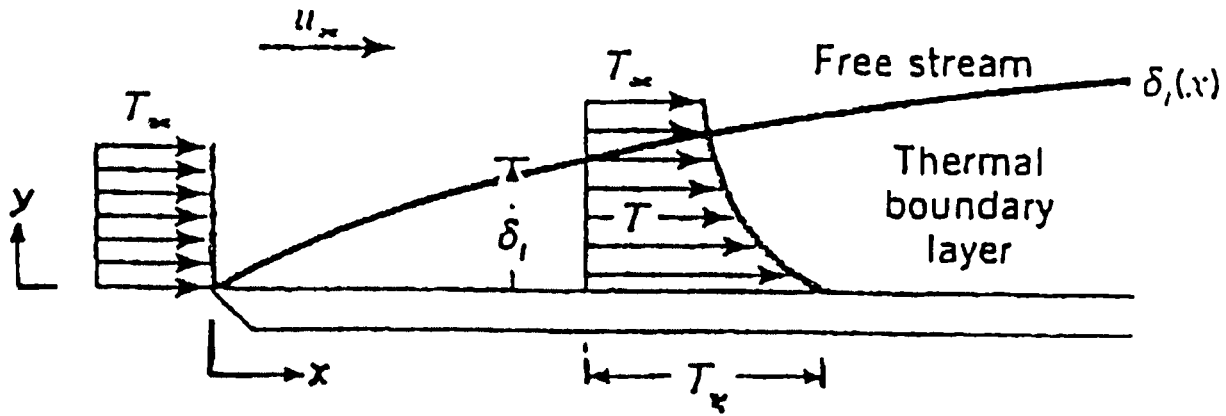
Figure 3.16: Thermal boundary layer development on an isothermal flat plate
(Incropera and DeWitt 2002).

Log-law layer

The log-law layer refers to a fluid flow in a turbulent region close to a smooth wall. Outside the

viscous sub-layer ($30 < y^+ < 500$), a region exists where viscous and turbulent effects are both

important. The shear stress, τ, varies slowly with the distance from the wall and within this

inner region it is assumed to be constant and equal to the wall shear stress. One further

assumption regarding the length scale of turbulence (mixing length, $l_m = \kappa y$) allows the

derivation of a dimensionally correct form of the functional relationship between u^+ and y^+

(Schlictung 1979):

$$u^+ = \frac{1}{\kappa}\ln y^+ + B = \frac{1}{\kappa}\ln(Ey^+) \qquad (3.68)$$

where κ is the von Karman's constant and E and B are constants. Numerical values for the

constants are found from measurements (Schlictung et al 1979). For smooth walls, $\kappa = 0.4$ and

$B = 5.5$ (or $E = 9.8$); wall roughness causes a decrease in the value of B. Due to the logarithmic

relationship between between u^+ and y^+, equation 3.68 is often referred to as the log-law and

the layer, where y^+ takes values between 30 and 500 the log-law layer. It is to be noted that y+

is a dimensionless distance between the wall and the next-to-wall grid point.

70

Outer layer

The *outer layer* refers to the inertia-dominated region far from the wall. Experimental measurements, as given by Schlictung et al (1979), show that the log-law is valid in the region $0.02 < y/\delta < 0.2$. For larger values of y, the velocity law equation provides the correct form of the expression required. In the overlap region, the log-law and the velocity-defect law have to become equal (Malalasekera 1995). Tennekes and Lunley 1972 show that a matched overlap is obtained by assuming the following logarithmic form:

$$\frac{U_{max} - U}{u_\tau} = \frac{1}{\kappa} \ln (y/\delta) + A \qquad (3.69)$$

where A is a constant and δ the layer thickness in relation to distance, y. Equation 3.69 is the *law of the wake*. Figure 3.15 shows the close agreement between theoretical equations (3.67) and (3.68) in their respective areas of validity and experimental data.

Similarly, for a flow over a surface, there exists a velocity layer and hence the existence of a surface friction. For a thermal boundary layer, however, convection heat transfer exist only if the surface and the free stream temperatures differ. Figure 3.16 shows the development of the thermal boundary layer on an isothermal flat plate. With increasing distance from the leading edge, the effects of heat transfer penetrate further into the free stream and the thermal boundary layer grows. Subsequently, the magnitude of the temperature gradient, $\partial T/\partial y \,|_{y=0}$, decreases with increasing x, and therefore heat flux, q_s'' and the heat transfer coefficient, h_c decreases with increasing x.

Comparison of 'wall function' and 'near-wall' modelling approach

A common approach to the treatment of near-wall regions as proposed by Launder and Spalding (1974) is to use the wall function method in a rearranged form. With this approach, no

attempt is made to compute the flow within the laminar and semi-laminar regions of the boundary layer where molecular diffusion is significant. Instead, the next-to-wall grid points are replaced in the fully-turbulent region, where laminar diffusion is overwhelmed by turbulent effects. A brief comparison of the two approaches for modelling the near-wall region, namely, the 'wall function' approach and the 'near-wall' modelling approach is made in this section to highlight the basic structure of each type as well as their merits and demerits.

With the *wall-function approach*, the viscosity-affected, inner region (viscous sub-layer) and buffer layer is not resolved (Figure 3.18(a)). Instead, semi-empirical formulae (wall-functions) are used to bridge the viscosity affected region between the wall and the fully turbulent region. In essence the wall-function method assumes the form of the velocity and temperature profiles within the boundary layer. In most turbulent, the wall function approach saves computational resources because the viscosity-affected near-wall region does not need to be resolved. It is economical, robust and reasonably accurate, and hence popular. The wall-function approach however, is inadequate in situations where the low Reynolds Number effects are pervasive in the flow domain, for example in buildings (weakly turbulent) and the hypothesis underlying the wall functions cease to be valid in the viscosity-affected area.

Launder and Spalding's wall functions are often referred to as the log-law wall functions because these functions originate from the logarithmic velocity profile for forced flow. The re-arraged form of Launder and Spalding's wall functions (Malalasekera 1995) are given as

$$\tau_{wall} = \frac{C_\mu^{1/4} \, k_P \rho u_P}{\left\{ \ln \left(E\rho\Delta x_P \, C_\mu 1/4 \, k_P^{1/2} \right)/ \mu \right\} 1/\kappa} \tag{3.70}$$

and

$$q'_{wall} = \cfrac{C_\mu^{1/4} \, k_P \rho C_p \, (T_P - T_{wall})}{\sigma_t \left[\cfrac{1}{\kappa} \ln\left\{ \cfrac{E\rho\Delta x_P C_\mu^{1/4} k_P^{1/2}}{\mu} \right\} + \left\{ \cfrac{\pi/4}{\sin \pi/4} \right\} \left[\cfrac{A}{k} \right]^{1/2} \left\{ \cfrac{Pr}{\sigma_t} - 1 \right\} \left\{ \cfrac{\sigma_t}{Pr} \right\}^{1/4} \right]} \qquad (3.71)$$

where the subscript P indicates the values at the next-to–wall grid points, Δx_P the distance from

the wall to the next-to-wall grid point (Figure 3.17), σ_t the turbulent kinetic energy, Pr the

Prandtl number, κ the von Karman's constant and A and E constants representing wall

roughness.
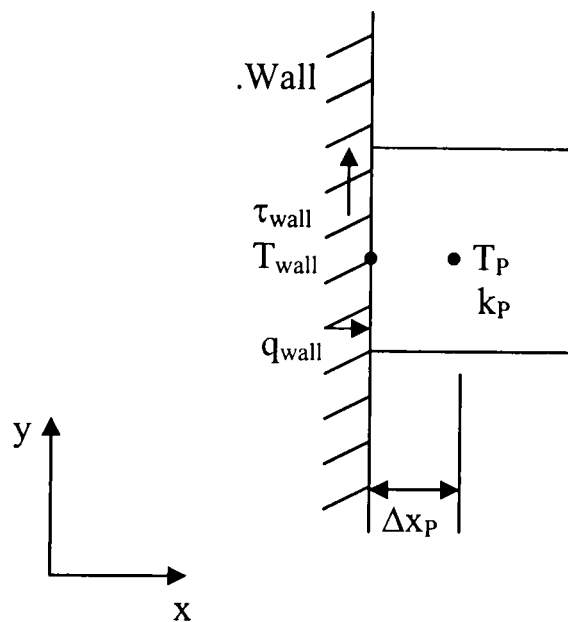
Figure 3.17: Wall functions.

The boundary condition coefficients must be updated at each solution iteration as the k solution

field evolves, since the turbulence kinetic energy of the next-to-wall grid points appears in the

wall functions. In essence the wall function approach assumes the form of the velocity and

temperature profiles within the boundary layer. The thermal wall function (Eq. 3.71) is used to

impose the influence of a wall's temperature on the room, and so predict the heat transfer from

the room air to the wall surface. It is apparent that if the wall functions approximate the profile

73

between the wall and the first grid point, it will result in errors in the wall shear and surface convection.

To resolve problems with surface convection predictions (over- and under prediction), Yuan et al (1994) developed a set of wall functions specifically for the case of natural convection along vertical surfaces in rooms. Yuan (1994) also showed that the logarithmic profile poorly approximated the velocities in the boundary layer for buoyancy-driven flows. Yuan further demonstrated the sensitivity of surface-convection prediction to the placement of the next-to-wall grid points. A functional form for the wall functions based on a dimensional analysis of the governing equations was eventually postulated. Consequently, the conclusion was drawn that the log-law model is not appropriate for natural convection flows (within indoor spaces).

Chen et al (1990) concluded from their observations that the log-law wall functions could result in significant errors in the prediction of surface convection for natural and mixed convection flows. The results obtained from such approach were found to be sensitive to the location of the next-to-wall grid points.

Niu and van der Kooi (1992) concluded from the comparison of numerical predictions to experimental results for buoyancy-driven flow within a building enclosure that, while the wall functions overpredicted the surface convection when the next-to-wall grid points were too close to the wall, underprediction of the surface convection resulted when they were placed too far away from the wall.

These observations illustrate the deficiences of the standard k-ε model with log-law wall functions in treating surface convection in room air flows. The log-law model, which has its

validity for the region $30 < y^+ < 500$ (Malalasekera 1995), is not relevant to air flow simulation of indoor spaces (weakly turbulent). This is because the log-law wall functions poorly characterise the boundary layer of many room air flows and also because in conjunction with the k-ε turbulence model it poorly predicts the turbulent diffusion in weakly turbulent regions.

An alternative approach to address the deficiences associated with the application of the log-law wall function and the k- ε model for room air flow simulation is through the near-wall modelling technique. For example, the low Reynolds Number k-ε model with embedded damping functions as provided by Lam and Bremhorst (1981) offers an acceptable solution with lesser stability problems. Similarly, within the configuration mechanism (Chapter 5) for the conflation of HAM and CFD models, a rules-based moisture control algorithm, whose controller has the capabilities to examine and appraise the prevailing flow conditions at the interface and subseq uently effects any remedial action required.

With the *near-wall approach*, the viscosity-affected region is resolved with a mesh all the way to the wall, including the viscous sub-layer as shown in Figure 3.18(b). Figure 3.18(a) illustrates the wall-function approach, which has its applicability within the turbulent core. These two approaches are shown schematically in Figure 3.18 (FLUENT User's Guide Volume 4.4, 1997). Other alternative near-wall treatments with the k- ε turbulence model as developed by Launder and Spalding (1974) Lam and Bremhorst (1981) as well as the two-layer model developed by Chen (1995) and Xu (1998) are presented in the next sub-section.

(a) Wall function approach   **(b) Near-wall model approach**
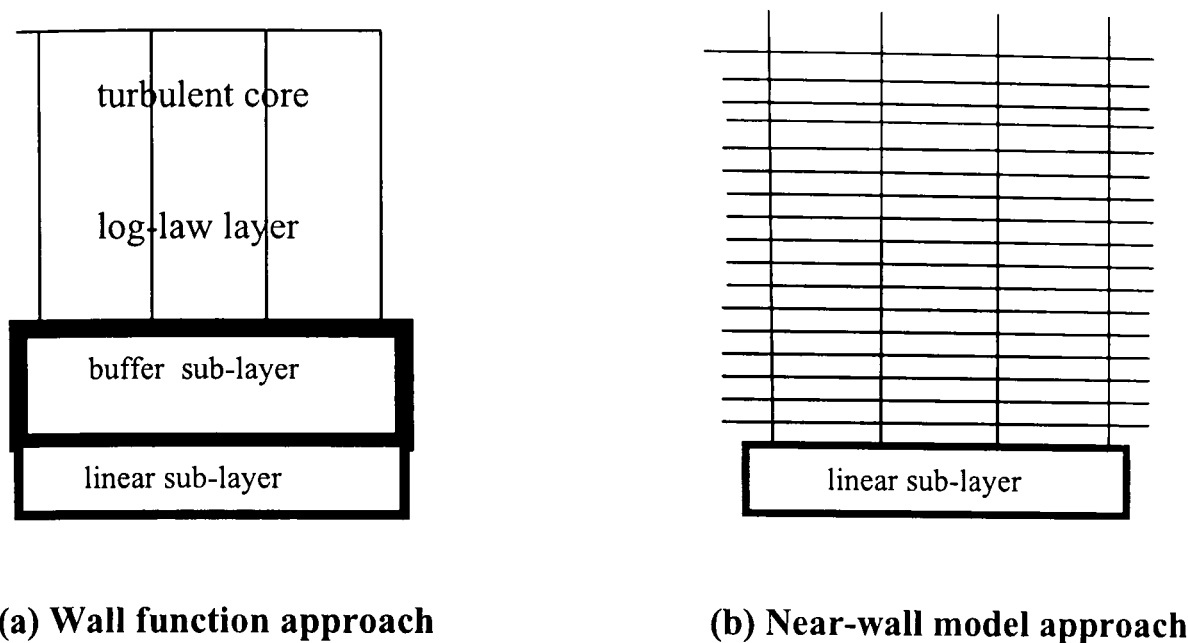
Figure 3.18: Near–wall treatments.

Low – Reynolds number modelling with k-ε model

Launder and Spalding (1974) describe the *low-Reynolds modelling method* as an alternative

approach for treating the near-wall regions with the k-ε model. In contrast to the wall-function

approach, grid points are placed within the boundary layer, including the laminar region. This

requires adjustments to the k and ε equations. In this regard, two of the empirical constants,

namely, C_μ and C_2 (Eqs. 3.59 and 3.61) are made to vary with the local turbulence Reynolds

number. Since the solution points are located within the laminar region of the boundary layer,

the wall shear and the thermal boundary conditions can be treated with the relations in Eqs.

3.10 –3.13. Unlike the wall-function method, the low Reynolds Number approach does not

assume the velocity and temperature profiles across the boundary layer. The computational

requirements with this approach is comparably higher due to the additional grid points required

in the boundary layer. Modifications to the k- ε model to enable it to cope with low Reynolds

Nimber flows are reviewed in Patel et al (1985). Wall damping functions are applied to ensure

that the viscous stresses take over from turbulent Reynolds stresses at low Reynolds numbers

and in the viscous sub-layer adjacent to solid walls. These functions contribute to stability improvement in the numerical solution. The equations of the low-Reynolds Number k-ε model (Malalasekera et al 1995) are

$$\mu_t = \rho C_\mu f_\mu \, k^2 / \varepsilon \qquad (3.72)$$

$$\frac{\partial(\rho k)}{\partial t} + \mathrm{div}(\rho k U) = \mathrm{div}\left[\left(\mu + \frac{\mu_t}{\sigma_k}\right)\mathrm{grad}\,k\right] + 2\mu_t E_{ij}.\,E_{ij} - \rho\varepsilon \qquad (3.73)$$

$$\frac{\partial}{\partial t}(\rho\varepsilon) + \mathrm{div}\,(\rho\varepsilon U) = \mathrm{div}\left[\left(\mu + \frac{\mu_t}{\sigma_\varepsilon}\right)\mathrm{grad}\,\varepsilon\right] + C_1 f_1 \frac{\varepsilon}{k} 2\mu_t E_{ij}.E_{ij} - C_2 f_2 \rho \frac{\varepsilon^2}{k} \qquad (3.74)$$

where f_μ, f_1 and f_2 are the wall damping functions given by equation 3.75. The most logical modification, is to include a viscous combination in the diffusion terms in (Eqs.3.72 – 3.74). In this regard the constants C_μ , C_1 and C_2 in the standard k-ε model are multiplied by wall-damping functions of the turbulence Reynolds number and /or similar parameters. Lam and Bremhorst (1981) put forward another low Reynolds-Number k-ε model. Rather than introduce new destruction terms to the k and ε equations, new formulations were added to make three of the constants (C1, C_2 and C_μ) vary with the local turbulence number. Lam and Bremhorst give the following wall-damping functions:

$$f_\mu = \left[1 - \exp(-0.0156 Re_y)\right]^2 \left\{1 + \frac{20.5}{Re_t}\right\}; \qquad (3.75)$$

$$f_1 = \left\{1 + \frac{0.05}{f_\mu}\right\}^3 ; \quad f_2 = 1 - \exp(-Re^2_t).$$

In function f_μ, the parameter Re_y is the local Reynolds number and is defined by $k^{1/2}/\nu$, where y is the co-ordinate direction normal to a solid wall and ν the kinematic viscosity. The turbulence Reynolds number, Re_t is defined as $Re_t = \vartheta l/\nu = k^2/(\varepsilon\nu)$, where the velocity scale, ϑ and length scale, l representative of the large scale turbulence can be expressed as follows

$$\vartheta = k^{1/2} , \quad l = k^{3/2}/l$$

Lam and Bremhorst use $\partial\varepsilon/\partial y = 0$ as a boundary condition.

Surface roughness can have a profound effect on heat transfer to surfaces beneath turbulent flow. The viscous sublayer adjacent to a smooth wall presents a high impedance to fluid transport to and from the surface. Protrusions that penetrate the viscous layer increase transfer rates between the surface and the fluid. They do so by generating irregular, turbulent motion and by extending into the flow (Durbin et al 2001). However, for indoor spaces, being a weakly turbulent case, these impedance to heat and mass transfer at the surfaces can be equally handled through application of the wall damping functions as developed by Lam and Bremhorst.

The two-layer model

The two-layer model (Chen 1995) is an alternate formulation of the k-ε model. Like the low-Reynolds number model, the two-layer model places the grid points within the laminar and semi-laminar regions of the boundary layer. Unlike the low-Reynolds models, however, the ε-equation is not solved within the near-wall region, but it is replaced by an algebraic equation. This leads to lesser grid points and one lesser differential equation to solve in the boundary layer. The two-layer model is more computational intensive than the standard k-ε model and proved to be less stable.

Xu et al (1998) developed a two-layer modelling approach for buoyancy-driven flows. Within the approach, the standard k-ε model is used in the regions from the walls, whereas the near-wall regions are treated with a one-equation near-wall model. Within the near-wall region only 7-10 grid points are required. The computational requirement is less than that for a low-Reynolds model.

Other alternative near-wall treatments including *'High Reynolds Number modelling with k-ε model'* and their relationship with the k- ε approach (Malalasekera 1995) are given in Appendix D. The next section is a review of the application of CFD to the resolution of indoor air quality. Within this traditional approach, however, moisture flow through the solid walls is not considered as a source term.

3.4 Application of CFD to indoor air quality

When applying CFD to the resolution of indoor air quality problems, for example, water vapour distribution within an indoor space, the transport equation with water vapour as the concentration as well as an equation for the mass fraction are required. This sub-section presents the relevant equations for water vapour, which is required in the resolution of the conflation problem. Consider the case where water vapour is introduced as the contaminant (construction moisture flux) into the interior space, with the intent to study its distribution at a large number of grid points in the three dimensional domain. It is assumed that the contaminant is carried purely by air flows. Consideration of water vapour as the contaminant with a concentration, C_w, yields the general transport equation:

$$\frac{\partial}{\partial t} C_w + (V. \nabla) C_w - \Gamma_{cw} \nabla^2 C_w = S_{cw} \tag{3.76}$$

where C_w is the concentration of water vapour, and Γ_{cw} the diffusion coefficient for water vapour, which is obtained from

$$\Gamma_{cw} = \frac{\mu}{Sc} + \frac{\mu_t}{\sigma_c} \tag{3.77}$$

where Sc is the Schmidt number, σ_c the turbulent Schmidt number and S_{cw} the source term due to vapour flux. The concentration, C_w is given by the product $\rho\phi$, where ϕ is the mass fraction of the water vapour. For buoyancy-driven flows, the Buossinesq approximation, which ignores the effect of pressure changes on density, is usually employed. The buoyancy-driven force is

then treated as a source term in the momentum equation. A turbulence model is usually applied for most indoor air flow problems in order to make the flow soluble using present computational capacity. The accuracy of CFD predictions is highly sensitive to the boundary conditions and the grid set-up. Normally, the boundary conditions for the CFD simulation of indoor air flow comprise the inlet (supply) and outlet (exhaust) characteristics, enclosure surfaces characteristics and internal objects representing furnishings. The temperature, velocity and turbulence of the air entering through diffusers or windows determine the inlet conditions, while the interior surface temperatures, vapour pressure and moisture or humidity fluxes are the essential boundary conditions for the enclosures.

Transport equation for the water vapour

The transport equation for the water vapour describes the manner in which an amount of water vapour in a particular parcel of air changes as a result of advectiom and condensation/ evaporation. For water vapour with vapour pressure, p_w, the specific transport equation is obtained from the general transport equation (Eq.3.76) given by

$$\frac{\partial}{\partial t}(\rho p_w) + \frac{\partial}{\partial x}\left[\rho u p_w - \left\{\frac{\mu}{Sc} + \frac{\mu_t}{\sigma_{pw}}\right\}\frac{\partial p_w}{\partial x}\right] + \frac{\partial}{\partial y}\left[\rho v p_w - \left\{\frac{\mu}{Sc} + \frac{\mu_t}{\sigma_{pw}}\right\}\frac{\partial p_w}{\partial y}\right]$$

$$+ \frac{\partial}{\partial z}\left[\rho w p_w - \left\{\frac{\mu}{Sc} + \frac{\mu_t}{\sigma_{pw}}\right\}\frac{\partial p_w}{\partial z}\right] = S_{pw} \tag{3.78}$$

where (ρp_w) is the concentration, C_w (in Eq.3.76), p_w the water vapour pressure (the variable of interest), μ and μ_t are the physical and the turbulent dynamic viscosities, Sc the Schmidt Number $= v/D$, where D is the diffusion coefficient of water vapour in air, and $\sigma_{pw} = 0.9$ is the turbulent Schmidt number; S_{pw} is the source term.

Equation for the mass fraction

The equation for the mass fraction is obtained through the thermodynamic relationship between the mass concentration and the partial pressure of water vapour,

$$p_w = p_m \cdot g_w\left\{\frac{R_w}{R_m}\right\} = p_m\left\{\frac{m_w}{m_w + m_L}\right\}\frac{R_w}{R_m} = p_m\left\{\frac{m_w}{m_w + m_L}\right\}\frac{R_w}{\left\{\frac{m_w}{m_w + m_L}\right\}R_w + \left\{\frac{m_L}{m_w + m_L}\right\}R_L}$$

$$= p_m\frac{m_w}{m_L}\cdot\frac{m_L}{m_L}\left\{\frac{R_w}{m_w R_w + m_L R_L}\right\} = \frac{p_m x}{\left[\left\{\frac{m_w R_w}{m_L R_w}\right\} + \left\{\frac{m_L R_L}{m_L R_w}\right\}\right]}$$

$$= \frac{p_m x}{\left\{x + \frac{R_L}{R_W}\right\}} = \frac{p_m x}{\left\{x + \frac{M_W}{M_L}\right\}} = \frac{p_m x}{(x + 0.622)} \tag{3.79}$$

are defined as follows: L is dry air, m is mixture and W is water vapour. The following data for the thermodynamic properties are relevant: $R_W = 461$ J/kgK, $R_L = 287.10$ J/kgK, $M_W = 18.02$ kg/kmol and $M_L = 28.96$ kg/kmol as given by Rogers and Mayhew (1995). Thus,

$$x = 0.622\left\{\frac{p_w}{p_L}\right\}; \quad p_w = p\left\{\frac{x}{(0.622 + x)}\right\}; \quad p_L = p\left\{\frac{0.622}{0.622 + x}\right\} \tag{3.80}$$

Also, the total pressure, p_T, is given by

$$P_T = p_L + p_w \tag{3.81}$$

where the partial pressure of dry air, p_L, is found from $p_L V = m_L R_L T$ and the partial pressure of water vapour p_w, is found from $p_w V = m_w R_w T$. The relative humidity, $\phi = p_w / p_s(t)$ and $p_s(t)$ is the saturated vapour pressure. These properties are required for the determination of the water vapour distribution within the computational domain. The next sub-section is a presentation on construction moisture as a source term contributor.

Construction moisture as a source term contributor

The situation with construction moisture combining with the air humidity within the enclosure calls for a different approach with regards to the imposition of the boundary conditions at solid

boundaries or near wall regions. Similarly, the assumption of zero-vapour gradient in this case is applicable at the outlet whilst a constant gradient or fixed flow rate (water vapour flux, $g_{constr.}$ = const.) is assumed for the inlet boundary condition. For the case of free convection , a suitable mass transfer coefficient correlation is prescribed and a Neumann boundary condition is imposed to replace the log-law wall functions (Beausoleil-Morrison 2000). For the resolution of the pivot–point, the following assumptions are relevant:

- both external and internal wall surfaces exchange mass with the ambient atmosphere by

surface convection occurs at the air–side and by molecular diffusion at the material-sid

For moisture to occur at the inside surface of the wall, the inside surface temperature, T_{is} must be greater than the dew-point temperature, T_{dp} of the air at that point; that is, $T_{is} \geq T_{dp}$. However, if the inside surface temperature of the wall is below the dew-point temperature, condensation occurs on the internal surface of the solid wall. This situation contributes to a negative source term, hence the assumption that no condensation occurs within the period under consideration. Under such condition (no condensation), the construction moisture flow is considered as a concentration source. This additional source term is added in the right-hand side of the transport equation. The next section considers the similarities and differences between HAM and CFD model. For an effective conflation, it is necessary that the commonalities between both models be established with the view to minimising their respective shortcomings.

3.5 Commonalities between HAM and CFD models

The main commonality between the two models is the fact that both are capable of undertaking transient thermal energy and mass flow simulations. A HAM model, however, considers the air within the zones as homogeneously mixed (Hens et al 1986). Furthermore, because momentum effects are neglected, intra-zone air movement cannot be accurately modelled and as a result of

the low resolution of local surface convection heat and mass transfer. Both HAM and CFD models apply conservation of mass and energy principles to predict temperature, flow rates, humidity, etc. within the components of the building and plant systems. The boundaries of the CFD model coincide with the internal surfaces defined for the HAM model. The HAM model assigns energy balances to the internal surfaces from which the surface temperatures and vapour pressures are determined. Unlike other simulation models, which employ the combination of numerical and analytical methods, both HAM and CFD use the conservative, finite volume method to discretise the differential equations, which yields an equivalent set of algebraic conservation equations. These algebraic equations differ only in the inter-volume interaction coefficients and source terms, which are specific for each system of equations. Both models represent a general structure and were conceived to deal with different geometries, which are subjected to distinct boundary conditions. As mentioned previously, HAM has the potential to predict the hygrothermal performance of the building envelope including uniform air flow properties within the zone. HAM models are usually limited to the computation of the conditions inside the zones at the macro-level, while CFD is capable of modelling gradients of air flow properties within the zones at the micro-level. The CFD boundary conditions are generally unknown, difficult to estimate and most often case-specific. From the above observations, a combination of the two models suggests itself as the way forward to minimise the short fall of each approach. Such a combination eliminates problems with the CFD assignation of the boundary conditions and numerical solution to the set of conservation equations. Figure 3.19 shows a building/plant energy flow schematic for which the conflated approach may be used to assess the air flow property gradients within the zone of interest. It shows an illustration of the indoor environment and the sources that act upon it. These sources originate from thermal processes, e.g. conduction, convection, radiation, advection, etc: air
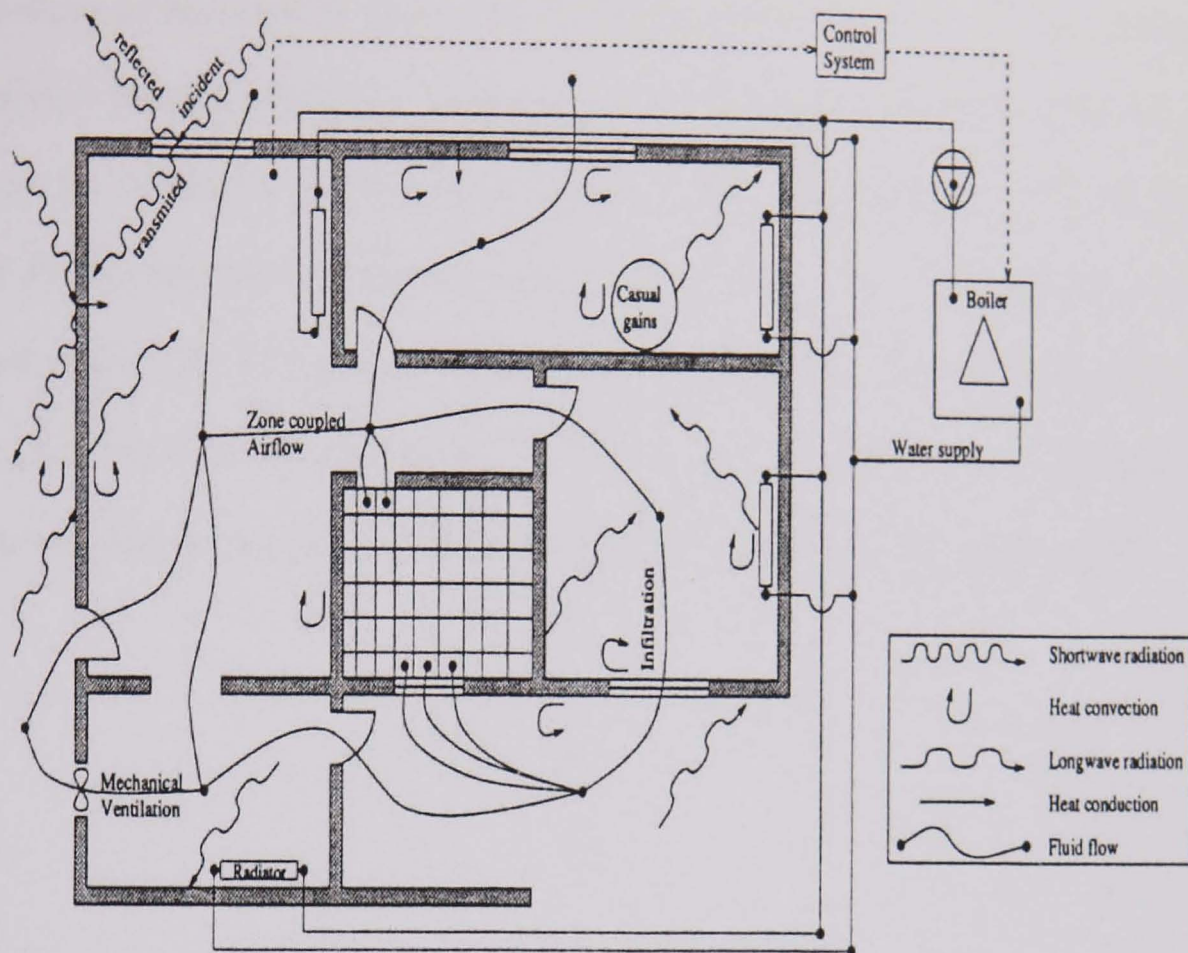
Figure 3.19:Building/plant and mass flow paths (Negrao 1995).

flow-induced process, e.g. through infiltration, mechanical ventilation, HVAC systems, etc;

moisture flow phenomenon, e.g. through moist air infiltration. Occupants activity, mass transfer

plants, vapour diffusion, vapour convection, etc. amongst others (Clarke 1985). It shows the

modelling of indoor air flow through the coupling of the nodes of the zonal network and that of

the CFD model through the zonal air point node of interest (Negrao 1995). Sources of casual

and latent heat gains within the building enclosure as well as the control systems and sensors to

ensure accurate monitoring of the indoor air flow parameters are also illustrated.

In conclusion, this chapter has reviewed the various approaches to indoor air flow modelling

with CFD with highlights on the limitations and capabilities of both HAM and CFD models.

The limitations of the zonal air flow network (ZN) approach to indoor air flow simulation was also discussed. From the findings, it became evident that for the determination of the pertinent parameters for indoor air quality assessment an integrated simulation of both HAM and ZN/CFD models provides a powerful simulation approach. For the resolution of the flow simulation within near-wall region the low-Reynolds Number k-ε model with embedded wall damping functions (Lam and Bremhorst 1985) could provide an acceptable performance results in comparison with the log-law wall function and the standard k-ε turbulence model.

4.1 Convective surface transfers

A review of the boundary layer theory is necessary due to the fact that the conflation of HAM and CFD models can either be effected using the air point node within the indoor space or at the internal surface node between the internal fabric surface and the air domain. The latter is the approach adopted in the present work, and is much dependent on the boundary layer phenomena. The effects of convection heat and mass transfer as a result of flow over a flat plate as well as the resultant boundary layer phenomenon, namely the velocity, thermal and concentration boundary layers are presented. The flow over a flat plate is characterised as being similar to the indoor air flow phenomenon hence the choice of this model as the basis for this review. The physical significance of the dimensional parameters and heat and mass transfer analogies that lead eventually to the establishment of the boundary conditions for energy transfer at material surfaces are also presented. These analogies form the basis for the correlations for the convection mass transfer coefficient presented in section 4.3.1.

Convective transfer problem

The local heat or mass flux and/or the total transfer rate are of paramount importance in the resolution of convective transfer problems. They depend on knowledge of the local and average convection coefficients and it is for this reason that the determination of these coefficients is viewed as the problem of convection. In addition to its dependency on numerous fluid properties such as density, viscosity, thermal conductivity and specific heat, the coefficients depend on the surface geometry and the flow conditions. The multiplicity of independent variables occur because convection transfer is determined by the boundary layers that develop on the surface. The development of the velocity, thermal and concentration boundary layers as

a result of flow over a flat plate is presented in the next sub-section.

4.2 Boundary layer classification

The boundary layer theory as it relates to this project is treated under three main classifications:

velocity, thermal and concentration types.

4.2.1 Velocity boundary layer

Consider a flow over the flat plate of Figure 4.1 (Incropera and DeWitt 2002). Fluid particles in

contact with the surface assume zero velocity. These particles then act to retard the motion of

particles in the adjoining fluid layer, which in turn acts to retard the motion of particles in the

next layer, and so on until at a distance $y = \delta$ from the surface the effect becomes negligible.

This retardation of the fluid motion is associated with shear stresses, τ, acting in planes that are

parallel to the fluid velocity as shown in Figure 4.1.The boundary layer velocity profile refers

to the manner in which velocity, u varies with distance, y through the boundary layer.
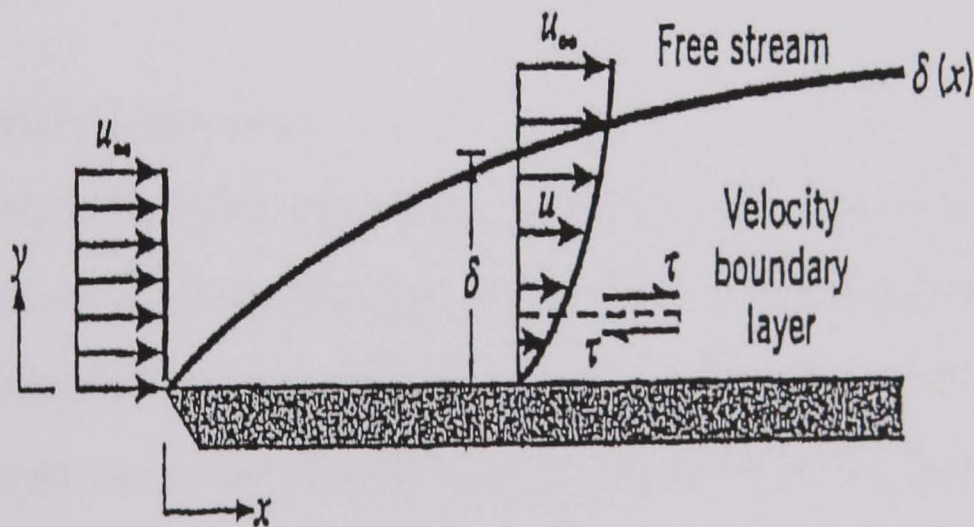
Figure 4.1: Velocity boundary layer development on a flat plate.

Accordingly, the flow is characterised by two distinct regions: a thin fluid layer (boundary

layer) in which velocity gradients and shear stresses are large and a region outside the boundary layer in which velocity gradients and shear stresses are negligible. With increasing distance from the leading edge, the effects of viscosity generates further into the free stream and the boundary layer thickness, δ, increases as distance, x, increases. This type is the *velocity boundary layer* which pertains to the fluid velocity. It develops whenever there is a fluid flow over a surface and is of fundamental importance to problems involving convection transport. For external flows, it provides the basis for the determination of the local friction coefficient, C_f

$$C_f \cong \tau_s / (\rho u^2_x / 2) \tag{4.1}$$

where C_f is a key dimensionless parameter from which the surface frictional drag is obtained, u_x, the velocity in the x-direction and τ_s the surface shear stress. For a Newtonian fluid, the surface shear stress is evaluated from the knowledge of the velocity gradient at the surface as given by the expression

$$\tau_s = \mu \left\{ \frac{\partial u}{\partial y} \right\}_{y=0} \tag{4.2}$$

where μ is the dynamic viscosity.

4.2.2 Thermal boundary layer

Just as a velocity boundary layer develops when there is fluid flow over a surface, a thermal boundary layer also develops if the fluid free stream and surface temperatures differ. For a flow over an isothermal flat plate as shown in Figure 4.2 (Incropera and DeWitt 2002), a uniform temperature profile is observed at the leading edge, with $T(y) = T_\infty$. Fluid particles that come into contact with the plate, attain thermal equilibrium at the plate's surface temperature. These particles in turn exchange energy with those in the adjoining fluid layer, and as a result of these

interactions a temperature gradient develops in the fluid. The region of the fluid in which these temperature gradients exists is the thermal boundary layer, and its thickness, δ_t, is typically defined as the value of y for which at the leading edge, the ratio

$$(T_s - T)/(T_s - T_\infty) = 0.99 .$$

(4.3)

With increasing distance from the leading edge, the effects of heat transfer penetrate further into the free stream and the thermal boundary layer grows. Figure 4.2 shows the development of the thermal boundary layer on an isothermal flat plate. At any distance, x, from the leading edge, the local heat flux may be obtained by applying Fourier's law to the fluid at y = 0:

$$q_s'' = -k_f \left\{ \frac{\partial T}{\partial y} \right\} \bigg|_{y=0}$$

(4.4)

where k_f is the thermal conductivity of the fluid. Equation 4.4 highlights the fact that at the surface there is no fluid motion and energy transfer occurs only by conduction.
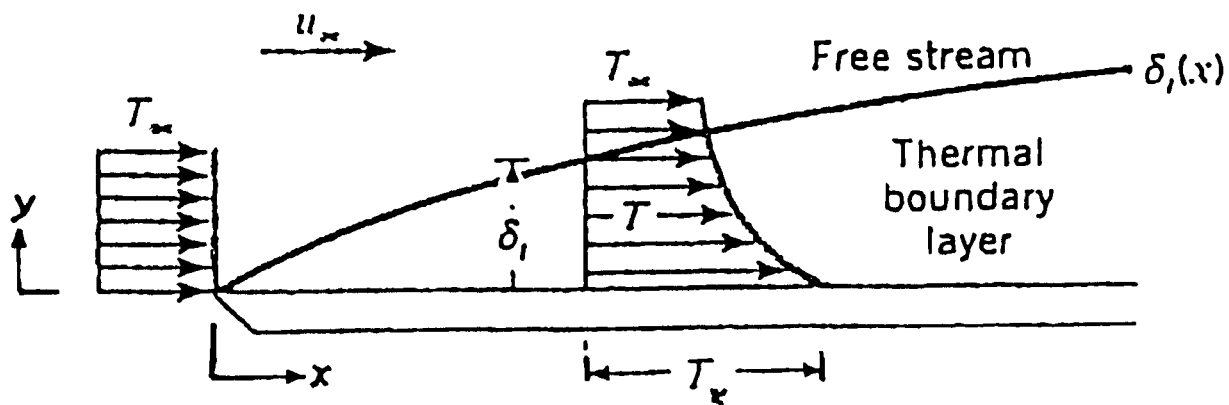
Figure 4.2: Thermal boundary layer development on an isothermal flat plate (Incropera and De Witt 2002).

Conditions in the boundary layer, which strongly influence the wall temperature gradient, $\partial T/\partial y \big|_{y=0}$, also determine the rate of heat transfer across the boundary layer. Accordingly, the

magnitude of $\partial T/\partial y$ |y=0 decreases with increasing x, and it follows that local heat flux, q_s"

decrease with increasing distance, x.

4.2.3 Concentration boundary layer

Just as the velocity and thermal boundary layers determine wall friction and convection heat

transfer, the concentration boundary layer determines convection mass transfer. For example, if

a binary mixture of chemical species A and B flows over a surface and the concentration of

species A at the surface, $C_{A,s}$, differs from that in the free stream, $C_{A,\infty}$, as shown in Figure 4.3,

a *concentration boundary layer* develops. This is the region of the fluid in which a

concentration gradient exists, and the layer thickness, δ_c, is typically defined as the value of y

for which

$$\left\{ (C_{A,s} - C_A)/(C_{A,s} - C_{A,\infty}) \right\} = 0.99. \qquad (4.5)$$

Species transfer by convection between the surface and the free stream fluid is determined by

conditions in this boundary layer. The molar flux associated with species transfer by diffusion

is given by Fick's law as

$$N_A'' = -D_{AB}\left\{ \partial C_A/\partial y \right\} \qquad (4.6)$$

where D_{AB} is the binary diffusion coefficient. Such flow phenomenon, as illustrated in Figure

4.3, is valid for laminar flow, for example, for the flow situation that moisture flow through the

wall is considered as a source term in the consideration of the combination of construction

moisture and indoor humidity

At any point corresponding to y > 0 in the concentration boundary layer of Figure 4.3

(Incropera and DeWitt 2002), species transfer is due to both bulk fluid motion and diffusion. At

y = 0, however, there is no fluid motion and species transfer is by diffusion only.
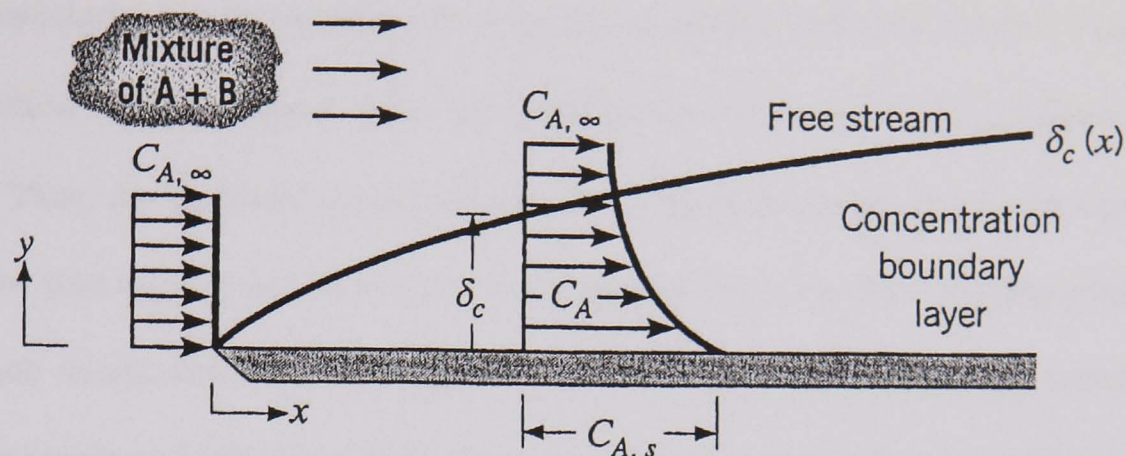
Figure 4.3: Species concentration boundary layer development on a flat plate.

Applying Fick's law at $y = 0$, the species flux at any distance from the leading edge is

$$N_A'' = -D_{AB} \left. \frac{\partial C_A}{\partial y} \right|_{y=0} . \tag{4.7}$$

Combination of equation 4.6 and the expression $N_A'' = h_m(C_{A,S} - C_{A,\infty})$ yields

$$h_m = -\frac{D_{AB} \left. \partial C_A/\partial y \right|_{y=0}}{C_{A,s} - C_{A,}} . \tag{4.8}$$

where h_m is the convective mass transfer coefficient, D_{AB}, the diffusivity of the mixture and C_A, the concentration of species A at the respective locations indicated. Conditions in the concentration boundary layer, which strongly influences the concentration gradient, $\partial C_A/\partial y |_{y=0}$, also influence the convection mass transfer coefficient, and hence the rate of species transfer into the boundary layer.

4.2.4 Transfer equations

In deducing the transfer equations for the different boundary layers a case is presented whereby simultaneous development of the velocity, thermal and concentration boundary layers occur over a surface. The velocity boundary layer is of extent $\delta_v(x)$ and is characterised by the

presence of velocity gradients and shear stresses. The thermal boundary layer is of extent $\delta_t(x)$ and is characterised by the presence of temperature gradients and heat transfer. Finally, the concentration boundary layer, $\delta_c(x)$, is characterised by concentration gradients and species transfer. Thus, the principal manifestations of the three boundary layers are surface friction, convection heat transfer and convection mass transfer. For each of the boundary layers, the appropriate convection transfer equations is presented considering the relevant physical processes involved. In this regard, the mass, momentum and energy conservation laws are applied to the various boundary layers for a two–dimensional flow.

Velocity boundary layer

For a steady two-dimensional flow of an incompressible fluid, the continuity and momentum equations are given by the following expressions.

Continuity Equation:

$$\frac{\partial(\rho u)}{\partial x} - \frac{\partial(\rho v)}{\partial y} = 0. \tag{4.9a}$$

Momentum Equation:

For a two-dimensional case, the expression for the x-direction is

$$\rho \left\{ u\frac{\partial u}{\partial x} + v\frac{\partial u}{\partial y} \right\} = -\frac{\partial p}{\partial x} + \frac{\partial}{\partial x}\left[\mu \left\{ 2\frac{\partial u}{\partial x} - \frac{2}{3}\left(\frac{\partial u}{\partial x} + \frac{\partial v}{\partial y} \right) \right\} \right]$$
$$+ \frac{\partial}{\partial y}\left[\mu \left\{ \frac{\partial u}{\partial y} + \frac{\partial v}{\partial x} \right\} \right] + X. \tag{4.9b}$$

Similarly, the expression for the y-direction is

$$\rho \left\{ u\frac{\partial v}{\partial x} + v\frac{\partial v}{\partial y} \right\} = -\frac{\partial p}{\partial y} + \frac{\partial}{\partial y}\left[\mu \left\{ 2\frac{\partial v}{\partial y} - \frac{2}{3}\left(\frac{\partial u}{\partial x} + \frac{\partial v}{\partial y} \right) \right\} \right]$$
$$+ \frac{\partial}{\partial x}\left[\mu \left\{ \frac{\partial u}{\partial y} + \frac{\partial v}{\partial x} \right\} \right] + Y. \tag{4.9c}$$

X and Y are the body forces in the x- and y-directions. The two terms on the left-hand side of equations 4.9b and 4.9c represent the net rate of momentum flow from a control volume. The terms on the right-hand side account for the net viscous and pressure forces, as well as the body force. These equations are satisfied at each point in the boundary layer, and with the continuity equation 4.9a they may be solved for the velocity field in the boundary layer. Equations 4.9a to 4.9c provide a complete representation of conditions in a two-dimensional velocity boundary layer.

Thermal boundary layer

The corresponding thermal energy equation is given as

$$\rho u \frac{\partial \rho}{\partial x} + \rho v \frac{\partial \rho}{\partial y} = \frac{\partial}{\partial x}\left\{ k \frac{\partial T}{\partial x} \right\} + \frac{\partial}{\partial y}\left\{ k \frac{\partial T}{\partial y} \right\} - \left\{ p \frac{\partial u}{\partial x} + \frac{\partial v}{\partial y} \right\} + \mu \Phi + q \qquad (4.10)$$

where the term $p \left\{ \frac{\partial u}{\partial x} + \frac{\partial v}{\partial y} \right\}$ represents a reversible conversion between kinetic and thermal energy. The viscous dissipation, $\mu \Phi$, is defined as

$$\mu \Phi = \mu \left[\left\{ \frac{\partial u}{\partial y} + \frac{\partial v}{\partial x} \right\}^2 + 2 \left(\left\{ \frac{\partial u}{\partial x} \right\}^2 + \left\{ \frac{\partial v}{\partial y} \right\}^2 \right) - \frac{2}{3} \left\{ \frac{\partial u}{\partial x} + \frac{\partial v}{\partial y} \right\}^2 \right]. \qquad (4.11)$$

originates from viscous shear stresses ⇓   viscous thermal stress ⇓

Equation 4.11 relates to the rate at which kinetic energy is reversibly converted to thermal energy due to viscous effects in the fluid. Using the concept of enthalpy, ($h = u + p/\rho$), equation 4.11 is re-arranged to obtain

$$\rho u \frac{\partial h}{\partial x} + \rho v \frac{\partial h}{\partial y} = \frac{\partial}{\partial x}\left\{ k \frac{\partial T}{\partial x} \right\} + \frac{\partial}{\partial y}\left\{ k \frac{\partial T}{\partial y} \right\} + \left\{ u \frac{\partial p}{\partial x} + v \frac{\partial p}{\partial y} \right\} + \mu \Phi + q. \qquad (4.12)$$

If the nature of the substance corresponds to an ideal gas for which $h = C_p dT$, then equation 4.12 becomes for the 2-dimensional case:

$$\rho C_p \left\{ u \frac{\partial T}{\partial x} + v \frac{\partial T}{\partial y} \right\} = \frac{\partial}{\partial x}\left\{ k \frac{\partial T}{\partial x} \right\} + \frac{\partial}{\partial y}\left\{ k \frac{\partial T}{\partial y} \right\} + \left\{ u \frac{\partial p}{\partial x} + v \frac{\partial p}{\partial y} \right\} + \mu \Phi + q.$$
$$(4.13)$$

Concentration boundary layer

Similarly, for the concentration boundary layer, and using Fick's Law to evaluate the diffusion flux, the corresponding transfer equation for the transportation of species A (e.g. water vapour) at the surface for the y-direction is given as

$$\frac{\partial}{\partial x}(\rho_A u) + \frac{\partial}{\partial y}(\rho_A v) = \frac{\partial}{\partial x}(D_{AB}\frac{\partial \rho_A}{\partial x}) + \frac{\partial}{\partial y}(D_{AB}\frac{\partial \rho_A}{\partial y}) + n_A. \qquad (4.14)$$

With the total mass density, ρ, assumed to be constant (for an incompressible flow), equation 4.14 reduces to

$$u\frac{\partial \rho_A}{\partial x} + v\frac{\partial \rho_A}{\partial y} = \frac{\partial}{\partial x}\left[D_{AB}\frac{\partial \rho_A}{\partial x}\right] + \frac{\partial}{\partial y}\left[D_{AB}\frac{\partial \rho_A}{\partial y}\right] + n_A. \qquad (4.15)$$

or in molar form:

$$u\frac{\partial C_A}{\partial x} + v\frac{\partial C_A}{\partial y} = \frac{\partial}{\partial x}\left[D_{AB}\frac{\partial \rho_A}{\partial x}\right] + \frac{\partial}{\partial y}\left[D_{AB}\frac{\partial \rho_A}{\partial y}\right] + N_A. \qquad (4.16)$$

With reference to equations 4.14 to 4.16, the terms on the left-hand side account for the net transport of species A due to bulk fluid motion (advection). Similarly, the terms on the right-hand side accounts for the net inflow due to diffusion and production due to chemical reactions. Equations 4.9a, 4.9b, 4.9c, 4.12, 4.15 and 4.16 constitute the convection transfer equations for motion of a fluid wih co-existing velocity, temperature and concentration gradients. At each point in the fluid, conservation of mass, energy, and chemical species as well as Newton's 2nd law of motion must be satisfied. Discussion on some dimensional parameters relevant to the present project are provided in Appendix E.

4.3 Heat and mass transfer analogy

From the expressions for the Nusselt number, Nu, and the Sherwood number, Sh (see Appendix E), it follows that the dimensionless temperature and concentration gradients were evaluated at the surface, and therefore their values are analogous. The analogy may also be used directly to

relate the convection heat transfer coefficients, h_c and the convection mass transfer coefficient, h_m. The analogy can be stated as follows: if a convection mass transfer problem has the same geometry, flow pattern and boundary conditions as a known heat transfer problem, then the heat transfer correlation may be converted to mass transfer correlation by replacing the convection heat transfer coefficient, h_c by the convection mass transfer coefficient, h_m, the Prandtl number, Pr by the Schmidt number, Sc, and the Nusselt number, Nu by the Sherwood number, Sh, for either laminar or turbulent flow. From the literature (Incropera and De Witt 2002), the Nusselt number, Nu and the Sherwood number, Sh are generally proportional to Pr^n and Sc^n respectively, where n is a positive exponent less than 1. In view of this dependence, the following relation follows from the analogy

$$\frac{h_c L / k}{P_r^{\,n}} = \frac{h_m L / D_{AB}}{S_c^{\,n}}$$

or

$$\frac{h_c}{h_m} = \frac{k}{D_{AB} \, L_e^{\,n}} = \rho \, C_p L_e^{\,(1-n)} \tag{4.17}$$

where Le is the Lewis number defined as Le = α / D_{AB} = Sc/Pr; with α being the thermal diffusivity and D_{AB} the mass diffusovity of species A in B, for example, water vapour in air (Incropera and De Witt 2002). Equation (4.17) is used in the determination of one convection coefficient, for example, h_c, from the knowledge of the other coefficient, h_m. The same relation is applicable to the average coefficients, h_c and h_m, and may be used for both turbulent and laminar flows. The product ρC_p is taken at the mean temperature, T. For most applications it is reasonable to assume the value of n = 1/3 (Incropera 2002). For gas mixtures, Le lies between 0.5 and 2 and for liquids, Le > 1. For all gas mixtures, Le lies near 1 and for an air/water vapour system, Le = 0.95 (Webb 1991). Mass transfer phenomenon often causes a slight 'blowing' effect at the wall, that is a *non-zero wall normal velocity, u_w,* caused by diffusion.

The basic reason for the blowing is that the wall acts as a barrier to the stream fluid B so the mass flux of species B at the wall is essentially zero: $g_{Bw} = 0$ for a binary mixture (White 1988). Generally, the effect of wall blowing is to reduce skin friction and wall heat transfer and therefore, by analogy, to reduce the wall mass transfer. This is true for both laminar and turbulent flow. Extensive computations of laminar flat plate flow with blowing have been reported by Hartnet and Eckert (1957). There is a weak effect of the Schmidt Number and a strong effect of the blowing parameter, which is defined as

$$\zeta = (u_w / U_\infty)R_{ex}^{\frac{1}{2}}$$
(4.18)

where u_w is the wall normal velocity. In most convective mass transfer problems, it is anticipated that both Nu and Sh drop to zero at $\zeta = 0.62$, whereby the boundary layer is said to have 'blown off'. In most practical cases, however, the operation is in the range $0 < \varsigma < 0.2$. The next section is a discussion on the correlations for the convection mass transfer coefficient.

4.3.1 Correlations for the convective mass transfer coefficient

Analogies, electro–thermal and hygric

Flows of electrical current, heat and water vapour are analogous to each the other. Each requires a driving force (potential, temperature and pressure difference) and the quantity transferred in each case is limited by a resistance (electrical, thermal or vapour). Vapour resistance is treated in a similar way to electrical and thermal resistances. The expression for the mass transfer rate, m_v, for convective mass transfer is given by

$$m_v = \delta A \left\{ \frac{\Delta p_v}{\Delta x} \right\}$$

$$= A \left\{ \frac{\Delta p_v}{R_v} \right\}$$
(4.19)

where $R_v = \Delta x / \delta$ is the vapour resistance (Ns/kg). For multu-layer construction, the composite

structure forms a number of resistances in series and the area is constant throughout. Thus, equation 4.19 becomes

$$m_v = A \left\{ \frac{p_{vi} - p_{vo}}{R_{TV}} \right\} \tag{4.20}$$

where R_{Tv} is the total vapour resistance for the composite structure (comparable with total thermal resistance), and $(p_{vi} - p_{vo})$ is the total vapour pressure difference (comparable with total temperature difference). The total vapour resistance, R_{TV}, is given by the expression

$$R_{TV} = \Sigma \left\{ \Delta x / \delta \right\} \tag{4.21}$$

The share of the total vapour pressure difference between the inside and outside air, which occurs across any section, s of a structure, is proportional to the vapour resistance. Thus, for any section, the corresponding vapour pressure difference is given by

$$\Delta p_x = R_{vs} \left\{ \frac{p_i - p_o}{R_{TV}} \right\} \tag{4.22}$$

For transient moisture transfer in rooms, it has been established that the mass flow rate of water vapour through structures is normally small compared with the mass flow rate of vapour between and within spaces.

Chilton-Colburn analogy

This analogy relates the heat and mass transfer in the form

$$j_H = j_M$$

where the Colburn j-factor for heat transfer, j_H, according to Eastop and Watson (1997) is given by the expression

$$St \, Pr^{2/3} = j_H = f/2 \qquad 0.6 < Pr < 60 \tag{4.23}$$

where St is the Stanton number given by $St = Nu/RePr = h_c / \rho u C_p$ and f the frction factor given

by f = friction factor = $\tau /(\rho u^2/2)$. In the expression for the friction factor, τ is the shear stress at the fluid surface, ρ the fluid density and u the fluid velocity across the surface. The modified Chilton-Colburn expression is appropriate for heat transfer in laminar flow only when the pressure gradient is approximately zero, in turbulent flow, however, the conditions are less sensitive to the effect of pressure gradient and the equation remains approximately valid. A similar analogy holds true for mass transfer. Chilton and Colburn defined a mass transfer Stanton number, St_M, as

$$St_M = Sh / ReSc = \frac{(h_m L \, p_{in})}{(\Delta p)} \left[\frac{v}{uL}\right] \left[\frac{D}{v}\right]$$

$$= h_m \, p_{in} / up \qquad (4.24)$$

where p_{in} is the logarithmic mean pressure, p the absolute pressure, Δp the pressure differential, v the kinematic viscosity, D the diffusivity and h_m the mass transfer coefficient. A j-factor for for mass transfer, j_M, is given as

$$j_M = St_M \, Sc^{2/3} \qquad 0.6 < Sc < 3000 \qquad (4.25)$$

and it has been shown experimentally that over a range of Prandtl numbers from 0.5 to 50, for both internal and external flows, $j_M = j_H$ (Eastop and Watson 1997).

From equations 4.23 and 4.25:

$$StPr^{2/3} = St_M Sc^{2/3}$$

that is

$$\frac{Nu \, Pr^{2/3}}{Re \, Pr} = \frac{Sh \, Sc^{2/3}}{Re \, Sc}$$

$$\frac{Nu}{RePr^{1/3}} = \frac{Sh}{ReSc^{1/3}} . \qquad (4.26)$$

Simplification of equation 4.26 gives

$$Sh = Nu \, \{Sc / Pr\}^{1/3} . \qquad (4.27)$$

Similarly, the Sherwood number, Sh is considered as the ratio of the mass transfer by

convection, h_m, to the mass transfer by molecular diffusion through a typical dimension, L. The

mass transfer by molecular diffusion is given as

$$m_d = \frac{DA\,p}{R_vTp_{in}}\left\{\frac{p_{vi}-p_{vo}}{L}\right\}.$$ (4.28)

and mass transfer by convection is

$$m_c = \frac{h_mA}{R_vT}(p_{vi}-p_{vo})$$ (4.29)

where A is the liquid-air interface surface area, T the absolute temperature of the air-vapour

mixture, R_v the specific gas constant for water vapour, p_{vi} the partial pressure of water vapour

at the liquid-air interface, p_{vo} the partial pressure of water vapour in the free stream, m_c the

mass transfer by convection, m_d the mass transfer by molecular diffusion, D the diffusion

coefficient for the water vapour-air mixture and p_{in} the logarithmic mean air pressure (Eastop

and Watson 1997). Therefore,

$$Sh = \frac{h_mA}{R_vT}\frac{R_vTp_{in}}{DAp}L = \frac{h_mL}{D}\left\{\frac{p_{in}}{p}\right\} \approx \frac{h_mL}{D}.$$ (4.30)

For most cases of water vapour in air, p_{in} is approximately equal to p and hence $Sh \approx h_mL/D$

(equation E.15 in Appendix E). Applying equation (4.27) to equation (4.30) gives

$$\frac{h_mLp_{in}}{Dp} = \frac{h_cL}{\lambda}\left\{\frac{Sc}{Pr}\right\}^{1/3}$$

hence

$$h_m = \frac{h_cDp}{\lambda p_{in}}\left\{\frac{Sc}{Pr}\right\}^{1/3}.$$ (4.31)

From equation 4.63, the ratio (Sc/Pr) is

$$\frac{Sc}{Pr} = \frac{\mu}{\rho D}\frac{\lambda}{C_p\mu} = \frac{\lambda}{\rho C_pD}.$$

Multiplying equation (4.31) by $\{\lambda/(\rho C_pD)\}$ and dividing by (Sc/Pr) yields

$$h_m = \frac{h_cDp}{\lambda p_{in}}\frac{\lambda}{\rho C_pD}\left\{\frac{Sc}{Pr}\right\}^{1/3}\left\{\frac{Pr}{Sc}\right\}$$

that is,

$$h_m = \frac{h_cp}{\rho C_pp_{in}}\left\{\frac{Pr}{Sc}\right\}^{2/3}.$$ (4.32)

For most cases of water vapour in air, the logarithmic mean air pressure, p_{in} is approximately equal to the absolute pressure, p of the air. Hence, in cases of mass transfer, where the heat transfer coefficient, h_c, of an equivalent geometry is known, the mass transfer coefficient, h_m can be obtained from the expression.

$$h_m = \frac{h_c}{\rho C_p} (Pr/Sc)^{2/3} \qquad (4.32a)$$

International Energy Agency

The International Energy Agency (IEA 1991) suggested that between the convective mass transfer coefficients, h_m, and the convective heat transfer coefficient, h_c, a relationship exists for building applications:

$$h_m = \frac{h_c(C_p R_a T\delta)}{C_p R_a T \rho_a \lambda_a}^{0.67} \qquad (4.33)$$

Mass transfer coefficient correlations

The average mass transfer coefficient may be measured directly (Matthews 1987), measured indirectly using the naphthalene sublimation technique (White 1988), estimated from published heat transfer correlations (e.g. Khalifa and Marshal 1990) using the heat and mass transfer analogy, or estimated from published mass transfer correlations. Mass transfer correlations typically relate a dimensionless form of the film coefficient, the average Sherwood number, Sh_L, with the surface flow Reynolds Number, Re_L, and the air phase Schmidt number, Sc. For a uniform flow parallel to a flat plate in the absence of wall blowing effect, White et al (1980) provides the following correlations.

For <u>laminar flow</u>, $Re_L \leq 500.000$:

a) local value: $Sh_x = \frac{h_m x}{D} = 0.332 \, Re_x^{1/2} Sc^{1/3}$ (4.34)

b) average value: $Sh_L = \frac{h_m L}{D} = 0.664 \, Re_L^{4/5} Sc^{1/3}$.

For <u>turbulent flow</u>, $Re_L \geq 500.000$ and with $Sc \approx 1.0$, the power law formulas may be used:

a) local value: $\qquad Sh_x = \dfrac{h_m x}{D} = 0.029\, Re_x^{4/5}\, Sc^{1/3}$

b) average value: $\qquad Sh_L = \dfrac{h_m L}{D} = 0.037\, Re^{4/5}\, Sc^{1/3}$ $\qquad\qquad$ (4.35)

where D is the diffusion coefficient for the water vapour-air mixture. Further discussion on boundary conditions as they relate to the building structure is presented in the next section.

.

4.4 Boundary conditions as they relate to the building structure

In addition to the boundary conditions specified previously for the HAM-model, air flow simulations and convective surface transfers, further discussion on boundary specifications for boundary layer diffusion as they relate to the building structure is presented. Building material surfaces are considered to be separated from the zone air by a film or boundary layer over which the species concentration varies from a near surface, air phase concentration, C_s, to the bulk air-phase concentration in the zone, C_{air}, as shown in Figure 4.4. For the case that the mass transport is only due to molecular and turbulent diffusion processes, the net mass transport rate from the bulk phase to the surface, m_v, may be approximated using steady-state mass transfer relations from the general boundary layer theory (White 1988):

$$m_v = h_m\, \rho A_s\, (C_{air} - C_s) \qquad\qquad (4.36)$$

where h_m is the average film mass transfer coefficient, ρ the film density (the average of the bulk and surface densities), and A_s the surface area of the wall. Both external and internal wall surfaces exchange mass with the ambient atmosphere by surface convection at the air side and by molecular diffusion at the material side.
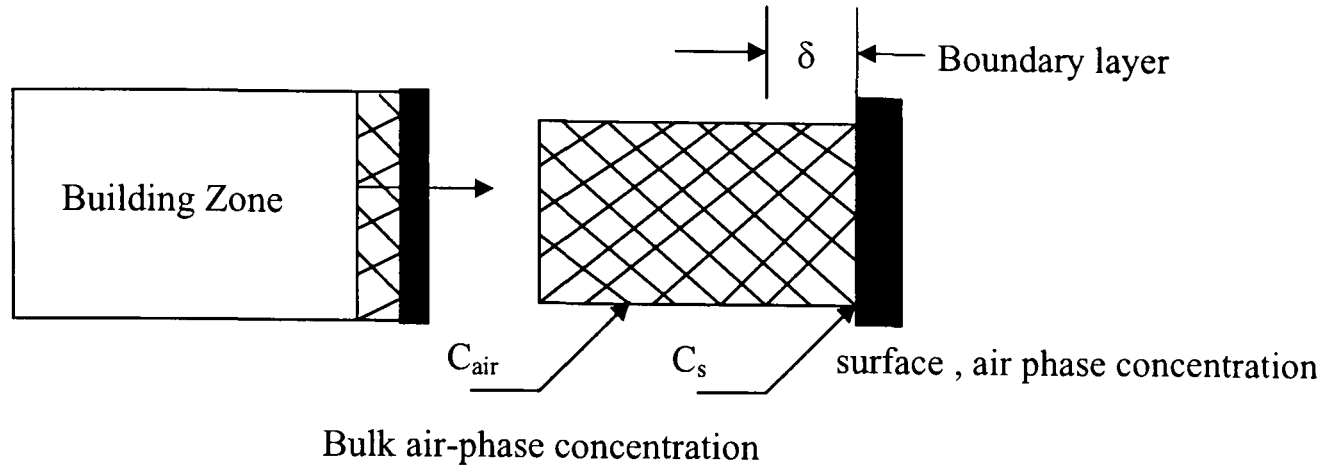
Figure 4.4: Boundary layer diffusion (White 1988)

In summary and with reference to Appendix E the complete set of boundary layer equations becomes

$$\frac{\partial u^*}{\partial x^*} + \frac{\partial v^*}{\partial y} = 0 \tag{4.37}$$

$$u^* \frac{\partial u^*}{\partial x^*} + v^* \frac{\partial u^*}{\partial y^*} = -\frac{dp^*}{dx^*} + \frac{1}{Re_L} \frac{\partial^2 u^*}{\partial y^{*2}}$$

$$u^* \frac{\partial T^*}{\partial x^*} + v^* \frac{\partial T^*}{\partial y^*} = \frac{1}{Re_L Pr} \frac{\partial^2 T^*}{\partial y^{*2}} \tag{4.38}$$

$$u^* \frac{\partial C^*_A}{\partial x^*} + v^* \frac{\partial C^*_A}{\partial y^*} = \frac{1}{Re_L Sc} \frac{\partial^2 C^*_A}{\partial y^{*2}}. \tag{4.41}$$

The boundary layer phenomenon, namely, the velocity, thermal and concentration boundary layers in relation to heat and mass transfer through porous medium has been highlighted. Their principal manifestations are surface friction, convection heat transfer and convection mass transfer in the order mentioned above. The review presented in this chapter was necessitated by the fact that the conflation of construction moisture and the indoor air humidity is effected at the interface between the solid surface and the building enclosure. This interface serves as the pivot point for the envisaged conflation. In particular, the relation between convection heat transfer coefficient, h_c, and convection mass transfer coefficient, h_m, was highlighted. It became evident that in most practical cases, for which the critical value for the blowing parameter,

$\xi = 0.62$, is not exceeded, the Lewis relation (Le) gives an appreciable results for the conversion of h_c to h_m and vice-versa.

5.1 Coupling approaches

Within this sub-section is a general discussion on coupling approaches for energy simulation (HAM) and the computational fluid dynamics (CFD) programs. Both models can play important roles in building design by providing complementary information about the building's environmental performance. The present study emphasizes the explicit coupling of individual HAM and CFD programs by exchanging the coupled boundary values. In order to bridge the disparities between HAM and CFD programs due to the different physical methods employed (Ch.3.5), the study suggests the staged coupling processes that may reduce the computing demands while keeping the advantages of the code coupling approach.

Code coupling

In the code coupling approach, convective heat and mass transfer from the enclosures are the most important information for the coupling. They are crucial for the energy analysis in HAM, as well as for the accurate specification of boundary conditions in CFD. The air temperature in the boundary layer of a surface and the convective mass transfer coefficient are two key factors determining the convective mass transfer. The next sub-section is a brief presentation on the staged coupling strategy.

5.1.1 Staged coupling

Three main discontinuities exist between HAM and CFD programs. The first one is a time-scale discontinuity: HAM has a characteristic time-scale of hours for building performance, but CFD is on the order of a few seconds for air. The second is a modelling discontinuity: the indoor environmental conditions predicted for each space in HAM are a spatial average, while

CFD presents field distributions of the variables. The third is a speed discontinuity: the execution time for energy simulation is of the order of a few seconds per zone per year, and the memory requirement is small (about 1MB), while a three-dimensional CFD analysis for a zone may take a few hours to a few days and require about 100 Mb of memory, even for a modest grid size (Srebic et al 1999). To bridge these discontinuities a staged coupling strategy is proposed. The staged coupling can be classified as being either *static* or *dynamic*. The latter type can be further classified as fully-dynamic or quasi-dynamic. These classifications are illustrated in Table 5.1.

Static coupling involves a one-step or two-step exchange of information between HAM and CFD programs, depending on the building performance and resolution requirement. Due to the few coupling steps and the static feature of the coupling operation, static coupling can usually be performed manually, with few changes in the HAM and CFD codes. Generally, the one-step static coupling is a good choice where HAM and CFD or both are not sensitive to the exchanged variables. If the information from CFD, such as the convection mass transfer coefficient, $h_{i,m}$, differs significantly from that used in the first HAM calculation, HAM may take this information from CFD for the new energy and temperature calculation. This is classified as a two-step static coupling. Two-step static coupling is sufficient for buildings in which the changes in the exchanged information are not significant, and the solution is not strongly dependent on the exchanged data.

Dynamic coupling involves coupling between HAM and CFD programs at every time-step. This is required when both HAM and CFD solutions depend on boundary conditions that vary significantly with time. There are three kinds of dynamic coupling:
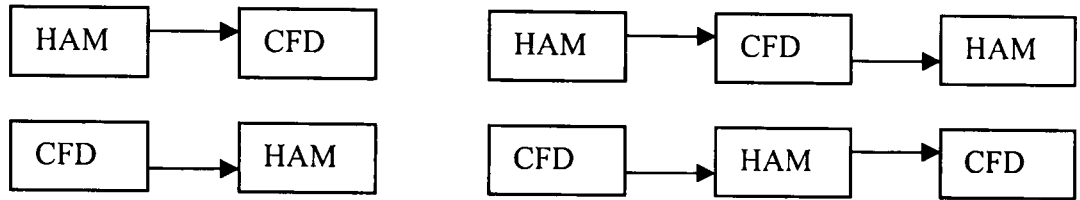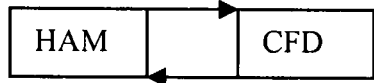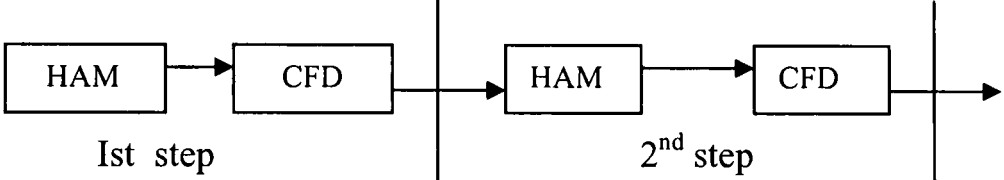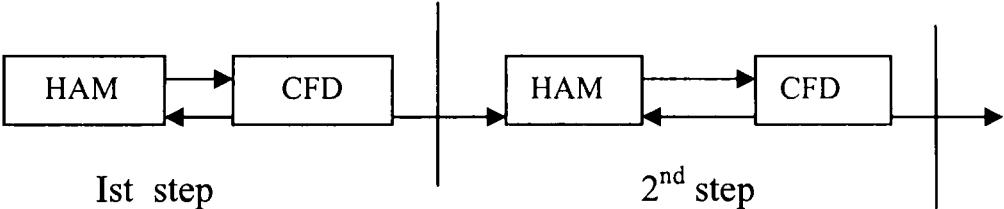
One-time step dynamic coupling, which focuses on the HAM/CFD coupling at one specific

time-step. The iteration between the two models is performed at this time-step until an acceptably consistent solution is obtained. Alternatively, HAM and CFD may iterate only one time at each coupling time step, and then move on to the next time step. This is the *quasi-dynamic coupling*. With the *full dynamic coupling*, HAM and CFD iterate at each coupling time step until convergence criteria are met. Full dynamic coupling is undoubtedly the most accurate, but also the most intensive computationally. Table 5.1 gives an illustration of the staged coupling strategy. The arrow from CFD to HAM indicates the transfer of indoor air water vapour pressure, $p_{i,air}$, and convective mass transfer coefficient, $h_{i,m}$, while the arrow from HAM to CFD indicates the transfer of inside surface water vapour pressure, $p_{s,i}$, and construction moisture flux, g_{constr}.

In general, the building characteristics and the purpose of the simulation determine which coupling process is the most appropriate for a particular case. The two-time step quasi-dynamic coupling is chosen for this project because of its adaptability to the loose-coupling algorithm process.

Within the coupling process, for example from 3-D model to 1-D HAM model, sources of error may be encountered through, for example, modelling, discretisation and interpolation amongst others. Discretisation errors, for example, are of major concern because they are dependent on the quality of the grids. The grid should be generated with due consideration given to such parameters as resolution, density, aspect ratio, orthogonality and zonal boundary interfaces. Similarly, interpolation errors occur at zonal interfaces where the solution of one zone is approximated on the boundary of the other zone (Mehta 1998). Other sources of error that can affect the coupling process may be traced to the use of 3-D simulation tools. For example,

Table 5.1: Illustration of staged coupling strategy

Coupling Type	Illustration of Methodology
Static	 One-step Two - step
Dynamic	 One time step dynamic coupling Quasi-dynamic coupling 1st step iterate till convergence 2nd step iterate till convergence Full dynamic coupling

3-D simulation tools such as the 3-D CFD model have had a number of restrictions imposed related to nodalization, field equations and other aspects of physical modelling. It is envisaged that the 3-D Navier-Stokes code for the CFD in this case is applied for the detailed analysis

of indoor air flow whilst the 1-D HAM code is used to provide the boundary conditions reflecting feedback from the balance of the system. Successful coupling therefore requires care in both the numerical and physical modelling. Since most CFD codes use fully implicit time differencing, coupling to a fully implicit 1-D code would therefore be most direct (Gibelling and Mahaffy 1992). The field equations in both models should at least match and the conservation of mass, momentum and energy made possible.

5.2 The conflation problem

The conflation problem is essentially concerned with the CFD boundary conditions and what takes place at the interface between the two computational domains. The interaction between the two systems occurs at the inside zone surfaces of the building envelope and at openings (doorways, windows, ducts, cracks, etc). By such interactions, as illustrated in Figure 5.1, the energy, mass and momentum balance equations must be connected (conservation principles).
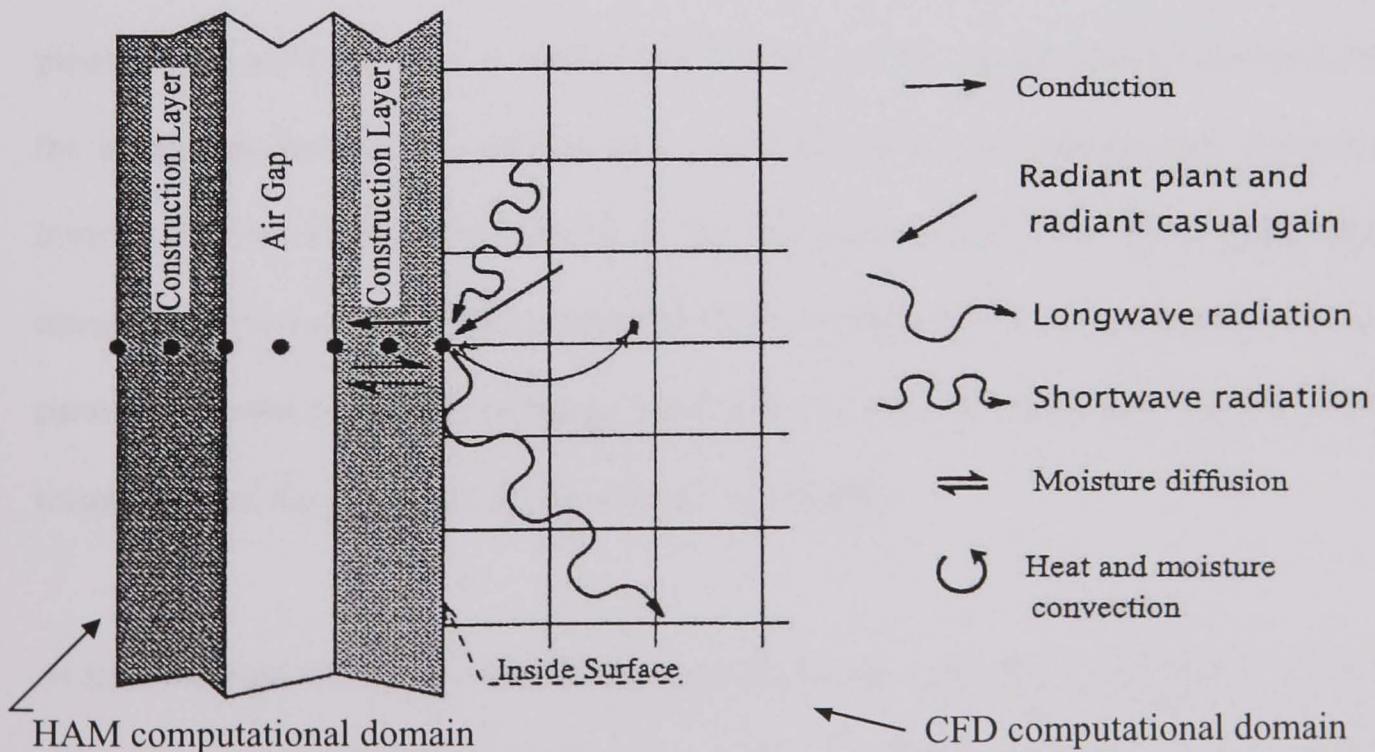
Figure 5.1: Energy interactions at inside zone surface within ESP-r.

imilarly, the combination of the two systems consists of substituting a HAM zone air volume by a CFD domain volume. The two systems thus need to communicate to each other in a co-operative manner, taking cognizance of their commonalities as mentioned in Chapter 3.5. For example, both models are capable of undertaking transient energy and mass flow simulations. Similarly, both HAM and CFD models apply the conservation of mass and energy principles to predict temperatures, flow rates, humidity, etc. within the components of the building and plant systems. Both models use the conservative, finite volume method to discretise the differential equations, which yields an equivalent set of algebraic conservation equations. These algebraic equations differ only in the inter-volume interaction coefficients and source terms, which are specific for each system of equations.

An illustration of such interaction between HAM and CFD nodes through the surface node at the internal fabric surface, K-K, is shown in Figure 5.2. It is at this surface that convection operates and, more specifically, where the handshaking between HAM and CFD models takes place. At the solid interface, a number of CFD cells, are in contact with an internal surface. By the interaction between the surface node and CFD cells it is observed that convection mass transfer between HAM solid node, (I-1), and the inside surface node, (I), is substituted by the interaction between the surface node and CFD air node, (I+1). As mentioned previously, the parameters involved in the exchange mechanism are the inside surface vapour pressure, the temperature of the wall and the convection mass transfer.

At the openings, CFD cells can also be in contact with other air nodes, internal or external, or plant component nodes. Mass flow rates, pressures, velocities and other scalar variables (such as temperature, humidity, etc.) are, in this case, the quantities to be interchanged.
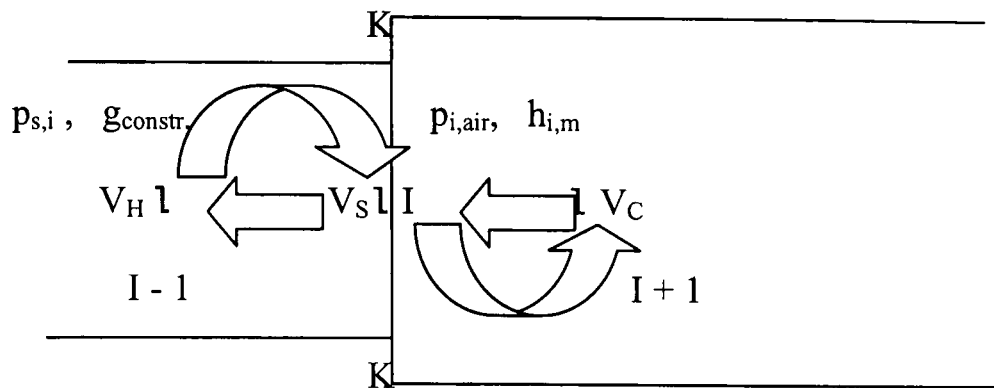
V_H = volume of HAM node (solid type); V_S = volume of internal surface node;

V_C = volume of CFD node (fluid type); $p_{s,i}$ = inside surface vapour pressure;

$g_{constr.}$ = construction moisture flux; $p_{i,air}$ = indoor air vapour pressure;

$h_{i,m}$ = convection mass transfer coefficient; K-K= internal fabric surface (interface).

Figure 5.2: Interaction between HAM and CFD nodes through the internal surface node.

5.2.1 Conflation technique

With the *close-coupled* simulation approach, the governing transport equations for HAM and CFD models are regarded as a combined mathematical system and solved using a global matrix formulation. An alternative simulation approach is the loose-coupled simulation approach which is performed in the time domain (Srebic and Novoselac 2002).

With the *loose coupled* - simulation approach, HAM and CFD models are simulated separately but are coupled through data exchange at the interface. Due to its adaptability to the two-time step quasi-dynamic staged coupling (Zhiqiang Zhai and Qingyan Chen 2001), it has been chosen for the conflation of construction moisture and indoor air humidity. It is also able to deliver a reasonable solution with acceptable computing effort. The *loose coupling* algorithm is shown in Figure 5.3, with the respective governing transport equations for HAM (1-D) and CFD (3-D) models. The most common way to realise the approach is by the selection of a

'master surface' for a variable of interest and interpolating or projecting the variable to the other domain at the beginning of the next time step. For the CFD/HAM conflation, the most natural combination is the selection of the HAM surface location (internal wall surface), the internal surface vapour pressure, $p_{s,i}$, and/or moisture flux, g_{constr}, as the master grid for the vapour distribution; and the indoor air (air point node) as the master grid for the variables, indoor air vapour pressure, $p_{i,air}$, and the convective mass transfer coefficient, $h_{i,m}$. The approach may be regarded as an iterative solution of the combined system. Each iterative process is composed of the following tasks:

- solve for CFD with imposed $p_{s,i}$ and g_{constr} from the HAM domain; and

- solve for HAM with imposed $p_{i,air}$, $h_{i,m}$ from the CFD domain.

The variables on the boundaries are transferred back and forth between the two domains by a master algorithm that directs the simulation (Loehner et al 1995). The convective mass transfer from the enclosure is the most important information for the coupling: the air temperature and water vapour pressure in the boundary layer of the surface and the convective mass transfer coefficient are the key factors for the determination of the convective mass transfer.

CFD performs the analysis of the air flow within the zones where the gradients are required. The input requirements for CFD are the domain boundary conditions. These include the inside zone surface vapour pressures and the air condition at inlet openings, such as mass flow rate, flow direction, temperature, inlet ambient pressure, vapour pressure and humidity. Similarly, HAM requires the air properties distribution, the convection mass transfer at inside zone surfaces and the air condition at the outlet openings of the CFD domain to compute the building's indoor air properties. This technique is shown schematically with the governing transport equations for both models, in Figure 5.3. The solution of the transport equations for the hygrothermal model can be attained using the two-nested iteration process (Appendix A) or

Hygrothermal Model:

Moisture balance term:

$$\rho_o \zeta \frac{\partial(p/p_s)}{\partial t} + \frac{dp_l}{dt} = \frac{\partial}{\partial x}\left[\delta^T_P \frac{\partial p}{\partial x} + D^P_T \frac{\partial T}{\partial x}\right] + S \quad . \qquad (2.4)$$

Energy balance term:

$$\left[\rho_o \left\{c_o + c_v u_v\right\} + c_l \rho_l\right]\frac{\partial T}{\partial t} + h_v \frac{\partial \rho_v}{\partial t} + h_l \frac{\partial \rho_l}{\partial t} = \frac{\partial}{\partial x}\left\{\lambda \frac{\partial T}{\partial x}\right\} - \frac{\partial}{\partial x} h_s J_v + g$$

$$(2.5)$$

Temperature/pressure field
Moisture field
Heat fluxes
Moisture fluxes

$p_{s,i}$

moisture flux, g_{constr}

$p_{s,i}$ = inside surface vapour pressure

$p_{s,i}$

$h_{i,m}$, $p_{i,air}$ (updated value)

-Averaging of variables to extract 3-D information for use by the 1-D calculations
-Grid transformation and data exchange
-Interpolation between grids
- h_m Control Algorithm :control laws / appraisal and examination of surface conditions/ h_m variation and source term adjustments.

$p_{s,i}$, g_{constr}

Temperature/pressure field
Convection mass transfer
fluxes Convection mass
transferc coefficients

$h_{i,m}$

$p_{i,air}$, indoor air vapour pressure

convection mass transfer coefficient

Computational Fluid Dynamics Model (in tensor notation for 3-D)

Continuity Equation:

$$\frac{\partial \rho}{\partial t} + \frac{\partial}{\partial x_I}(\rho u_i) = 0 \quad . \qquad (3.2)$$

Navier-Stokes Equations:

$$\frac{\partial}{\partial t}(\rho u_i) + \frac{\partial}{\partial x_j}(\rho u_i u_j) = -\frac{\partial p}{\partial x_i} + \frac{\partial}{\partial x_j}\left[\mu\left\{\frac{\partial u_i}{\partial x_j} + \frac{\partial u_j}{\partial x_i}\right\}\right] - \rho g \beta (T_\infty - T) \quad . \qquad (3.3)$$

Energy Equation:

$$\frac{\partial}{\partial t}(\rho C_p T) + \frac{\partial}{\partial x_i}(\rho u_i C_p T) = \frac{\partial}{\partial x_i}\left[k\frac{\partial T}{\partial x_i}\right] + S_c \qquad (3.4)$$

Concentration (water vapour) Equation

$$\frac{\partial}{\partial t}(\rho p_w) + \frac{\partial}{\partial x}\left[\rho u\, p_w - \left\{\frac{\mu}{Sc} + \frac{\mu_t}{\sigma_{pw}}\right\}\frac{\partial p_w}{\partial x}\right] + \frac{\partial}{\partial y}\left[\rho v p_w - \left\{\frac{\mu}{Sc} + \frac{\mu_t}{\sigma_{pw}}\right\}\frac{\partial p_w}{\partial y}\right] + \frac{\partial}{\partial z}\left[\rho w p_w - \left\{\frac{\mu}{Sc} + \frac{\mu_t}{\sigma_{pw}}\right\}\frac{\partial p_w}{\partial z}\right]$$

$$= S_{pw} \qquad (3.78)$$

for k-transport:

$$\frac{\partial}{\partial t}(\rho k) + \frac{\partial}{\partial x_j}(\rho u_j k) = \frac{\partial}{\partial x_j}\left\{\frac{\mu_t}{\sigma_k}\cdot\frac{\partial k}{\partial x_j}\right\} + \mu_t\left\{\frac{\partial u_i}{\partial x_j} + \frac{\partial u_j}{\partial x_i}\right\}\frac{\partial u_i}{\partial x_j} - \rho \varepsilon - g\beta\frac{\mu_t}{\sigma_t}\frac{\partial T}{\partial z} \qquad (3.60)$$

for ε-transport:

$$\frac{\partial}{\partial t}(\rho \varepsilon) + \frac{\partial}{\partial x_j}(\rho u_j \varepsilon) = \frac{\partial}{\partial x_j}\left\{\frac{\mu_t}{\sigma_\varepsilon}\frac{\partial \varepsilon}{\partial x_j}\right\} + C_1 \varepsilon \mu_t\left\{\frac{\partial u_i}{\partial x_j} + \frac{\partial u_j}{\partial x_i}\right\}\frac{\partial u_i}{\partial x_j} - C_2 \rho\frac{\varepsilon^2}{k} - C_1 \varepsilon\, g\beta\mu_t\frac{\partial T}{\partial z} \qquad (3.61)$$

Figure 5.3: Loose coupling algorithm.

by processing the coupled moisture/energy equations separately, but under global iteration control to handle the coupling effects because of the non-linearity behaviour associated with the moisture equation (Clarke 2001). With reference to the latter solution approach, the coupled moisture/energy equations of Eqs. 2.4 and 2.5 can be expressed by

$$\begin{bmatrix} \mathbf{E} \\ \mathbf{M} \end{bmatrix} \times \begin{bmatrix} \mathbf{T} \\ \mathbf{P} \end{bmatrix} = \begin{bmatrix} \mathbf{B_e} \\ \mathbf{B_m} \end{bmatrix} \tag{5.1}$$

where $\mathbf{E}$ and $\mathbf{M}$ are the energy and moisture coefficient matrices respectively, $\mathbf{T}$, $\mathbf{P}$ the temperature and water vapour pressure vectors, and $\mathbf{B_e}$, $\mathbf{B_m}$ the energy and moisture boundary conditions. The solution approach enables each equation set to be integrated at different frequencies depending on the system's characteristics (Clarke 2001). Due to the non-linear behaviour of the moisture system, the moisture flow equations are solved by the Gauss-Seidel method. To guard against convergence instabilities, for example, in the case of strong non-linearity, etc. linear under-relaxation is employed within the solution process. Most often the moisture solution is constrained to advance at a time-step equal to or greater than that imposed on the energy equation.

For the energy equations, the matrix partitioning technique as illustrated in Clarke (2001) is employed. This has the advantage of enabling variable time-stepping with iteration incorporated for non-linear cases. For highly coupled cases, however, both equation systems are solved at matched and small time-step. For the humidity coupling, the inside wall surface vapour pressure, p_{si} and the vapour flux $g_{constr.}$ are supplied through the data exchange station to the CFD model to establish the required boundary conditions for the simulation run by the CFD model.

The CFD solution follows the sequential and iterative solution approach provided in Appendix C (Figure C1.1) to obtain the values for the convective mass transfer coefficient, h_{im}, and the indoor air vapour pressure, $p_{i,air}$, required for the next HAM simulation run for the 2nd time-step after these values have been updated at the data exchange station. The set criterium for the acceptance of the value for $h_{i,m}$ is based on the value of h_{im}, that can be obtained when an analogous convection heat transfer coefficient, h_c, and the Lewis relations are used for its evaluation.

The CFD model uses the finite volume method to solve the Navier-Stokes equations for the co-located grid arrangement. The solution of the momentum equations enables the velocity distribution of the room air flow to be obtained. The continuity equation is modified to yield a pressure correction equation to facilitate the resolution of the problem with pressure-velocity coupling on co-located grids (Ferziger and Peric 1995). The pressure-correction equation is employed to obtain the pressure distribution through the use of the SIMPLE algorithm (or variants thereof, notably the SIMPLEC-algorithm). Turbulence conditions are catered for by the standard version of the k-ε turbulence model (Launder and Spalding 1974). The model can be configured to account for the time dependent conditions at the internal fabric surfaces. The configuration mechanism discussed in section 5.3 considers the resolution of problems with moisture migration at the internal surface through a moisture control algorithm for the variation of the convective mass transfer coefficient, h_{im}, and adjustment of the source terms of the HAM and CFD models.

An equation governing the water vapour distribution in the room (Eq. 3.78), is added to the CFD model for the determination of the spatial variation of relative humidity as a function of the spatial humidity sources by the CFD model:

$$\partial(\rho p_w)/\partial t \; + \; \partial\{\rho u p_w - \{\mu / Sc + \mu_t/\sigma_{pw}\} \; \partial p_w/\partial x\}/\partial x +$$
$$\partial\{\rho v p_w - \{\mu / Sc + \mu_t/\sigma_{pw}\}\partial p_w/ \partial y\}/ \partial y + \partial \{\rho_w p_w-\{\mu / Sc + \mu_t/ \sigma_{pw} \}\partial p_w/ \partial z\}/\partial z = S_{pw}$$

$$(3.78)$$

where μ and μ_t are the physical and the turbulent dynamic viscosities, Sc the Schmidt number = v/D, where D is the diffusion coefficient of water vapour in air, v the kinematic viscosity and $\sigma_{pw} = 0.9$ the turbulent Schmidt number; S_{pw} is the source term. The accuracy of CFD predictions is highly sensitive to the boundary conditions. Essentially, the flow inside the CFD solution domain is driven by the boundary conditions. Normally, the boundary conditions for CFD simulation of indoor air flows relate to the inlet (supply), outlet (exhaust), enclosure surfaces, and intenal objects or furnishings (Malalasekera 1995). The pressure, temperature, velocity and turbulence of the air entering from diffusers, windows or through infiltration determine the inlet conditions, while the interior surface vapour pressures, temperatures and/or heat or moisture fluxes are important thermal and hygric boundary conditions for the enclosures. From Figure 5.3 it is implied that, the hygrpothermal model establishes the Temperature/pressure field, moisture field, as well as the heat and moisture fluxes. The data exchange station is a stage within the solution process, whereby averaging of variables, grid transformation, data exchange between models, interpolation between grids, resolution of the moisture migration problems through the moisture control algorithm, etc are carried out. Consequently, the CFD model establishes the conditions within the building enclosure. These are the Temperature/pressure field, convection heat and mass transfer fluxes and heat and mass transfer coefficients. The next sub-section presents the two-time step dynamic coupling method.

5.2.2 Two time step dynamic coupling

Within this coupling approach, the HAM model solves a system of moisture and energy balance equations and applies a one-dimensional finite difference method to calculate the heat conduction and moisture flux through the building envelope.

The schematic diagram of the two-time step coupling, as shown in Figure 5.4, consists of an illustration of the governing transport equations for the HAM and CFD models and a configuration unit responsible for the data exchange at each time step of the coupling process.

$p_{s,i}$ = inside surface vapour pressure of solid wall ; $g_{constr.}$ = moisture flux

$p_{i,air}$ = indoor air vapour pressure; $h_{i,m}$ = convective mass transfer coefficient.

HAM inputs; inlet air temperature, $p_{i,air}$; inside wall surface temperature, $p_{s,i;}$

inlet air pressure (ambient), p_a ; inlet partial water vapour pressure, p_v .
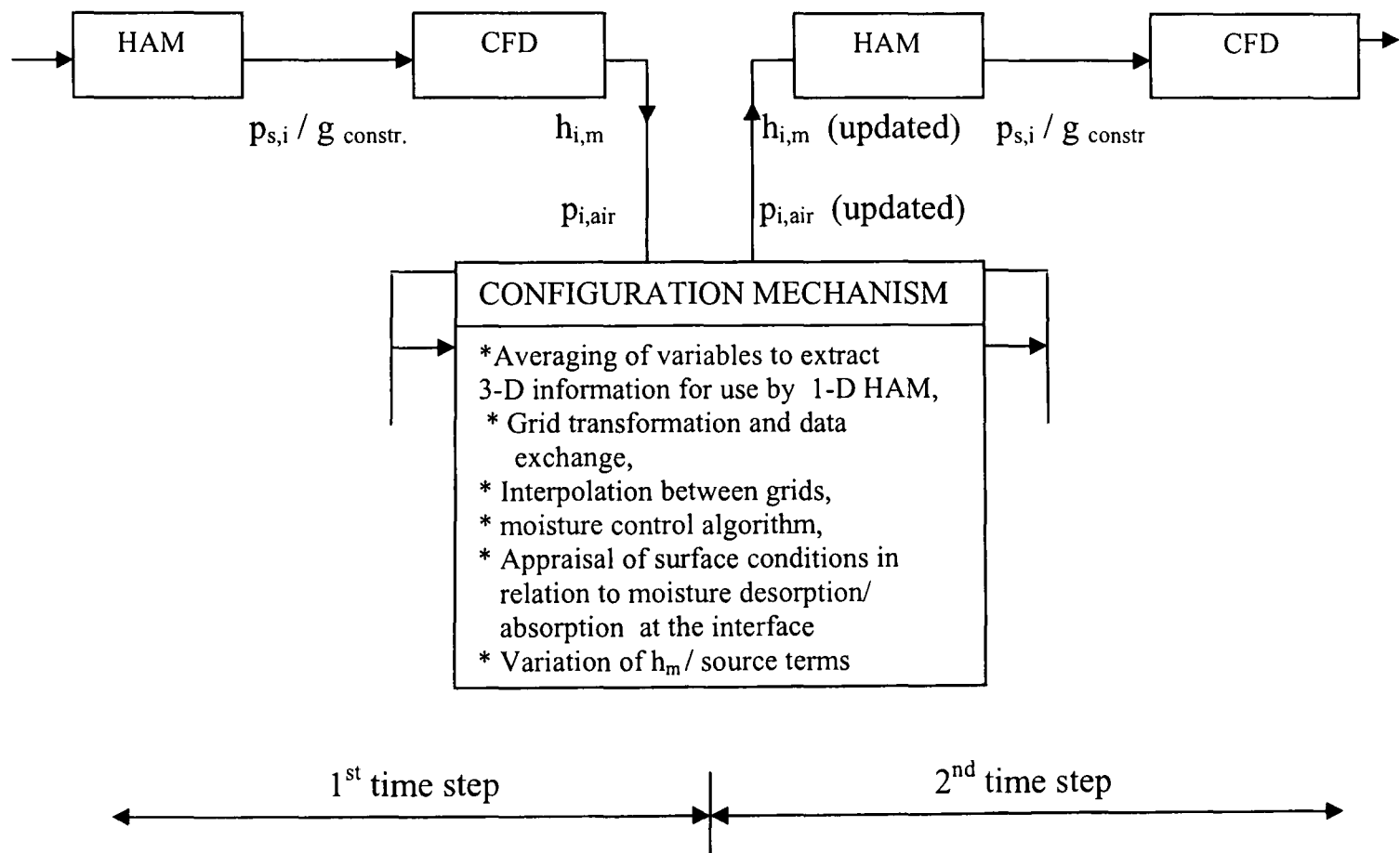
Figure 5.4: Two time step dynamic coupling.

116

This has been illustrated in Figure 5.3 to highlight on the governing transport equations for the conflating models and to facilitate the understanding of the coupling schematic presented in Figure 5.4. Discussions on the energy transfer mechanism associated with the pertinent nodes in HAM and CFD domains, namely, the solid type, the surface node and the fluid or air-point node for the data exchange within the framework of ESP-r's simulation methodology (Clarke 2001) is provided in Appendix F.

For the coupling of HAM and CFD models, the energy and humidity balance equations for the zone air and that for the convective mass transfer coefficient are relevant. For a 1-D case considering conduction as the dominant heat flux through the porous medium, the corresponding energy balance equation is given as

$$\left[\rho_o \left(c_o + c_v u_v\right) + c_l \rho_l\right]\frac{\partial T}{\partial t} + h_v\frac{\partial \rho_v}{\partial t} + h_l\frac{\partial \rho_l}{\partial t} = \frac{\partial}{\partial x}\left\{\lambda\frac{\partial T}{\partial x}\right\} - \frac{\partial}{\partial x}h_s J_v + g \tag{2.5}$$

where J_v is the vapour mass flux (kg/m^{2}s due to phase change, J_v is negative for adsorption and condensation and positive for desorption and evaporation phenomena); h_v, h_l and h_s the enthalpies (J/kg) of vapour, liquid and moisture flux source respectively. The source term, g, represents a source of heat. The driving potential for the energy term is the temperature gradient. Similarly, the moisture balance term is given as

$$\rho_o\zeta\frac{\partial (p/p_s)}{\partial t} + \frac{d\rho_l}{dt} = \frac{\partial}{\partial x}\left[\delta^T_P\frac{\partial p}{\partial x} + D^P_T\frac{\partial T}{\partial x}\right] + S \ . \tag{2.4}$$

where ρ is density (kg/m^3; 0 and 1 denote porous media and liquid respectively) and S is the moisture source term. For moisture transport by vapour diffusion, the driving potential is the difference in partial water vapour pressure across the porous medium.

Boundary condition

For the inside surface of the external wall, the boundary condition $T(L,t)$ is determined from Eq. A.29 with reference to Figure A1.2 in AppendixA:

$$\left\{\begin{array}{l}\text{Inward heat}\\\text{conduction}\end{array}\right\} = \left\{\begin{array}{l}\text{Convection from}\\\text{the inside surface}\end{array}\right\} + \left\{\begin{array}{l}\text{Radiation exchange}\\\text{between inner surface}\\\text{and other surfaces}\end{array}\right\} + \left\{\begin{array}{l}\text{Heat required}\\\text{for the}\\\text{evaporation}\\\text{of liquid water}\end{array}\right\} + \left\{\begin{array}{l}\text{heat influx}\\\text{to the room}\\\text{due to air}\\\text{infiltration}\end{array}\right\}$$

(A.29)

$$-k\frac{\partial T}{\partial x}\bigg|_{=L} = h_{c,i}[T(L,t) - T(t)] + \sum_{j=1} h_{r,j}[T(L,t) - T(n,t)] + \rho_i h_{i,m} U_i(L,t)[w(L,t) - w_r(t)]h_{fg}.$$

$$+ m_a C_{pa}[T(L,t) - T(t)]$$

(A.30)

where w is the air humidity ratio, $h_{i,m}$ the convective mass transfer coefficient, $h_{i,c}$ the convective heat transfer coefficient, ρ_i the inside air density and U the moisture content.

Air humidity balance for the zone air

A humidity balance equation represent the humidity that is exchanged by infiltration, ventilation and air change with adjacent zones. Humidity is also exchanged by convective mass transfer between the zone air and the building envelope as a result of which moisture is either released or absorbed from or to the porous medium. The humidity balance equation for the zone air is given as

$$\Sigma G = G_{constr} + G_{vent} + G_{sys}.$$

(2.18c)

Equation (2.18c) represents the summation of the vapour flux into the zone from all available sources as detailed below. Thus

$$V \cdot \rho_{air}(w^{new} - w^{old}) / \Delta t = \Sigma G$$

(2.18)

where V is the volume of the zone, w the air humidity ratio and ρ_{air} the density of the zone air.

The humidity transfer between the construction surfaces and the zone air is governed by the convective mass transfer coefficient, which may be determined from

$$G_{constr} = \sum_{constr} A_{surf} h_m (p_{surf} - p_{air}) \qquad (2.18a)$$

where $G_{constr.}$ is the vapour flux through the porous medium, A_{surf} the wall surface area, h_m the convective mass transfer coefficient, p_{surf} the partial pressure of the water vapour at the inside wall surface, p_{air} the partial water vapour pressure of the zone air and ρ_{air} the density of the water vapour. Vapour contributed to the zone air by ventilation, G_{vent} is determined by summation of all sources:

$$G_{vent} = \sum_{Air\ sources} n_{vent} . V \rho (w_{vent} - w_{air}) \qquad (2.18b)$$

where w_{vent} is the humidity ratio of the air as it enters the zone (from the outside or from another zone) and n_{vent} is the associated air change rate.

Moisture contributions may originate from people (metabolism) and from other moisture loads (e.g. washing machine, ccoker, etc) in the zone. Such influences on the indoor air humidity vary according to defined schedules or various control strategies. The humidity contribution from these sources may be combined into a single quantity, G_{sys}. This parameter indicates the mass of water vapour induced to the air per unit time (kg/h). The total humidity balance for the zone is obtained by inserting the different moisture constituents in equation (2.18c):

$$\Sigma G = G_{constr} + G_{vent} + G_{sys}. \qquad (2.18c)$$

The next sub-section is an overview of the CFD model in relation to its control equation and the associated boundary conditions.

CFD – control equation and boundary conditions

CFD involves the application of numerical techniques to solve the Navier-Stokes equations for fluid flow. For a transient incompressible flow, the standard differential equation, which invariably serves as the control equation for CFD is given as

$$\frac{\partial(\rho\phi)}{\partial t} + \text{div}\,(\rho\nabla\phi - \Gamma_\phi\nabla\phi) = S_\phi \qquad (3.1)$$

where ϕ is a general variable that can stand for any mean scalar variable or velocity component ϕ (= 1 for continuity); u, v, and w are the velocity components in the x, y and z directions; k represents the turbulent kinetic energy; ε represents the energy dissipation; while C and T represent the concentration and temperature respectively. The diffusion coefficient, Γ_ϕ, and the source terms, S_ϕ, are provided in the literature (Malalasekera 1995).

Coupling of HAM and CFD models

For humidity coupling, the problem of model coupling is focused on how to treat the convective mass transfer in HAM and CFD models. Within the code coupling method, HAM and CFD programs are coupled directly and exchange information on convective mass transfer after their individual simulation runs. In the light of the foregoing discussions, a pragmatic approach is to supply the surface average of the air vapour pressure, $p_{i,air}$, computed by CFD at the flow grid next to the wall surface together with the corresponding averaged convective mass transfer coefficient, $h_{i,m}$, to the HAM model. The indoor air average partial water vapour pressure of the indoor air, $p_{i,air}$, is obtained from the CFD control equation Eq.3.1, through the substitution of ϕ = p, where p is the scalar variable of interest (partial water vapour pressure) for the simulation. The average indoor air vapour pressure and average convective mass transfer coefficient provided by CFD are used in the HAM model through the humidity balance

equation (2.18c). For a particular surface, i, for example

$$\text{Vapour flux, } g_{i,m} = G_{constr.}/A = h_{i,m} (p_{s,i} - p_{i,air}) . \tag{5.2}$$

that is,

$$\text{Vapour flux, } g_{i,m} = h_{i,m} (p_{s,i} - p_{i,air}) = h_{i,m} (p_{s,i} - p_{room}) - h_{i,m} \Delta p_{i,air} \tag{5.3}$$

where $\Delta p_{i,air} = p_{i,air} - p_{room}$, and p_{room} is the design partial water vapour pressure of the air in the room. After finishing each CFD simulation, HAM obtains the updated $p_{i,air}$ and $h_{i,m}$ values from CFD, substituting them into equation 5.3. HAM then solves the humidity and energy balance equations (2.5 and 2.18c) with this new Eq. 5.2 to obtain new surface water vapour pressures and room air water vapour pressure for the humidity coupling. The CFD program then uses the outputs from the HAM simulation to determine the pertinent indoor air quality indicators, for example, relative humidity distribution, temperature distribution, vapour pressure distribution, etc. The level of acceptance of the average convective mass transfer coefficient, h_m, obtained from the CFD simulation run is based on the value of h_m obtained through the use of the Lewis relation and and analogous convective heat transfer coefficient, h_c, Figure 5.5 summarises the conflation technique in terms of the data exchange between HAM and CFD for the humidity coupling.
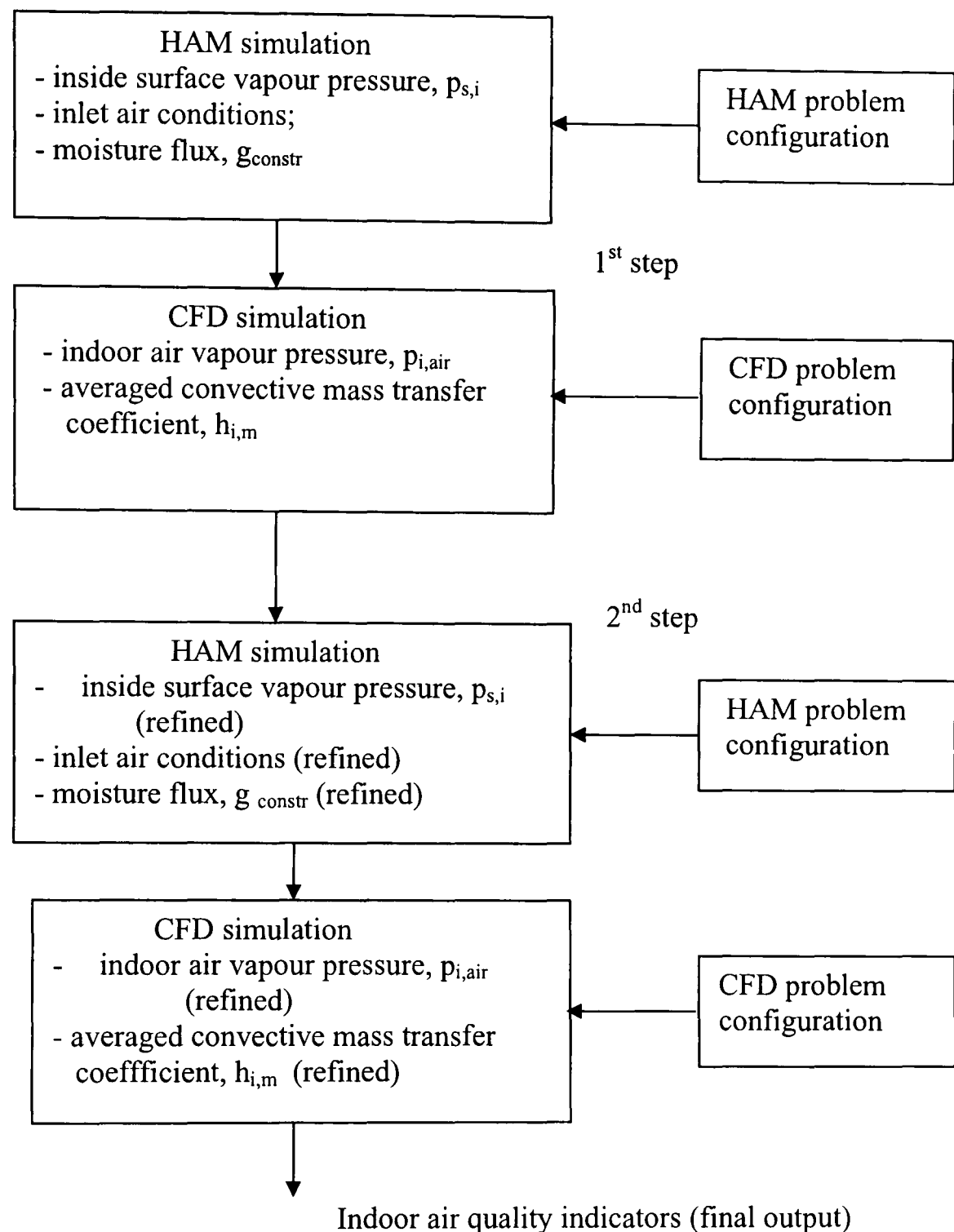
Figure 5.5: Illustration of the two time step conflation technique.

5.2.3 Coupling 1-D HAM model to 3-D CFD model

In finite volume methods, the conservation property can be used to transfer the mass fluxes and residuals from the fine (e.g. 3-D CFD model) to the coarse grid (e.g. 1-D HAM model) and vice versa. The co-located grid arrangement is used for the discretisation of the CFD domain

to facilitate the solution of the Navier-Stokes equations due to its computing advantages as mentioned in Chapter 3 (section 3.2). Grid co-location is basically a process of averaging values of dependent variables at the interface through interpolation using the central differencing scheme or the mid-point rule to obtain the discretised equation for the node or cell concerned. In the course of this discussion, an interface is defined as a rectangular surface that separates adjacent cells, for example, cell h_1 (solid node) for the 1-D HAM and cell c_1 (fluid node) for the 3-D CFD model separated by the internal fabric surface or interface, Y-Y in Figure 5.6.
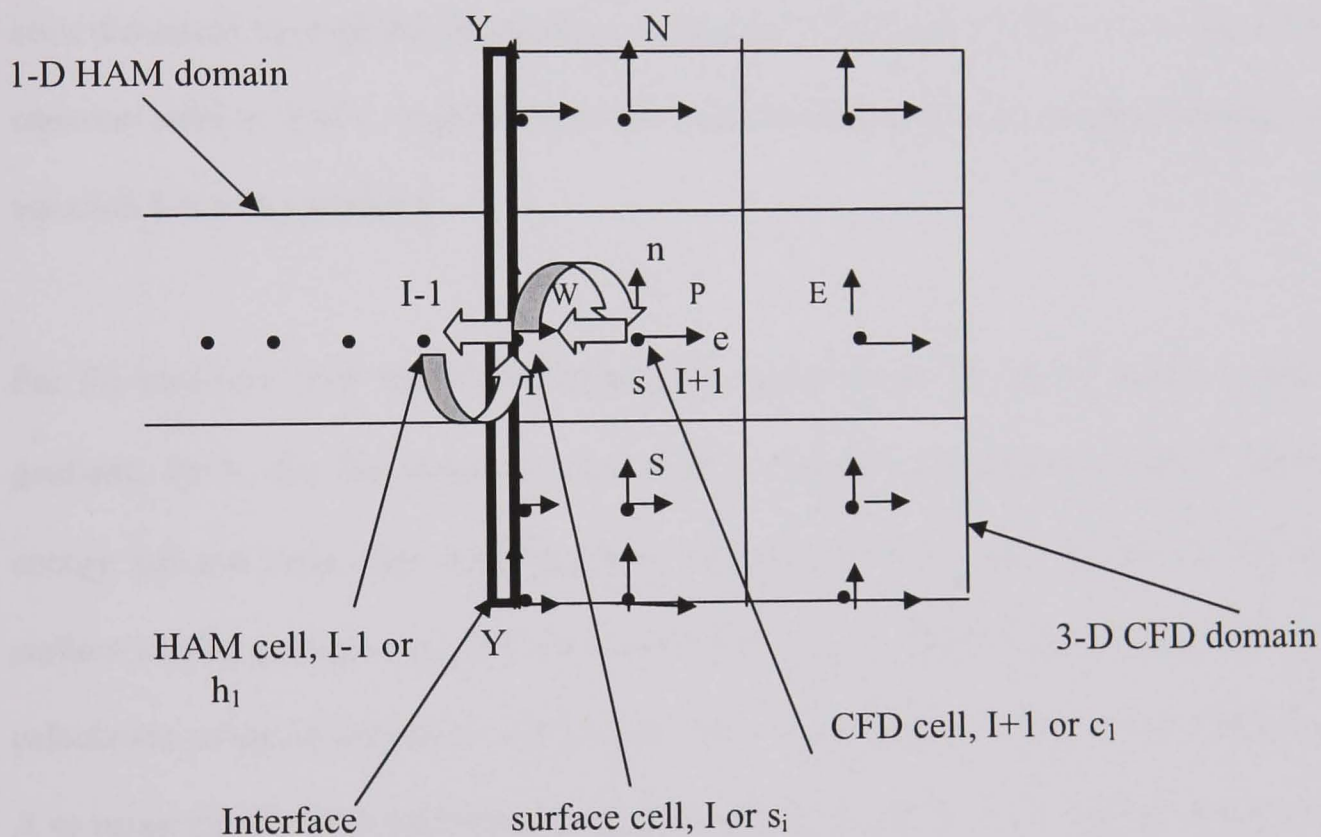
Figure 5.6:The interface and its adjacent cells.

Interfaces are described by heat and mass flow equations while cells are described by balance equations, for example, the heat balance equation, moisture balance equation and the humidity balance equation amongst others and the state laws. It could be inferred from Figure 5.6, that the two adjacent cells, h_1 and c_1, exchange data, e.g. inside surface vapour pressure, $p_{s,i}$, and

moisture flux, g_{constr}, from the solid type node or cell h_1 (HAM domain) through the surface node I or cell s_i, at the interface to cell c_1. In return, the fluid type node or cell c_1 (CFD domain) supplies cell h_1 (HAM) through the surface node I or cell s_i, with the averaged values for the convective mass transfer coefficient, $h_{i,m}$, and the vapour pressure of the indoor air, $p_{i,air}$, at the end of the time step used to effect the handshaking or the conflation of the two models. Figure 5.7 also shows a 1-D HAM model in conflation with a 3-D CFD model, with their relevant transport equations and a data exchange station. Characterisation of the energy transfer mechanism at the surface node, I, in relation to the solid node, I-1, and the fluid node, I+1, has been discussed through the illustrations in Figures F.1(a) and F.1(b) in Appendix F. The basic equation used in ESP-r, together with the self-coupling and cross-coupling terms, is given by equation F.6 of Appendix F.

For the moisture flow model, the dependent variables are the partial water vapour pressure gradient, $\partial p/\partial x$, for the moisture balance term and the temperature gradient, dT/dx, for the energy balance term. The input interface variables for the HAM model are the inside wall surface vapour pressure, $p_{s,i}$, and the vapour flux, g_{constr}.. These are determined from the HAM calculation using an iteration procedure of two nested iteration steps as provided in Appendix A or using the Gauss Seidel iteration process for the solution of the moisture equations and the matrix partitioning technique (Clarke 2001), for the solution of the energy equations as described previously. The inside surface vapour pressure, $p_{s,i}$ and the vapour flux, g_{constr}, are calculated from the HAM simulation run. These values are then supplied through the surface cell, s_i (data exchange station), to the CFD fluid cell, I+1, or c_1, to establish the boundary conditions for the CFD model. Similarly, for the CFD model the input variables are the room vapour pressure and temperature, the inlet air temperature and pressure, inlet air flow rate and

Figure 5.7:1-D HAM model in surface conflation with a 3-D CFD model

Hygrothermal Model:

Moisture balance term:

$$\rho_o \zeta \frac{\partial (p/p_s)}{\partial t} + \frac{dp_l}{dt} = \frac{\partial}{\partial x}\left\{ \delta^T{}_P \frac{\partial p}{\partial x} + D^P{}_T \frac{\partial T}{\partial x}\right\} + S \quad . \qquad (2.4)$$

Energy balance term:

$$\left[\rho_o \left\{ c_o + c_v u_v \right\} + c_l \rho_l\right]\frac{\partial T}{\partial t} + h_v \frac{\partial \rho_v}{\partial t} + h_l \frac{\partial \rho_l}{\partial t} = \frac{\partial}{\partial x}\left\{ \lambda \frac{\partial T}{\partial x}\right\} - \frac{\partial}{\partial x} h_s J_v + g$$

Temperature/pressure field ; moisture field; heat fluxes; moisture fluxes

Data Exchange station

-Averaging of variables to extract 3-D information for use by the 1-D calculations
-Grid transformation and data exchange
-Interpolation between grids
- Moisture control algorithm / appraisal of surface conditions
-Variation of h_m/ variation of source terms

Vapour pressure field, Temperature field; Convective mass transfer fluxes; convectve mass transfer coefficient

Computational Fluid Dynamics Model (in tensor notation for 3-D)

Continuity Equation:

$$\frac{\partial \rho}{\partial t} + \frac{\partial}{\partial x_I}(\rho u_i) = 0 \quad . \qquad (3.2)$$

Navier-Stokes Equations:

$$\frac{\partial}{\partial t}(\rho u_i) + \frac{\partial}{\partial x_j}(\rho u_i u_j) = -\frac{\partial p}{\partial x_i} + \frac{\partial}{\partial x_j}\left[\mu \left\{\frac{\partial u_i}{\partial x_j} + \frac{\partial u_j}{\partial x_i}\right\}\right] - \rho g \beta (T_\infty - T) \quad . \qquad (3.3)$$

Energy Equation:

$$\frac{\partial}{\partial t}(\rho C_p T) + \frac{\partial}{\partial x_i}(\rho u_i C_p T) = \frac{\partial}{\partial x_i}\left[k \frac{\partial T}{\partial x_i}\right] + S_c \qquad (3.4)$$

Concentration (water vapour) Equation

$$\frac{\partial}{\partial t}(\rho p_w) + \frac{\partial}{\partial x}\left[\rho u\, p_w - \left\{\frac{\mu}{Sc} + \frac{\mu_t}{\sigma_{pw}}\right\}\frac{\partial p_w}{\partial x}\right] + \frac{\partial}{\partial y}\left[\rho v p_w - \left\{\frac{\mu}{Sc} + \frac{\mu_t}{\sigma_{pw}}\right\}\frac{\partial p_w}{\partial y}\right] + \frac{\partial}{\partial z}\left[\rho w p_w - \left\{\frac{\mu}{Sc} + \frac{\mu_t}{\sigma_{pw}}\right\}\frac{\partial p_w}{\partial z}\right] = S_{pw} \qquad (3.78)$$

for k-transport:

$$\frac{\partial}{\partial t}(\rho k) + \frac{\partial}{\partial x_j}(\rho u_j k) = \frac{\partial}{\partial x_j}\left\{\frac{\mu_t}{\sigma_k} \cdot \frac{\partial k}{\partial x_j}\right\} + \mu_t \left\{\frac{\partial u_i}{\partial x_j} + \frac{\partial u_j}{\partial x_i}\right\}\frac{\partial u_i}{\partial x_j} - \rho \varepsilon - g \beta \frac{\mu_t}{\sigma_t}\frac{\partial T}{\partial z} \qquad (3.60)$$

for ε-transport:

$$\frac{\partial}{\partial t}(\rho \varepsilon) + \frac{\partial}{\partial x_j}(\rho u_j \varepsilon) = \frac{\partial}{\partial x_j}\left\{\frac{\mu_t}{\sigma_\varepsilon}\frac{\partial \varepsilon}{\partial x_j}\right\} + C_1 \varepsilon \mu_t\left\{\frac{\partial u_i}{\partial x_j} + \frac{\partial u_j}{\partial x_i}\right\}\frac{\partial u_i}{\partial x_j} - C_2 \rho \frac{\varepsilon^2}{k} - C_1 \varepsilon\, g \beta \mu_t \frac{\partial T}{\partial z} \qquad (3.61)$$

velocity, as well as the relative humidity. Solution for the CFD model is obtained using the sequential solution procedure as detailed in Appendix C. The output from CFD after the 1st time step, and subsequent resolution of the internal fabric surface through the configuration mechanism (section 5.3), are the average convective mass transfer coefficient, h_{im}, and the indoor air vapour pressure, $p_{i,air}$. These updated values from the CFD model serve as the input variables for the 2nd time step simulation run by HAM. By 'updated values', it is implied that the average value obtained for the convective mass transfer coeffcient, h_{im}, is acceptable by the controller via a moisture control algorithm when such value compares favourably with that obtained when the convective heat transfer coefficient, h_{ic}, and the Lewis relations as given by equation 4.17 (Table 5.3) is used for its determination. At the end of which the pertinent data for indoor air quality, e.g. vapour pressure distribution, temperature distribution, relative humidity distribution, etc within the building enclosure are determined.

5.3 Configuration mechanism

The configuration mechanism in relation to the conflation of the HAM and CFD models involves the appraisal of the conditions at the internal fabric surfaces taking cognizance of the influencing factors for the determination of the convective mass transfer coefficient, h_{im}. These factors are: the prevailing vapour pressure gradient, $\partial p_v / \partial x$, the surface-to-air vapour pressure difference, the surface-to-air temperature difference, the nature and type of convective flow depending on the prevailing Grashof number, Gr, Rayleigh number, Ra, and Reynolds number, Re. For the convective heat transfer coefficient, $h_{i,c}$, the prevailing temperature gradient, dT/dx, and the surface-to-air temperature difference are considered. It is important that the respective solvers corresponding to the building's thermal/ zonal network air flow/ moisture flow (HAM),

electrical power, HVAC and CFD conservation equation sets are arranged to act co-operatively. The configuration mechanism ensures that the turbulence model is properly configured at each time step. Through the use of a moisture control algorithm via a controller, which operates on a set of control laws, appraisal of the internal fabric surfaces is carried out for eventual variation of the convective mass transfer coefficient, $h_{i,m}$, and/or variation of the source terms in either CFD or HAM or both for the resolution of moisture migration problems across the interface.

Moisture migration across the interface results in moisture absorption into the building envelope for a positive vapour pressure gradient across the interface, for example during cold weather in winter the vapour pressure inside a building is usually higher than that outside, resulting in vapour diffusion through the walls from the indoor space, through the porous medium (solid walls), to the outside environment. The result is the general increase in thermal conductance of each cell element and hence the overall U value. For the scenario that the building enclosure is colder compared to the outside environment, a negative vapour pressure gradient results in the moisture diffusion from the outside environment through the porous medium into the building enclosure (moisture desorption). The next sub-section is a discussion on factors that impact the convective mass transfer coefficient, $h_{i,m}$, and the convective heat transfer coefficient, $h_{i,c}$.

5.3.1 Factors that impact on the convective heat and mass transfer coefficients

The important parameters for the information exchange at the interface between HAM and CFD models for the hygro-thermal coupling are the convective mass transfer coefficient for the humidity coupling and the convective heat transfer coefficient for the thermal coupling. For the humidity coupling, which is the main theme for this project, much emphasis is placed on the

parameter, convective mass transfer coefficent, $h_{i,m}$. This is very much dependent on the prevailing partial water vapour pressure gradient, $\partial p_v/\partial x$, normal to the internal surface of the wall, surface-to-air vapour pressure difference, surface-to-air temperature difference, the temperature gradient, Rayleigh number, Ra, Grashof number, Gr, and the Reynolds number, Re at the internal fabric surface and within the building enclosure. This may be expressed as

$$h_{i,m} = f\ \partial p_v/\partial x,\ p_{vs},\ p_{v,i,air},\ \Delta p_{v\ s\to i,air},\ \Delta T_{s\to i,air},\ dT/dx;\ \text{flow conditions (Ra,Gr and Re)}.\quad (5.4)$$

Table 5.2 shows the classification of the type of convective flow regimes in relation to the dimensionless parameters, Ra, Gr and Re (Beausoleil 2000), and the dependent parameters for the determination of the convective mass transfer coefficient, $h_{i,m}$.

Table 5.2: Convection heat and mass transfer coefficient and its dependent variables.

Convective heat and mass transfer coefficient, h_{ic} $h_{i,m}$			
Type of convective flow regimes	**Prevailing water vapour pressure gradient at the interface, $\partial p_v/\partial x$**	**Prevailing surface-to -air vapour pressure difference, $\Delta p_{v\ s\to air}$**	**Prevailing surface-to-indoor air temperature difference $\Delta T_{s,i\to i,air}$**
Free convection $Gr/Re^2 \gg 1$		Surface vapour pressure higher than indoor air vapour pressure, $p_{v,s} > p_{v\ i,air}$	surface temperature warmer than indoor air temperature, $T_{s,i} > T_{i,air}$
Forced convection $Gr/Re^2 \ll 1$	Moisture absorption $\partial p_v/\partial x > 0$		
Mixed convection $Gr = Re^2$	Moisture desorption $\partial p_v/\partial x < 0$		
Laminar flow $Re < 2300$		Surface vapour pressure lower than indoor air vapour pressure, $P_{v,s} < p_{v\ i,air}$	Surface temperature colder than indoor air temperature, $T_{s,i} < T_{i,air}$
Turbulent flow $Re > 2300$	Zero vapour pressure gradient $\partial p_v/\partial x \approx 0$		

5.4 Moisture control algorithm

Due to the presence of the solid boundary (interface) the flow behaviour and turbulence structure are considerably different from the free turbulent flow within the building enclosure.

It is assumed that free and natural convection prevails within the building enclosure but other cases might lead to the occurrence of forced or mixed convection flow within the enclosure, for example through localised infiltration and/or high velocity air flows located within the enclosure can be considered using similar approach together with the Lewis relations and analogous convection heat transfer coefficient.

.

Control laws

Since the convective mass transfer coefficient, h_m, depends on the water vapour pressure gradient, the surface–to-air vapour pressure difference, the surface-to-air temperature difference as well as the type and nature of convective flow at the surface (Table 5.2), it is evident that the envisaged moisture control algorithm evolves around these parameters for the formulation of the operating control laws. These control laws adapt the convection heat and mass transfer calculations in response to the prevailing conditions at the internal fabric surfaces and within the indoor air space, for example, moisture absorption or desorption due to existing vapour pressure difference across the porous medium (wall) or buoyancy-driven indoor air motion due to surface–to-indoor air temperature difference.

The first control law represents a typical cold weather condition:

1. $\partial p_v/\partial x > 0$

This control law relates to a condition that, the existing vapour pressure difference across the wall results in moisture absorption at the internal fabric surface, with the flow direction from inside the building enclosure through the porous medium to the outside environment.

Similarly, the second control law represents a typical summer/autumn weather condition.

2.. $\partial p_v/\partial x < 0$

The resultant negative surface-to-air vapour pressure difference results in moisture desorption at the interface, with moisture flow direction from the outside environment through the porous medium into the building enclosure.

In both cases, $\partial p_v/\partial x$ represents the vapour pressure gradient at the interface and it is the drive potential for moisture diffusion through the porous medium with the vapour pressure as the dependent variable in the moisture balance equation (Eq. 2.4). Considering the characteristics of Air-Vapour mixtures, it may be recalled that when there is a difference in concentration of the water vapour between two points of a solid material, there is a corresponding difference in partial pressure, The difference in partial pressure of the water vapour cause a flow of the water vapour from the point of higher concentration to the lower. When a partial pressure difference exists between the two sides of a material, for example, a porous medium, water vapour will diffuse through the material until the partial pressures of the water vapour are equalized. The rate of water vapour diffusion is determined by the partial pressure difference, Δp_v, the length of the flow path, Δx and the permeability of the water vapour, δp_v, of the water vapour flow through the porous medium. The maximum amount of water vapour is limited by the temperature. In this regard, the water vapour gradient may be defined as the ratio of the difference in partial pressure of the water vapour, Δp_v, to the length of the flow path in the x-direction, Δx of the porous medium.

A third control law relates to the condition that room air flow may be caused by surface-to-air temperature difference resulting in buoyant condition within the indoor air space, whereby the inside surface is colder than the indoor air.

3. $T_{s,i} < T_{i,air}$

where $T_{s,i}$ is the inside surface temperature and $T_{i,air}$ the indoor air temperature.

Alternatively, for the condition that the driving force due to surface-to-air temperature difference results in the inside surface being warmer than the indoor air (stratified condition), the corresponding control law is given by

4. $T_{s,i} > T_{i,air}$

Depending upon the surface-to-air temperature difference, a flow within a room may be buoyant or stably stratified for thermal simulation. For humidity coupling, however, the surface-to-air vapour pressure difference is used for classification of the prevailing flow regime at the internal fabric surface. With horizontal surfaces, for example the ceiling or floor, a test is performed using the air point and the surface temperature prior to the setting of the flag by the controller (Beausoleil-Morrison 2000). Within this project emphasis is placed on vertical surfaces relating to flow through porous medium or solid walls.

Controller

With reference to the moisture control algorithm shown in Figure 5.8, the controller operates via the set of control laws mentioned previously. It examines and appraises the condition at the internal fabric surfaces taking into consideration the type and nature of convective flow, for example, free convection, forced convection, etc and other factors that impact on the convective mass and heat transfer coefficients, h_m and h_c, as presented in Table 5.2. The controller is empowered to address humidity-related problems, for example due to inaccurate CFD mass transfer coefficient predictions after the first time step, which can lead to errors in the simulation results for the HAM model. In principle, the algorithm appraises a configuration through the Controller to assign an appropriate convective mass transfer coefficient, h_m correlation (Table 5.3) to each internal surface, with minimal data input from the user. As the simulation evolves, the algorithm toggles between the h_m correlations in response to the

131

prevailing convective regime at the internal surface. A scheme is adapted within the algorithm in which the applicable control law for the flow regime at the internal surface is attributed with an ICOR flag to associate it with a suitable h_m correlation, for example, ICOR flag 1, represents the application of control law 1, that relates to the case of moisture absorption at the internal fabric surface for free convection flow.

The selection of an appropriate scheme by the Controller relates to its capabilities to prescribe the nature and type of convective flow as well as the examination and appraisal of prevailing surface condition at the internal fabric surfaces. This facilitates the resolution of moisture migration problems at the interface by the Controller through variation of the convection mass transfer coefficient, h_m using the available h_m correlations or through source term adjustments on the CFD and HAM models via the respective governing equations.

Figure 5.8 shows an illustration of the moisture control algorithm. With reference to the control algorithm of Figure 5.8, the following functional signals can be initiated by the controller using the flagging concept for the simulation as follows:

A1.Free convection flow regime at the internalconvection flow at the internal fabric surface,

A2.Forced convection flow regime at the internal fabric surface, and

A3.Mixed convection flow at the internal fabric suraface.

The next sub section relates to the case of free convection flow, A1, at the internal fabric surface.

5.4.1 Free convection flow

For the case that free convection flow regime, A1, prevails at the internal fabric surface and with reference to control laws 1 and 2 relating to moisture absorption and desorption at the

interface, the moisture control algorithm of Figure 5.8 can be interpreted as follows:

1   prevailing vapour pressure gradient, $\partial p_v/\partial x > 0$ or moisture absorption ;

2   prevailing vapour pressure gradient, $\partial p_v/\partial x < 0$ or moisture desorption,

1a CFD adjustments involving either the variation of the convective mass transfer coefficient, h_m or source term adjustments of the governing equations or variation of the standard k-ε turbulence model, namely, the Low-Reynolds Number k-ε model, (LRNKEM) with its embedded wall damping functions or a combination of these corrective measures for the scenario that moisture absorption occurs at the interface;

2a HAM model adjustments involving source term adjustments of the governing equations for the occurrence of moisture desorption at the interface;

Depending upon the type and nature of prevailing convective flow regime at the internal fabric surface, for example for the condition that $Gr/Re^2 \gg 1$ (Table 5.2), free convection flow exist. Using the flagging concept, the controller sets the ICOR flag at A1 indicating the existence of free convective flow regime at the internal fabric surface (Figure 5.8). Upon the establishment of the type of convective flow regime, the next step is the examination and appraisal of the surface condition. The process of surface examination and appraisal by the controller is based on the control laws, which in turn evolves from consideration of the factors that impact on the the convection heat and mass transfer coefficients, h_c and h_m. For example, for the flow situation that a positive partial vapour pressure gradient (moisture absorption) exist at the interface, the controller calls for flag number 1, signifying that, the operating control law relates to that for a prevailing vapour pressure gradient at the internal fabric surface. Similarly, setting of flag 2 relates to a flow situation that a negative partial water vapour pressure gradient exist at the interface.

133

To facilitate the corrective measures to be effected towards the resolution of a prevailing moisture migration interfacial problems by the controller, a call is made for flag 1a, after the interogation to signify that CFD adjustment is required to be effected by the controller through:

- variation of convective mass transfer coefficient, h_m via the available convective mass transfer correlation shown in Table 5.3,

- adjustment of source terms of the governing equations for the CFD model, and

- variation of the standard k-ε turbulence model, namely the Low Reynolds Number k-ε model,

For the case that moisture desorption occurs at the interface,.the controller sets ICOR flag 2a for HAM model adjustments after the interogation for similar resolution..

to Controller

Controller

prescribes type & nature of convective flow

Free Convectio, A1

examines and appraises internal fabric surfaces

Surface condition 1 or 2

1 2

1 = moisture absorption
2 = moisture desorption
1a = CFD adjustment
2a = HAM adjustment

Moisture Absorption
$\partial p_v/\partial x > 0$

Moisture Desorption
$\partial p_v/\partial x < 0$

corrective measures by Controller

1a

2a

CFD adjustments

HAM adjustments

1a

2a

- h_m variation set ICOR to C!, C3 via h_m - correlation

- Source term adjustments

- Variation of k-ε turbulence model (LRNKEM)

Source term Adjustments on governing equations for HAM model

Is h_m value acceptable?

Is source term adjustment acceptable ?

no

no

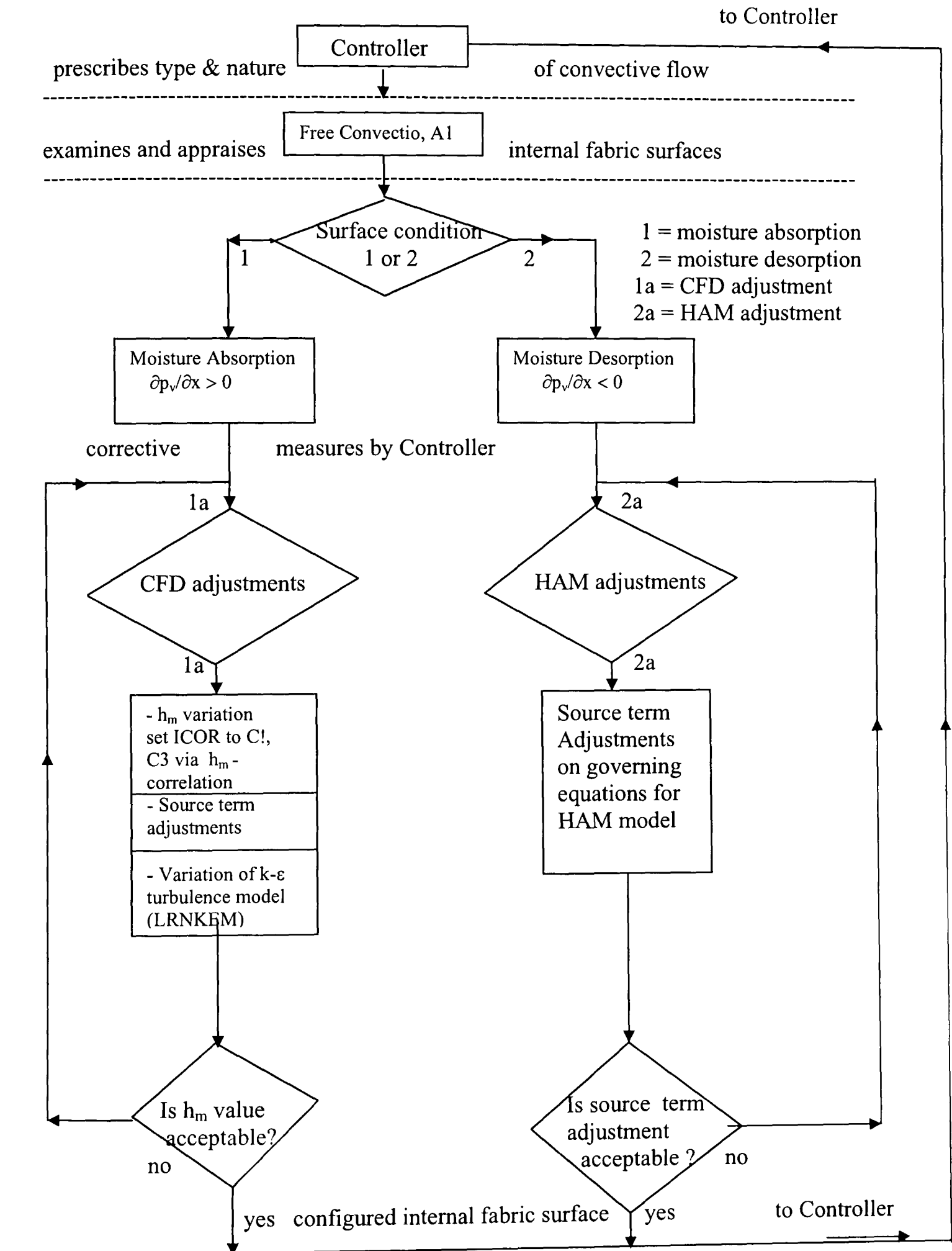yes   configured internal fabric surface   yes

to Controller

Figure 5.8: Moisture control algorithm – Free convection flow

Free convection flow within the building enclosure and at the internal fabric surfaces is considered within this project. Other cases that might lead to the occurrence of forced or mixed convection flow conditions within the enclosure. for example, through localised infiltration and/or high velocity air flow can be treated using similar approach as for the free convection flow. Attribution of convective heat transfer coefficient, h_c, to convective surfaces from available correlations for convective heat transfer coeffiicients with regards to thermal simulation (Beausoleil 2000), however calls for a different approach to address moisture migration problems at the interface. For humidity coupling and subsequently for hygrothermal simulation. the convective mass transfer coefficient, h_m, is obtained from the analogous h_c value and the Lewis relation or from the h_m orrelations presented in Table 5.3.

As mentioned previously in section 5.2.2 (two time step coupling) and 5.4.1, h_m variation is carried out by the CFD model until an acceptable average value is obtained for subsequent use by the HAM model. The average convective mass transfer coefficient, h_m, as supplied by the CFD model at the end of the 1st time step through the data exchange station (Figure 5.7) to the HAM model, is considered accurate and acceptable when the value obtained for h_m compares favourably with the analogous value for the convective heat transfer coefficient, h_c, and the Lewis relations or with other h_m correlation as presented in Table 5.3. For example. based on the Lewis relations and h_c, h_m is determined from equation (4.17) as

$$\frac{h}{h_m} = \frac{k}{D_{AB} L_e^n} = \rho C_p L_e^{(1-n)}. \tag{4.17}$$

where Le is the Lewis number and equals 0.95 for an air water vapour system. For all gas mixtures Le lies near 1 (Webb 1991). In equation 4.17. ρ is the density of air, C_p the specific heat at constant pressure. and h_c the heat transfer coefficient for water vapour. For most

building applications, the blowing parameter, $\zeta \leq 0.35$, is far below the critical value of 0.62, hence the h_m values based on the analogous relationship between h_c and the Lewis relations are considered to give satisfactory simulation results (White F.M 1988).

Table 5.3: Correlations for convective mass transfer coefficient, h_m.

Equations	Type of surface	Applicability	h_m correlations
Lewis relations, Le C1	building walls, floors, ceiling,	laminar/weakly turbulent flows, Indoor air flow	$\dfrac{h_c}{h_m} = \rho C_p Le^{(1-n)}$
Chilton-Colburn C2	building walls, floors, ceiling	laminar/weakly turbulent flows, Indoor air flow	$h_m = \dfrac{h_c}{\rho C_p}\left[\dfrac{Pr}{Sc}\right]^{2/3}$
International Energy Agency (IEA) C3	building walls, floors, ceiling	laminar/weakly turbulent flows, Indoor air flow	$h_m = \dfrac{h_c.\delta}{\lambda_a} = 7.4E-9\, h_c$
White, F.M. C4	walls and horizontal surfaces	Laminar flow $Re \leq 500,000$	$\dfrac{h_m L}{D_{va}} = 0.664\, Re_L^{4/5}\, Sc^{1/3}$.
		Turbulent flow $Re \geq 500,000$	$\dfrac{h_m L}{D_{va}} = 0.037\, Re^{4/5}\, Sc^{1/3}$

With reference to Table 5.3 (Chapter 4.3.1), Pr is the Prandtl number, Sc the Schmidt number, δ the water vapour permeability, λ_a the thermal conductvity of air and D_{va} the diffusion coefficient for air.

5.5 Moisture desorption/absorption at the interface

The maximum amount of water that can exist as vapour is set by the temperature, which also establishes the saturated vapour pressure. In practice it is better for a wall to have a more permeable surface so that it can dry to the interior if necessary. Vapour cconvection involves small air flows carrying moist air through penetrations (e.g. cracks, openings). Moist air can flow into a crack in a ceiling or wall assembly and find a path to an uninsulated area or to a colder part of the wall and form condensation. To control moisture flow, there is the need to treat the interior surface as an air barrier. Since convection impacts on small air flows finding their way into openings and uninsulated spaces, keeping a place well ventilated by opening windows or using fans can reduce the moisture level in the air within the enclosure if the exterior air is drier. As illustrated in Figure 5.8, moisture desorption or absorption at the interface can be resolved through variation of the convection mass transfer coefficient, h_m, as well as through source term adjustments or variation of the standard k-ϵ turbulence model of the CFD model and also through source term adjustment on the equations of the HAM model. The next section is a discussion on corrective measures through CFD adjustments

5.5.1 CFD model adjustments

Adjustment through the CFD model towards the enhancement of the resolution of the internal fabric surface within the framework of the surface conflation with the HAM model can be carried out through variation of the convective mass transfer coefficient, source term

adjustment on the governing equations or variation of the k-ε turbulence model, namely, the Low Reynolds Number k-ε model for the resolution of flow in the near-wall flow regime.

Variation of convective mass transfer coefficient, h_m

The humidity transfer between construction surfaces and the room air is governed by the convective mass transfer coefficient, h_m and the surface-to-air vapour pressure difference as well as the surface-to-air temperature difference. Figures 5.9(a) and 5.9(b) illustrate the mechanism for heat and vapour transfer through a solid wall. The mechanism includes their drive potentials, namely the temperature differences between the inside wall surface and the indoor air, $\Delta T_{s \to i,air}$, for the thermal simulation and vapour pressure difference between the inside wall surface and the indoor air vapour pressure, $\Delta p_{vs \to i,air}$ for the humidity transfer. To determine the heat transfer coefficient, for example, it is necessary to determine the real physical effect, represented by the heat transfer flux, q, (Figure 5.9a). In which case, h_c is dependent on the surface-to-air

temperature difference or the temperature gradient, dT/dx, across the interface as well as the type and nature of the prevailing convective flow regime at that surface. Similarly, to determine h_m, it is necessary to determine the physical effect represented by the convective mass transfer coefficient (Figure 5.9(b)). The mass transfer coefficient depends on the surface-to-air vapour pressure difference or the vapour pressure gradient, $\partial p_v / \partial x$ across the interface as well as on the type and nature of the prevailing convective flow regime at the interface (Maliska 2001). As described previously, the h_m variation is effected over the control-equation (equation 5.3) for humidity coupling at the data exchange station in Figure 5.7. Depending on the h_m output from the CFD model after the 1st time step and at the instance of the controller, a signal is initiated for a corrective measure to be effected.
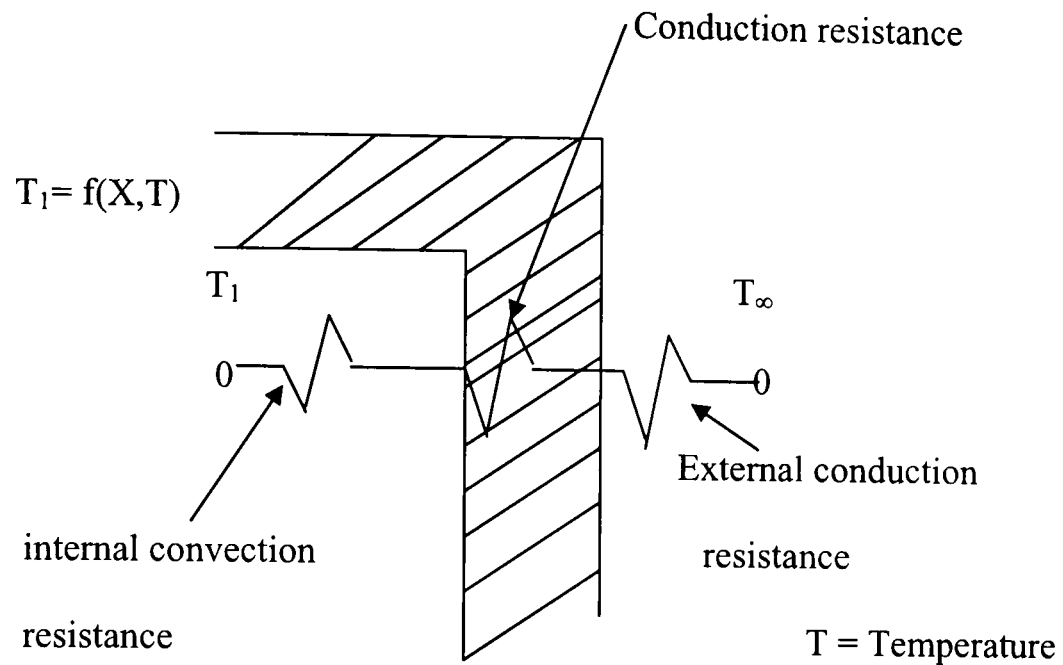
Figure 5.9(a): Global heat transfer coefficient (Maliska 2001).
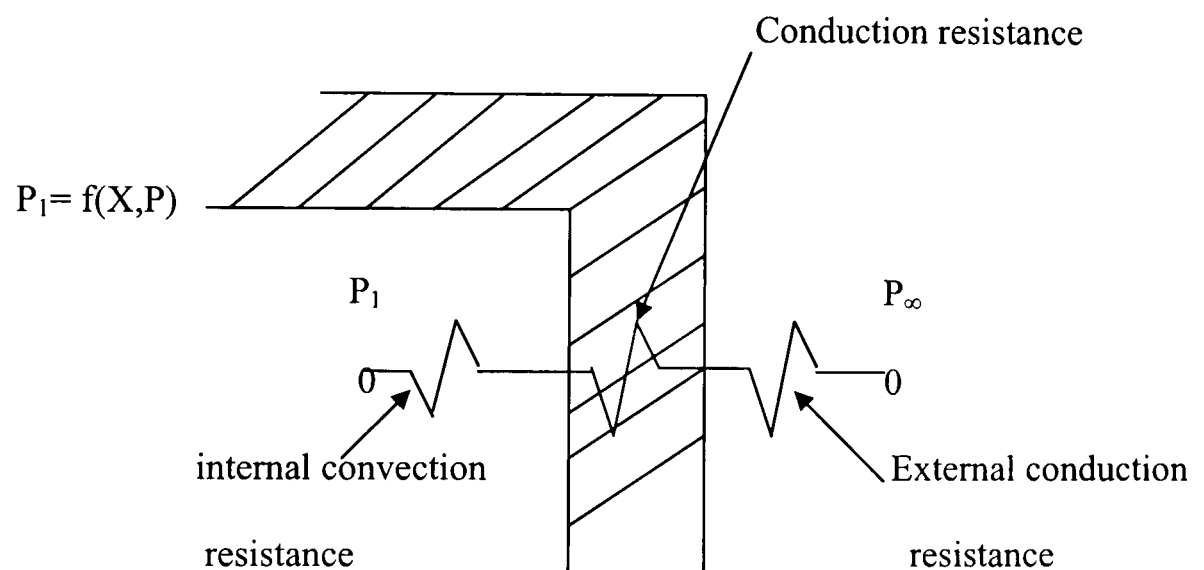

Figure 5.9(b): Global mass transfer coefficent (Maliska 2001).

As per the illustration of the algorithm (Figure 5.8), the variation of the convective mass transfer coefficient, is carried out via the h_m correlation shown in Table 5.3. For example, with the ICOR set at C3, the equation as presented by the International Energy Agency (IEA), which is applicable for indoor suefaces, namely, walls, floors, ceiling, etc.is invoked for the h_m variation. The value so obtained is then compared with the value obtained with the ICOR set at

C1, which relates to the h_m equations for Lewis relation. The h_m value obtained from the application of Lewis relation is considered as the benchmark for the h_m variation using other correlations, such as Chilton Colburn correlation, C2 as well as White correlation, C4, depending upon the prevailing control law as shown in the algorithm. Thus, the value of h_m obtained through the application of h_m correlations C2, C3 and C4 is deemed acceptable when the value obtained after the variation compares favourably with the value for h_m obtained from the Lewis relation calculation. The h_m value so obtained through Lewis relation is acceptable for most building application (White 1988). In the case that constant heat transfer coefficients are used for the simulation, a default value of $2.0.10^{-8}$ (m/s) may be used for the convective mass transfer coefficient at indoor surfaces (Carsten Rode 2001). Invariably the h_m variation could be effected directly with the ICOR flag set at C1 for the CFD adjustments.

Source term adjustments

Adjustments to the CFD model can be effected via the source terms of the governing transport equations to resolve problems with moisture absorption and desorption at the internal fabric surface. Buoyancy-induced convection conditions within an enclosure are induced entirely by thermal effects. With the introduction of buoyancy, two further parameters enter the flow field description: the temperature distribution, T (x, y, z), and the density distribution, ρ (x, y, z). The temperature field is expressed in the form of a thermal transport equation based on the energy conservation law, taking into account diffusion effects and thermal conductivity, while the density distribution is linked to the temperature and pressure fields by the equation of state for an ideal gas. The pattern of flow withinan enclosure is driven by conditions at the boundary and by the characteristics of the source terms within the enclosed volume as provided in standard literature (Malalasekera 1995). In order to establish the correct flow pattern, it is

necessary to ensure that the flow adjacent to the boundaries follows the boundary layer theory (Chapter 4). For infiltration or natural ventilation dominated air flow within the enclosure, the infiltrating flow rate must be included as part of the boundary source terms. Localised infiltration and/or high velocity flow gives rise to high values of diffusion coefficients for mass, momentum and heat. The flow breaks down in such instances generating a large number of small scales and undergoes a rapid transition to the fully turbulent regime. Such localised infiltration within the enclosure may be considered also as part of the boundary source term within the framework of turbulence modelling. The simulation of buoyancy generated flow and the transfer of heat and mass between boundaries is dependent on the accurate representation of the thermal and hygric properties at the boundaries as well as heat, air and moisture sources. In the case of convective sources, for example this is achieved by expressing the thermal characteristics of the sources in terms of temperature and heat transfer coefficients or U-values.

Pollutant sources, for example water vapour, are described by means of an emission characteristic and location within the grid. Source terms may be constant (for example, thermally insulated or adiabatic surfaces) or time dependent (e.g. through periodic heat or mass injection to obtain a desired simulation result). Within the enclosure, source terms such as heat supply and pollutant generation are represented by identifying the relevant grid location and specifying the source value. As the iteration proceeds, values at source locations are maintained at their pre-defined static or time-varying settings. As mentioned in Chapter 3.1 the boundary conditions enter the discretised equations by the suppression of the link to the boundary side and modification of the source terms. The appropriate coefficient of the discretised equation is set to zero and the boundary side flux, exact or linearly approximated, is introduced through the source terms S_u and S_P. The linearised source coefficients, S_u and S_P, may be heat or moisture

flux source at node P (domain cell of interest) for the u-velocity equation (subscript, u = u-velocity component; p = boundary cell of interest at point P). This approach is used to fix the flux of a variable at a cell face (Figures 3.7 and 3.8). For example, to set the variable ϕ at node P to a value ϕ_{fix}, the following source term modification is used in its discretised equation:

$$S_P = -10^{30} \text{ and } S_u = 10^{30} \phi_{fix} \qquad (5.5)$$

Addition of these sources to the discretised equations gives the expression (equation 3.6)

$$(a_P + 10^{30})\phi_P = \Sigma \; a_{nb} \; \phi_{nb} \; + \; 10^{30} \; \phi_{fix} \qquad (5.6)$$

where ϕ is the variable of interest (= P_v, T, C, etc). Since the source term, S_P, may be arbitrarily set so long as it is very large compared with all the coefficients in the original discretised equation, and if a_P and a_{nb} are also negligible, then the discretised equation implies that

$$\phi_P = \phi_{fix} \qquad (5.7)$$

which fixes the value of ϕ at P.

The discretised equations for one-, two- and three dimensional diffusion problems, for example, have been found to take the following general form (same as equation 3.6)

$$A_P \; \phi_P = \Sigma a_{nb}\phi_{nb} + S_u \qquad (5.8)$$

where Σ indicates the summation over all neighbouring nodes (nb), a_{nb} the neighbouring coefficients, a_W, a_E in 1-dimension, a_W, a_E, a_S, a_N in 2-dimension, a_W, a_E, a_S, a_N, a_B, a_T in 3-dimension and ϕ_{nb} the values of the property, ϕ at the neighbouring nodes and (S_u +$S_P\phi_P$) is the linearised source term. In all cases the coefficents around point P satisfy the following relation

$$a_P = \Sigma a_{nb} - S_P . \qquad (5.9)$$

Similarly, source terms can be included by identifying their linearised form $S \; \Delta P = S_u + S_P\phi_P$ and specifying values for S_u and S_P as previously described.

Variation of standard k-ε turbulence model

With reference to Figure 3.15 (Ch. 3), which shows a typical velocity distribution of flow near a solid wall (Malalasekera 1995), it is observed that, close to the wall the flow is influenced by the viscous effects. The mean flow velocity, U within the inner region depends on the distance y from the wall fluid density, ρ, viscosity, μ, and the wall shear stress, τ_w (equation 3.62).

$$U = f(y, \rho, \mu, \tau_w) .$$

(3.62)
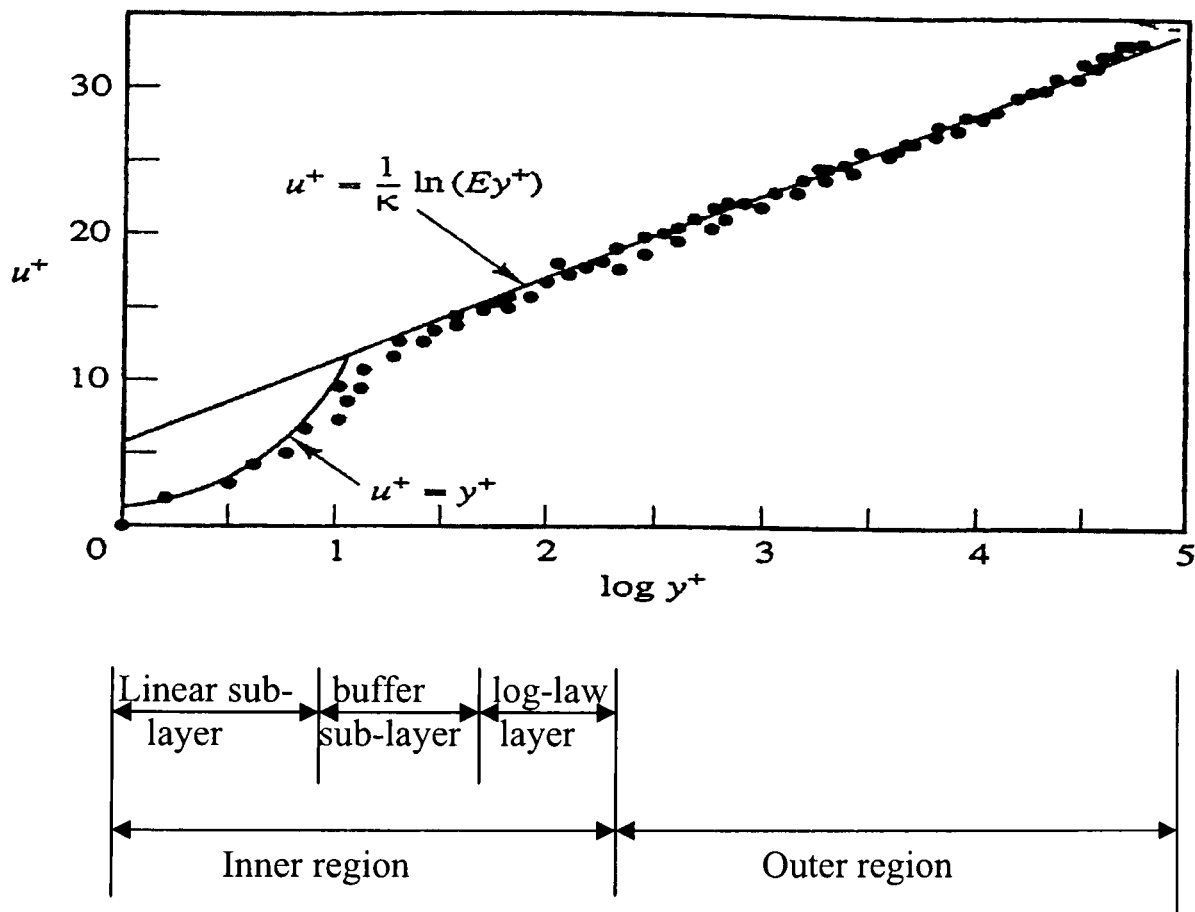
Figure 3.15: Velocity distribution near a solid wall.

Similarly, within the linear sub-layer, viscous stresses dominate the flow adjacent to the surface and the resolution of such flow conditions within the indoor space requires the application of the near-wall modelling concepts (Ch.3). For the reasons mentioned previously, the log-law wall function in combination with the standard k-ε turbulence model is not applicable for indoor air flow simulation (Ch.3). An alternative approach for the resolution of the flow

144

conditions near the solid wall is through the application of the extended k-ε turbulence model, the low-Reynolds Number k-ε model (LRNKEM). Wall damping is applied through the embedded damping functions to ensure that the viscous stresses take over from the turbulent stresses at low Reynolds numbers and within the viscous sub-layer adjacent to the solid wall (Figure 3.15). Application of damping functions contribute to the minimization of instabilities (from oscilatory behaviour) within the numerical solution. An approach is to include a viscous combination in the diffusion terms in equations (3.59 – 3.61) (Ch.3) for the CFD model through modification of the wall functions or through modification of the source terms.

$$\mu_t = C_\mu \rho k^2 / \varepsilon \tag{3.59}$$

where C_μ is an empirical constant and ρ the fluid density. The local distributions of k and ε require the solution of two additional transport equations, which are defined from the Navier-Stokes equations.

The **k–transport equation** is given by

$$\frac{\partial}{\partial t}(\rho k) + \frac{\partial}{\partial x}(\rho u k) + \frac{\partial}{\partial y}(\rho v k) + \frac{\partial}{\partial z}(\rho w k) = \frac{\partial}{\partial x}\left[\frac{\mu_t}{\sigma_k}\frac{\partial k}{\partial x}\right] + \frac{\partial}{\partial y}\left\{\frac{\mu_t}{\sigma_k}\frac{\partial k}{\partial y}\right\} + \frac{\partial}{\partial z}\left\{\frac{\mu_t}{\sigma_k}\frac{\partial k}{\partial z}\right\}$$

$$+ \mu_t\left\{\frac{\partial u}{\partial x} + \frac{\partial u}{\partial x}\right\}\frac{\partial u}{\partial x} + \mu_t\left\{\frac{\partial v}{\partial y} + \frac{\partial v}{\partial y}\right\}\frac{\partial v}{\partial y}$$

$$+ \mu_t\left\{\frac{\partial w}{\partial z} + \frac{\partial w}{\partial z}\right\}\frac{\partial w}{\partial z} - \rho\varepsilon - g\beta\frac{\mu_t}{\sigma_t}\frac{\partial T}{\partial z} \tag{3.60}$$

where σ_k is an empirical constant and μ_t is the eddy viscosity. The last terms in equations (3.60) and (3.61) represent the production of turbulence energy by buoyancy as given by Rodi et al (1980). Empiricism is introduced into the model through the five constants C_μ, σ_k, σ_ε, C_1 and C_2.

Similarly, the *ε-transport equation* is given by

$$\frac{\partial}{\partial t}(\rho\varepsilon) + \frac{\partial}{\partial x}(\rho u\varepsilon) + \frac{\partial}{\partial y}(\rho v\varepsilon) + \frac{\partial}{\partial z}(\rho w\varepsilon) = \frac{\partial}{\partial x}\left\{\frac{\mu_t}{\sigma_\varepsilon}\frac{\partial\varepsilon}{\partial x}\right\} + \frac{\partial}{\partial y}\left\{\frac{\mu_t}{\sigma_\varepsilon}\frac{\partial\varepsilon}{\partial y}\right\}$$

$$+ \frac{\partial}{\partial z}\left\{\frac{\mu_t}{\sigma_\varepsilon}\frac{\partial\varepsilon}{\partial z}\right\} + \frac{C_1\varepsilon\mu_t}{k}\left\{\frac{\partial u}{\partial x}+\frac{\partial u}{\partial x}\right\}\frac{\partial u}{\partial x}$$

$$+ \frac{C_1\varepsilon\mu_t}{k}\left\{\frac{\partial v}{\partial y}+\frac{\partial v}{\partial y}\right\}\frac{\partial v}{\partial y} + \frac{C_1\varepsilon\mu_t}{k}\left\{\frac{\partial w}{\partial z}+\frac{\partial w}{\partial z}\right\}\frac{\partial w}{\partial z}$$

$$- \frac{C_2\rho\varepsilon^2}{k} - C_1\frac{\varepsilon g\beta\mu_t}{k}\frac{\partial T}{\sigma_t\partial z} . \tag{3.61}$$

Launder and Spalding (1974) recommended values for these constants, as obtained from data-fitting for a wide range of turbulent flows:

$$C_\mu = 0.09; \quad \sigma_k = 1.00; \quad \sigma_\varepsilon = 1.30; \quad C_1 = 1.44; \quad C_2 = 1.92.$$

In this regard, the constants C_μ, C_1 and C_2 in equations 3.59 – 3.61 are multiplied by the wall damping functions f_μ, f_1 and f_2 respectively. These functions are themselves functions of the turbulence Reynolds number and/or similar parameters (equations 3.72 to 3.74). The equations of the low-Reynolds Number k-ε model (Malalasekera et al 1995) are

$$\mu_t = \rho C_\mu f_\mu k^2 / \varepsilon \tag{3.72}$$

$$\frac{\partial(\rho k)}{\partial t} + \text{div}(\rho kU) = \text{div}\left[\left[\mu + \frac{\mu_t}{\sigma_k}\right]\text{grad } k\right] + 2\mu_t E_{ij}.E_{ij} - \rho\varepsilon \tag{3.73}$$

$$\frac{\partial}{\partial t}(\rho\varepsilon) + \text{div}(\rho\varepsilon U) = \text{div}\left[\left[\mu + \frac{\mu_t}{\sigma_\varepsilon}\right]\text{grad }\varepsilon\right] + C_1 f_1 \frac{\varepsilon}{k} 2\mu_t E_{ij}.E_{ij} - C_2 f_2\rho\frac{\varepsilon^2}{k} \tag{3.74}$$

The wall–damping functions as given by Lam and Bremhorst (1981) in equation (3.75) are relevant in the resolution of problems of moisture migration at the interface. These are

$$f_\mu = \left[1 - \exp(-0.0156Re_y)\right]^2 \left\{1 + \frac{20.5}{Re_t}\right\}; \tag{3.75}$$

$$f_1 = \left\{1 + \frac{0.05}{f_\mu}\right\}^3 ; \quad f_2 = 1 - \exp(-Re^2_t) .$$

In function f_μ, the parameter Re_y is defined by $k^{1/2}y/v$, where y is the co-ordinate direction

146

normal to a solid wall and v the kinematic viscosity. The turbulence Reynolds number, Re_t is

defined as $Re_t = \vartheta l/v = k^2/(\varepsilon v)$, where the velocity scale, ϑ and length scale, l representative of

the large scale turbulence can be expressed as follows

$$\vartheta = k^{1/2} \; , \; l = k^{3/2}/l$$

The boundary condition may be taken as $\partial \varepsilon/\partial y = 0$, as proposed by Lam and Bremhorst et al

(1981). Similarly, in the consideration of the standard k-ε model for the modelling of buoyant

flows, the momentum equation in the direction of gravity should include the body force

resulting from buoyancy. For example, in two–dimensional flows with buoyancy in the y-

direction, the v-momentum equation is given by

$$\frac{\partial}{\partial t}(\rho v) + \frac{\partial}{\partial x}(\rho uv) + \frac{\partial}{\partial y}(\rho vv) = \frac{\partial}{\partial x}\left\{\mu\frac{\partial v}{\partial x}\right\} + \frac{\partial}{\partial y}\left\{\mu\frac{\partial v}{\partial y}\right\} - g(\rho - \rho_0) - \frac{\partial p}{\partial y} + S_v \qquad (5.10)$$

where $-g(\rho - \rho_0)$ is the buoyancy term, ρ_0 is a reference density and S_v the source term. Severe

under-relaxation is often required in the resolution of buoyancy-related problems. Additional

modification to the standard k-ε turbulence model for turbulent buoyant flow application is

made through the inclusion of a generation term relating to buoyancy in the k-equation.

5.5.2 Source term adjustments – HAM model

With reference to the two-time step dynamic coupling discussed in section 5.2.2, it is evident

that, the main adjustments required for the resolution of moisture migration problems via the

HAM model is through the adjustment of the source terms of the transport equations. Hence

the moisture and energy term balance equations (2.4 and (2.5) are given below. For the

moisture balance term (in one dimension):

$$\rho_0\xi \frac{\partial}{\partial t}(p/p_s) + \frac{d\rho_l}{dt} = \frac{\partial}{\partial x}\left\{\delta^T{}_P \frac{\partial p}{\partial x} + D^P{}_T \frac{\partial T}{\partial x}\right\} + S_g \qquad (2.4)$$

where ρ is density (kg/m^3; 0 and 1 denote porous media and liquid respectively), ξ the moisture storage (kg/kg), p the partial water vapour pressure (Pa), p_s the saturated vapour pressure (Pa), δ^T_p the water vapour permeability due to vapour pressure gradient when the second driving potential is the temperature gradient (kg/Pa.m.s), D^P_T the moisture diffusion coefficient when the second driving potential is the vapour pressure gradient, S_g the moisture source term. For moisture transport by vapour diffusion, the driving potential is the partial water vapour pressure gradient. For the energy balance term (in one dimension):

$$\left[\rho_0\left\{c_0 + c_v u_v\right\} + c_l\rho\right]\frac{\partial T}{\partial t} + h_v\frac{\partial\rho_v}{\partial t} + h_l\frac{\partial\rho_l}{\partial t} = \frac{\partial}{\partial x}\left[\lambda\frac{\partial T}{\partial x}\right] - \frac{\partial}{\partial x}h_s J_v + g \qquad (2.5)$$

where c is the specific heat of water vapour, u the moisture content, T the teperature, λ the thermal conductivity, J_v the vapour mass flux (kg/m^{2}s due to phase change, J_v is negative for adsorption and condensation and positive for desorption and evaporation phenomena); g the source of heat, h_v, h_l and h_s the enthalpies (J/kg) of vapour, liquid and moisture flux source respectively. From equations (2.4) and (2.5) the source term contributions are;

1. S_g = moisture source term in the moisture balance equation (Eq. 2.4) and

2. g = source of heat flux in the energy balance equation (Eq. 2.5).

Due to difficulties associated with the dependence of the heat flux term on the moisture flow direction, heat flux due to vapour transfer, $h_s J_v$ (or $h_s.m_{vdot}$) in equation (2.5) is treated as a source term. This implies that source term adjustment can be carried out through the variation of this parameter via its dependent variables, notably the partial water vapour pressure.

Heat flux due to vapour flux = $h_s J_v$; where J_v is the vapour mass flux = $h_m (p_{v,s} - p_{vi,air})$, h_s the enthalpy of vapour flux (J/kg), $p_{v,s}$ the partial water vapour pressure at the inside surface of the wall and $p_{vi,air}$ the partial water vapour pressure of the indoor air.

In summary, a conflation approach has been presented in this chapter. The approach entails the application of a moisture control algorithm which operates via a controller for the examination and appraisal of the prevailing surface conditions as well as for the resolution of moisture migration related problems, for example, moisture absorption or desorption at the internal fabric surfaces during the simulation. The control laws for the algorithm are based on the factors impacting specifically on the convective mass transfer coefficient for the humidity coupling and on the convective heat transfer coefficient for the thermal coupling. The resolution of the moisture absorption problem is achieved through the variation of the convective mass transfer coefficient via a set of correlations for convective mass transfer coefficients, having the correlation C! (Table 5.3, Lewis relation) as its benchmark, source term adjustments and through the variation of the standard k- ε turbulence model through application of the Low Reynolds number k- ε model with its embedded wall damping functions within the framework of near-wall modelling for the CFD model adjustments and through source term adjustment for the HAM model in the case of moisture desorption at the internal fabric surface.

6.1 Conclusion

The quality of the indoor air is often expressed as the extent to which human requirements are met. Indoor air quality is influenced by changes in building operation, occupant activity and the outdoor climate. Humidity in indoor spaces is one of the most important factors in the determination of indoor air quality. Humidity extremes can create indoor air quality problems because excessively high or low relative humidities can cause discomfort to occupants, while high relative humidities can promote the growth of mould and mildew on building surfaces. Regulating the indoor temperature and humidity in buildings (usually between 19^0C and 26^0C and 50% and 60% RH), plays a dominant role towards the mitigation of the effects of higher humidities within building enclosures. Thus, moderation of the indoor relative humidity is an important requirement for a healthy indoor environment because it affects the perception of air quality, occupant health (asthma, respiratory illness, etc.), building durability, material emissions and energy consumption. Other non-relative humidity factors (e.g. VOCs, $CO2$, etc). influencing indoor air quality have been discussed in Chapter 1. Similarly, application of appropriate building materials, which are vapour permeable and highly hygroscopic can contribute to the maintenance of good air quality.

The conceptual framework laid down through this thesis for the subsequent development of the analytical tool addresses these humidity-related problems through the coupling of a heat and mass transfer (HAM) and computational fluid dynamics (CFD) model. From the findings of the IEA enquiries, it is evident that for the determination of the essential parameters for indoor air quality an integrated simulation of both HAM and CFD models is required.

Modelling of moisture transfer processes to determine potential moisture-related problems in building components is severely limited by the lack of reliable data on moisture transfer and storage propeties of building materials. The mathematical description for the prediction of building hygrothermal dynamics is complex, due to the non-linearities and inter-dependence among several variables, for example, vapour pressure, temperature, etc. The parametric uncertainties in the modelling, simulation time-steps, external climate, building schedules, ground temperature, the pattern of pore size and shape distribution that exist in the porous medium and how the voids are inter-connected etc. also contribute to increase this complexity. The predictive ability of HAM model simulation depends on the accuracy and reliability of the material properties used, such as dry and wet heat capacity, dry and moist thermal conductivity, sorption and desorption isotherms, suction curves, water vapour permeability, moisture diffusivity, thermal moisture diffusivity and air permeabilities in both dry and wet stages Nathan Mendes 2001). These limitations have been the set back for the development of 2D and 3D HAM models.

The co-located grid arrangement, unlike the staggered grid type, uses the same control volume for all the variables in the solution of the discretised Navier-Stokes equations and so has been adopted in this project. The mass flux through any control volume face is determined by interpolating the velocities at two nodes on either side of that face. Comparatively, the co-located grid approach converges faster and offers implementation advantages as well savings in computational time. Theoretical adaptation of the Navier-Stokes equations is proposed that may be incorporated within existing code that employ the staggered grid arrangement.

Approaches to the turbulence modelling of indoor air flow systems have been presented, with due consideration given to the boundary conditions at the wall and for the building

enclosure (inlet, outlet, etc.). The use of the low-Re k-ε model as a tool to represent flow in the near-wall zone utilising embedded damping functions (Lam and Bremhorst 1981) has been highlighted. The log-law model is not relevant to simulation in indoor spaces (weakly turbulent). This is because the log-law wall functions poorly characterise the boundary layer of many room air flows and also because with the k-ε model it poorly predicts the turbulent diffusion in weakly turbulent regions. The pattern of flow within an enclosure is driven by conditions at the boundary and by the charateristics of the source terms within the enclosed volume. It is necessary to ensure that flow adjacent to surfaces within the building enclosure conforms to the boundary layer theory.

The principal manifestations of the three classified boundary layers, namely velocity, thermal and concentration are friction, convection heat transfer and convection mass transfer. Based on the analogous relations between heat and mass transfer for a particular geometry, it follows that if a convection mass transfer problem has the same geometry, flow pattern and boundary conditions as a known heat transfer problem, then the heat transfer correlation may be converted to a mass transfer correlation by replacing h_c by h_m, Pr by Sc, and Nu by Sh, for either laminar or turbulent flow. It is evident from the review that for most building applications, the Lewis relation for the conversion of convection mass transfer coefficient, h_m, to convection heat transfer coefficient, h_c, and vice-versa, provides satisfactory simulation results so long as the critical value for the wall blowing parameter (ζ = 0.62) is not exceeded. In most practical cases, the operation is in the range $0 \leq \zeta \leq 0.2$ (White 1988).

The conceptual framework for the conflation of HAM and CFD models utilises a configuration mechanism which functions over a moisture control algorithm.

A controller, whicg is responsible for the examination and appraisal of the surface conditions at the internal fabric surface during the simulation, gives an indication of the the type of surface conditions prevailing at the interface based on a set of control laws and effects an appropriate action within the capabilities of the configuration mechanism to resolve moisture absorption and desorption at the interface. Depending on the outcome of the surface appraisal by the controller, the required adjustments (as discussed in section 5.5.1 and 5.5.2) are carried out on either the CFD or HAM model or both models if required.

In comparison with other indoor air quality prediction tools, the conceptual framework presented for the subsequent development of an analytical tool considers construction moisture desorption and absorption at the interface and has the capabilities to capture the interaction between the building materials, the sources of moisture flow through the porous medium, namely, through vapour diffusion, vapour convection, etc. and the indoor air within the enclosed volume.

6.2 Future work

6.2.1 Coding

To evaluate the building hygrothermal performance, a code extension to the existing CFD programm (e.g. esrudfs), which uses the staggered grid arrangement must be carried out to include a co-located grid arrangement for the discretisation process; a source term contribution from the construction moisture into or out of the building enclosure; the loose coupling algorithm for the conflation activity; the configuration mechanism; and the incorporation of the low-Reynolds number k-ε model to capture the flow characteristics of the near-wall region. It is recommended that a CFD code, which is adaptable to the co-located grid arrangement, be used for the extension to the standard k-ε turbulence model

6.2.2 Material properties

The surveyed literature indicates that there is a lack of data concerning material properties such as vapour permeability, moisture diffusivity, etc. Future experiments on building materials should concentrate on the study of sorption behaviour of building and furnishing materials to obtain more data on sorption and desorption rates.

6.2.3 Moisture transport models

There is a need to improve upon the existing moisture transport models to facilitate a statistical variation of material properties and outdoor weather conditions to assess the importance of uncertainties in input data. Such models will permit an assessment of the importance of material properties and identify target properties for manufacturers and designers to strive for. From the findings of the IEA 24 enquiry, it is evident that most modellers either over-simplify the analysis assumptions due to lack of data or due to negligence on the part of the modellers, the former being more pronounced. Promotion of a data acquisition scheme for hygric properties of building materials through a merit award scheme for participants would contribute immensely towards the improvement in the modelling of moisture transport prediction tools with specific reference to future conflation of 2D and 3D HAM models to 3D CFD models.

6.2.4 Experiments

An experimental laboratory, where varied experiments under hygrothermal conditions for building materials may be undertaken in order to demonstrate, at the full-scale, the interaction between indoor spaces, building envelope components and furnishings. It is essential to develop standard test methods to evaluate the hygrothermal performance of building systems using full-scale experiments and to allow systematic verification and validation of numerical models to facilitate future research work in this area.

APPENDIX A   MATHEMATICAL MODEL FOR HEAT AND MOISTURE

TRANSPORT THROUGH POROUS MEDIUM

For moisture flow only, considering the differential element in Figure A1.1. For a stationary, homogeneous, isotropic control volume (CV) with internal mass generation and without phase change, the law of mass conservation states that

$$
\left\{
\begin{array}{l}
\text{The rate of the } i_{th} \text{ species} \\
\text{mass storage in the} \\
\text{control volume}
\end{array}
\right\}
=
\left\{
\begin{array}{l}
\text{the rate of the } i_{th} \text{ species} \\
\text{mass entering through} \\
\text{the contol volume} \\
\text{bounding surface}
\end{array}
\right\}
+
\left\{
\begin{array}{l}
\text{the rate of } i_{th} \\
\text{species mass} \\
\text{generation in the} \\
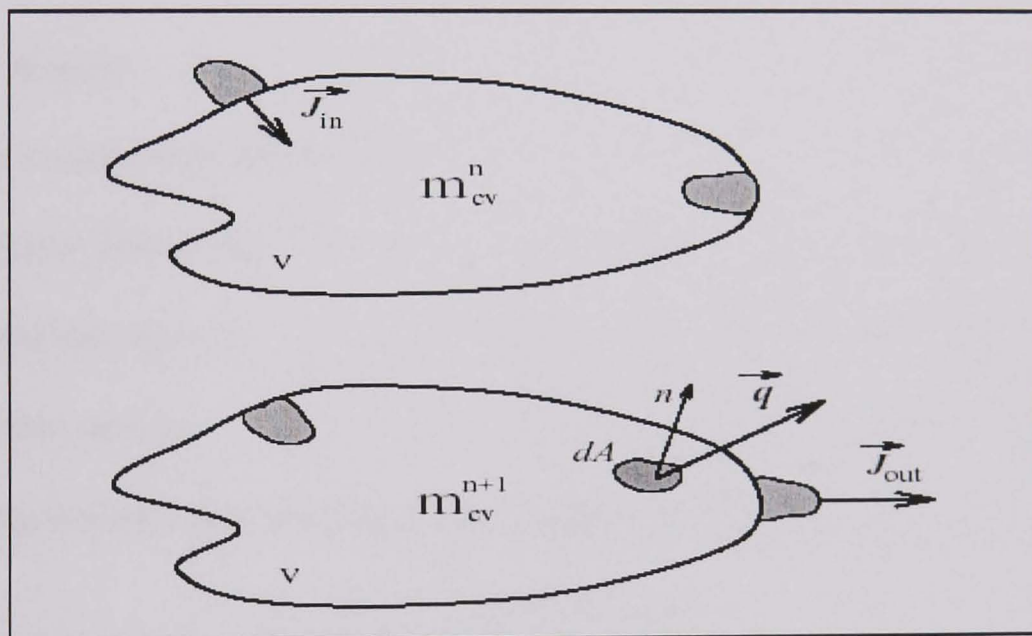\text{control volume.}
\end{array}
\right\}
\tag{A1}
$$

Figure: A1.1: Differential element for mass diffusion.

For 1-dimensional analysis:

$$
\rho_0 \, \frac{\partial u_i}{\partial t} = - \, \nabla.\vec{J}^F_i + S_i .
\tag{A.2}
$$

From Fick's law:

$$
\vec{J}^F_i = -D_F \, \nabla F .
\tag{A.3}
$$

Substitution of equation (A.3) in equation (A.2) gives

155

$$\rho_0 \frac{\partial u_i}{\partial t} = \nabla \, [D_F . \nabla F] + S_i \; . \tag{A.4}$$

For a constant diffusion coefficient, equation (A.4) simplifies to

$$\rho_0 \frac{\partial u_i}{\partial t} = D_F . \nabla^2 F + S_i \; . \tag{A.5}$$

There are four distinct stages in the wetting process of a porous system:

- the absorption stage at low relative humidity;

- vapour transfer stage;

- vapour and liquid transfer stage, and

- liquid transfer stage at high relative humidity.

Due consideration must be given to both water vapour and liquid water transfer in the modelling of moisture flow through building materials.

Vapour transfer

Moisture transfer may occur via

- molecular diffusion;

- thermal diffusion, or

- filtration motion.

According to Fick's law, the molecular diffusion is defined as

$$J^D_v = -D_{Pv} \nabla \rho_v \tag{A.6}$$

where J^D_v is the diffusion vapour flux (kg/m^{2}s), ρ_v the vapour concentration (kg/m^3) and D_{Pv} the diffusion coefficient in the porous medium (m^2/s). Similarly,

$$D_{Pv} = \upsilon \chi D_v \tag{A.7}$$

where υ is the tortuosity factor, χ, the volume fraction of air-filled open pores and D_v, the diffusion coefficient of vapour in air. Applying the perfect gas law upon the assumption that vapour behaves as an ideal gas in building applications gives

$$\rho_v = \frac{P_v}{R_v T} \; . \tag{A.8}$$

Substitution of equation (A.8) into equation (A.7) gives

$$\vec{J}^D_v = - D_{P_v} \frac{\nabla P_v}{R_v T} + D_{P_v} \frac{P_v \nabla T}{R_v T^2} \tag{A.9}$$

Thermal vapour diffusion is that caused solely by the temperature gradient through

a porous material. It is defined as

$$\vec{J}_{vT} = - D_T \nabla T \tag{A.10}$$

where D_T is the vapour thermal diffusion coefficient (kg/msK). Filtration flow of the

vapour occurs when a total pressure gradient exists. By Fick's law, vapour filtration motion

through bodies is given by

$$\vec{J}_v^{Ptot} = - D_{Ptot} . \nabla P_{tot} \tag{A.11}$$

where D_{Ptot} is the vapour filtration coefficient (s).

Liquid transfer

Liquid transfer may occur via molecular diffusion, thermal diffusion or filtration motion.

Liquid transfer by molecular diffusion through saturated porous materials can be expressed

by Darcy's law:

$$\vec{J}_l^D = - \rho_l \kappa \nabla \phi \tag{A.12}$$

where $\vec{J}_l^D$ is the liquid flux due to molecular diffusion (kg/m^{2}s), ρ_l the water density,

(kg/m^3); κ the material hydraulic conductivity (m/s) and ϕ the total hydraulic head (m). For

unsaturated media (Galbraith 1992), a modified form of Darcy's law can be used:

$$J_l^D = - D_{l,\gamma} \nabla \gamma \tag{A.13}$$

where $D_{l,\gamma}$ is the liquid permeability (s) and γ the the hydraulic potential (m^2/s).

The hydraulic potential consists of two elements:

- the *matrix potential, γ_m*, which is related to the pore water pressure caused by capillary

effects; and

- the *gravity potential, γ_g*, which is related to gravitational effects. Thus,

$$\gamma = \gamma_m + \gamma_g \qquad\qquad (A.14a)$$

or
$$\gamma = \frac{P_l}{\rho_l} + zgk \qquad\qquad (A14b)$$

where P_l is the pore water pressure (N/m^2), g the gravitational acceleration (m/s^2). z the height over a reference level (m) and k a unit vector in the positive z-direction. Substitution of Eq.(A.14) in Eq. (A.13) yields:

$$J_l^D = - D_{l,\gamma} \nabla P_l - D_{l,\gamma} \rho_l g k \Delta z \qquad\qquad (A.15a)$$

or
$$J_l^D = - D_{l,Pl} \cdot \nabla P_l - D_{l,z} \Delta z \quad . \qquad\qquad (A.15b)$$

The liquid molecular diffusion due to the gravity gradient may be in a lateral direction for some building elements, e.g. walls, and thus warrants a 2- or 3-dimensional analysis. However, for a 1-dimensional analysis, its effects may be neglected.

Liquid thermal diffusion in porous materials on the other hand, is estimated from the expression

$$\overrightarrow{J_l^T} = -D_{l,T} \nabla T \qquad\qquad (A.16)$$

where $D_{l,T}$ is the thermal liquid diffusion coefficient (kg/msK). Liquid filtration flow occurs when there is a total pressure gradient. The liquid filtration flux can be estimated by utilising an empirical diffusion coefficient, $D_{l,Ptot}$, expressed in units of seconds as

$$\overrightarrow{J_l^{Ptot}} = - D_{l,Ptot} \cdot \nabla P_{tot} \qquad\qquad (A.17)$$

It is evident that all the diffusion flux types can be expressed by Fick's law for which the diffusion coefficients are empirical. If liquid molecular diffusion due to the gravitational force, vapour and liquid filtration flows are neglected, then for a 1-dimensional analysis the total moisture transport may be estimated:

$$\overrightarrow{J_{tot}} = \overrightarrow{J_v} + \overrightarrow{J_l} = \overrightarrow{J_v^D} + \overrightarrow{J_v^T} + \overrightarrow{J_l^D} + \overrightarrow{J_l^T} \qquad\qquad (A18a)$$

or

$$J_{tot} = - \frac{D_{Pv} \nabla P_v}{R_v T} + \left\{ \frac{D_{Pv} P_v}{R_v T^2} - D_T - D_{l,T} \right\} \nabla T - D_{l,Pl} \nabla P_l \quad . \qquad (A.18b)$$

For a 2-or 3-dimensional analysis, the liquid molecular diffusion due to gravity cannot be neglected. It must be considered in the analysis (e.g.walls, corners etc), in which case

$$\vec{J}_{tot} = \vec{J}_v + \vec{J}_l = \vec{J}_v^D + \vec{J}_v^T + \vec{J}_l^D + \vec{J}_l^T \ . \tag{A.19a}$$

or

$$J_{tot} = -\frac{D_{P_v}}{R_v T}\nabla P_v + \left\{\frac{D_{P_v} P_v}{R_v T^2} - D_T - D_{l,T}\right\}\nabla T - D_{l,P}\nabla P_l - D_{l,z}\Delta z \tag{A.19b}$$

Equations A.18b and A.19b contain three dependent variables, P_v, T and P_l. The number of variables can be reduced to two, using the approach by Galbraith and McLean (1993). In this approach, a formula based on Kelvin's equation, which relates the vapour pressure gradient to the liquid pressure gradient is given for a 1-dimensional case as

$$\nabla P_l = \frac{R_v T \rho_l}{P_v}\nabla P_v + R_v \rho L \left\{\ln \phi - \frac{L}{R_v T}\right\}\nabla T \tag{A.20}$$

where ϕ is the relative humidity ($\phi = P_v/P_s$), P_s the vapour saturation pressure (N/m^2) and L the latent heat of vapourization (J/kg). Substituting Eq.(A.20) into Eq.(A.19) reduces the dependent variables to P_v and T. Hence Eq.(A18) can be expressed in a simplified form:

$$J_{tot} = -D_{P_v}^T \nabla P_v - D_T^{P_v} \nabla T \ . \tag{A.21}$$

Here, $D_{P_v}^T$ is a moisture diffusion coefficient due to the vapour pressure gradient when the second driving potential is the temperature gradient. Similarly, $D_T^{P_v}$ is a moisture diffusion coefficient due to the temperature gradient when the second driving potential is the vapour pressure gradient. It is very essential to check for the set of driving potentials when dealing with a diffusion coefficient. The moisture equation for 1-dimension in the x-direction is

$$\rho_o \frac{\partial u_i}{\partial t} = -\nabla J_1 + I_i + S_i \qquad I = 1, 2, \tag{A.22}$$

According to Galbraith (1992) and Laan (1994), filtration flow due to the total pressure between inside and outside environment is negligible. except when severe winds occur. In other words vapour and liquid transport by the filtration mechanism is not considered. Accordingly, for the case of combined heat and moisture transfer, the moisture balance

equation becomes

$$\rho_0 \frac{\partial u_{tot}}{\partial t} = \frac{\partial}{\partial x}\left\{\delta_P{}^T \frac{\partial P}{\partial x} + D_T{}^P \frac{\partial T}{\partial x}\right\} + S \qquad (A.23)$$

where S is the source term. Since

$$u_{tot} = u_1 + u_2$$

noting that

$$-\nabla J_1 - \nabla J_2 = \frac{\partial}{\partial x}\left\{\delta_P{}^T\frac{\partial P}{\partial x} + D_T{}^P\frac{\partial T}{\partial x}\right\}$$

$$\sum_{i=1}^{2} I_i = 0 . \qquad S = S_1 + S_2$$

$$\rho_0 \frac{\partial u_v}{\partial t} + \rho_0 \frac{\partial u_1}{\partial t} = \frac{\partial}{\partial x}\left\{\delta_P{}^T \frac{\partial P}{\partial x} + D_T{}^P \frac{\partial T}{\partial x}\right\} + S \qquad (A.24)$$

where u_v is the moisture content with vapour enthalpy and u_1 is the moisture content with

liquid enthalpy , that is;

$$u_v = \begin{cases} u_{tot} & \text{when } u_{tot} < u_{max} \\ u_{max} & \text{when } u_{tot} > u_{max} \end{cases}$$

$u_1 = u_{tot} - u_v$; where $u_{max} = u(\phi_{max})$

In order to reduce the number of dependent variables in Eq. (A.24) by one, the moisture

storage term is recast as

$$\rho_0 \frac{\partial u_v}{\partial t} = \rho_0 \frac{\partial u_v}{\partial \phi} \cdot \frac{\partial \phi}{\partial t} = \rho_0 \xi \frac{\partial (P/P_s)}{\partial t}$$

Hence for 1-Dimensional case in the x-direction, the moisture term, Eq.(A.24) becomes;

$$\rho_0 \xi \frac{\partial (P/P_s)}{\partial t} + \frac{d\rho_1}{dt} = \frac{\partial}{\partial x}\left\{\delta_P{}^T \frac{\partial P}{\partial x} + D_T{}^P \frac{\partial T}{\partial x}\right\} + S \qquad (A.25)$$

Similarly, for a 1-dimensional case considering conduction as the dominant heat flux

through the porous medium, the corresponding energy equation can be written as

$$\left[\rho_0(c_0 + c_v u_v) + c_1 \rho_1\right]\frac{\partial T}{\partial t} + h_v \frac{\partial \rho_v}{\partial t} + h_1 \frac{\partial \rho_1}{\partial t} = \frac{\partial}{\partial x}\left\{\lambda \frac{\partial T}{\partial x}\right\} - \frac{\partial h_s J_v}{\partial x} + g \qquad (A.26)$$

where h_s is the enthalpy at the source of moisture flux. It is positive if the moisture is

entering the control volume, otherwise it is negative. The governing equations for the

combined heat and moisture transport equations A.25 and A.26 contain 3 dependent

variables (P, T and ρ_1). A third equation, the condensation/evaporation control equation is

therefore needed to solve these equations (Nakhi 1995). The control equation is assumed to be a function of the saturation pressure only.

Boundary conditions of an external wall

Taking cognizance of the contributions of the sensible and latent infiltration loads as well as the air humidity exchanges between the zone air and the interior of the external wall, the boundary condition at T(0,t), as shown in Figure A1.2, may be expressed as

$$
\left\{ \begin{array}{l} \text{Solar radiation} \\ \text{absorbed} \end{array} \right\} + \left\{ \begin{array}{l} \text{Radiation exchange} \\ \text{between outside} \\ \text{surface, the sky} \\ \text{and surroundings} \end{array} \right\} + \left\{ \begin{array}{l} \text{Latent heat of condensation} \\ \text{of liquid water condensed} \\ \text{on the outside surface} \end{array} \right\} + \left\{ \begin{array}{l} \text{Heat influx} \\ \text{due to air} \\ \text{infiltration} \end{array} \right\}
$$

(A.27)

$$
= \left\{ \begin{array}{l} \text{convection from} \\ \text{outside surface} \end{array} \right\} + \left\{ \text{inward conduction} \right\}
$$

$$
\alpha It + \varepsilon \Delta R + \rho_o h_{m,o} U(0,t)[w_o(t) - w(0,t)]h_{fg} + m_a C_{pa}[T(0,t) - T_o(t)]
$$

(A.28)

$$
= h_{c,o}[T_o(t) - T(0,t)] - k \left. \frac{\partial T}{\partial x} \right|_{x=0}
$$

For the inside surface of the external wall, boundary condition T(L,t) can be determined from

$$
\left\{ \begin{array}{l} \text{Inward heat} \\ \text{conduction} \end{array} \right\} = \left\{ \begin{array}{l} \text{Convection from} \\ \text{the inside surface} \end{array} \right\} + \left\{ \begin{array}{l} \text{Radiation exchange} \\ \text{between inner surface} \\ \text{and other surfaces} \end{array} \right\} + \left\{ \begin{array}{l} \text{Heat required} \\ \text{for the} \\ \text{evaporation} \\ \text{of liquid water} \end{array} \right\} + \left\{ \begin{array}{l} \text{heat influx} \\ \text{to the room} \\ \text{due to air} \\ \text{infiltration} \end{array} \right\}
$$

(A.29)

$$
-k \frac{\partial T}{\partial x} \bigg|_{=L} = h_{c,i}[T(L,t) - T(t)] + \sum_{j=1} h_{r,j} [T(L,t) - T(n,t)] + \rho_i h_{m,i} U_i(L,t) [w(L,t) - w_r(t)]h_{fg}
$$

$$
+ m_a C_{pa} [T(L,t) - T(t)]
$$

(A.30)

The use of equations A.25 and A.26 allows the solution of the three dependent variables, P,

T and ρ_l, for each control volume within a multi-layered construction when evolving through time under the influence of boundary heat and mass transfers being simultaneously resolved within ESP-r.
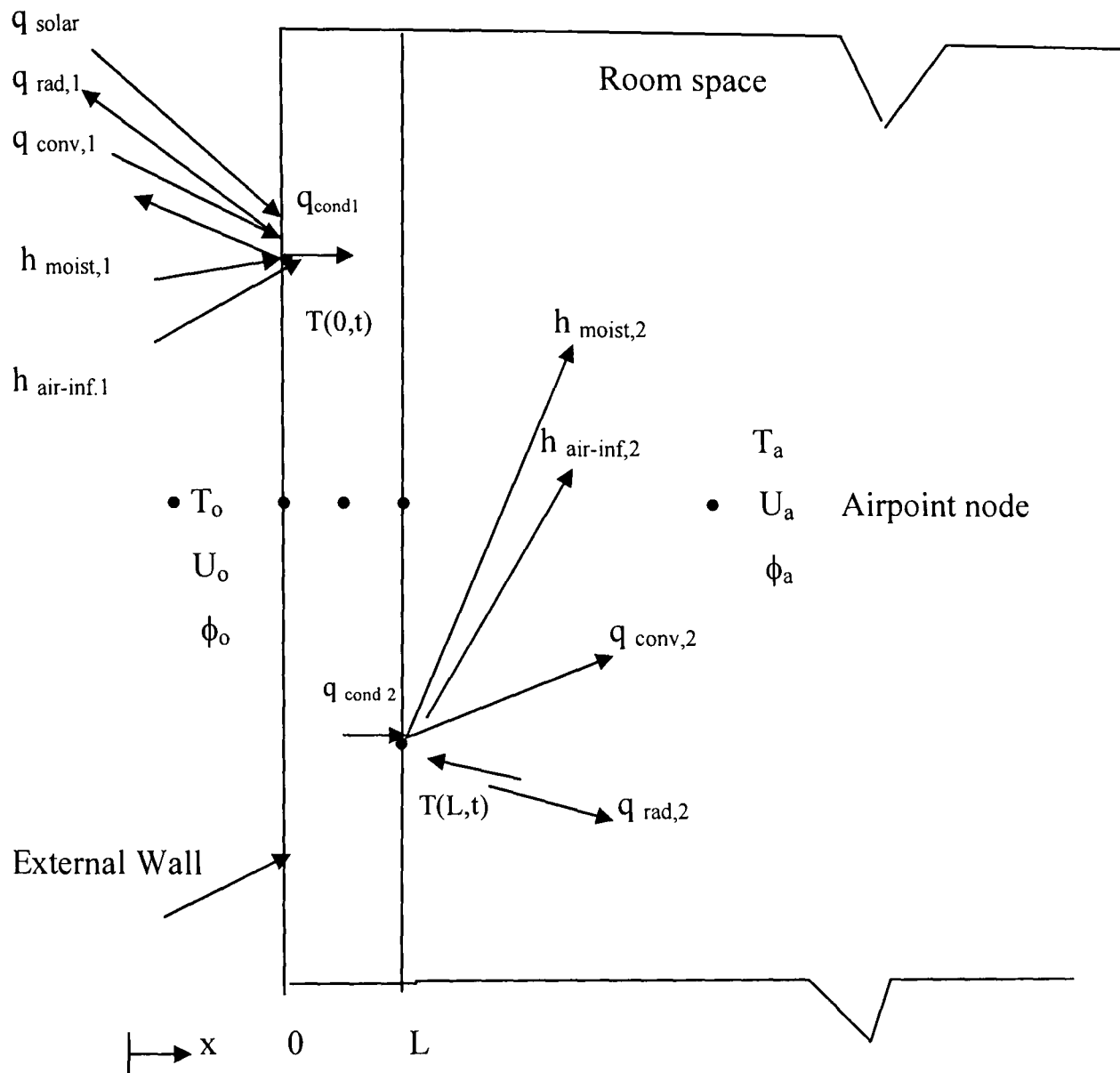

Figure A1.2 : Boundary conditions of an external wall.

The next sub-section is a presentation of the numerical model uitlised towards the solution of the governing transport equations for the moisture and energy balance terms, equations A.25 and A.26 respectively.

By applying the two-point finite difference formulae to these equations the following finite difference approximations are derived (Nakhi 1995), giving for the moisture balance term.

$$a_i^{n+1}P_i^{n+1} + \sum_{j=1}^{2} a_j^{n+1}P_j^{n+1} + (m_l)_i^{n+1} - \gamma\Delta t \; S_i^{n+1}$$

$$= a_i^{n} P_i^{n} + \sum_{j=1}^{2} a_j^{n}P_j^{n} + (m_l)_i^{n} + (1-\gamma) \Delta t \; S_i^{n}$$

$$+ \sum_{j=1}^{2} b_j^n (T_j^n - T_i^n) + \sum_{j=1}^{2} b_j^{n+1} (T_j^{n+1} - T_i^{n+1}) \tag{A.31}$$

where, γ is the degree of implicitness, n and n+1 relates to the present and future time-rows. Δt the time step (s), m the specific mass (kg/m^3), and

$$a_j^{n+1} = - [\gamma (\delta^T P)_{j \to i}^{n+1} A \Delta t] / \Delta X_{j \to i}$$

$$a_j^{n} = [(1 - \gamma) (\delta^T P)_{j \to i}^{n} A \Delta t] / \Delta X_{j \to i}$$

$$a_i^{k} = [\rho_0 \xi_i V(P_s)_i^{k} - a_{i-1}^{k} - a_{i+1}^{k}]$$

$$b_j^{n+1} = - [\gamma (D^P T)_{j \to i}^{n+1} A \Delta t] / \Delta X_{j \to i}$$

$$b_j^{n} = [(1 - \gamma) (D^P T)_{j \to i}^{n} A \Delta t] / \Delta X_{j \to i}$$

$$m_l^{k} = V \rho_l^{k} \text{ (kgmoisture)}$$

$$S_i^{k} = V s_i^{k} \text{ (kgmoisture/sec)}$$

where A is the area (m^2), ΔX the flowpath length (m) and V the node volume (m^3).

For the energy term

$$a_i^{n+1} T_i^{n+1} + \sum_{j=1}^{2} a_j^{n+1} T_j^{n+1} - \gamma G_i^{n+1} \Delta t - \gamma (h_s m_v)^{n+1} \Delta t$$

$$= a_i^{n} T_i^{n} + \sum_{j=1}^{2} a_j^{n} T_j^{n} + (1 - \gamma) G_i^{n} \Delta t + (1 - \gamma) (h_s m_v)^{n} \Delta t$$

$$- (h_l)_i^{n+1} [(m_l)_i^{n+1} - (m_l)_i^{n}] - (h_v)_i^{n+1} [(m_v)_i^{n+1} - (m_v)_i^{n}] \tag{A.32}$$

where,

$$a_j^{n+1} = - \gamma A \lambda^{n+1}_{j \to i} \Delta t / \Delta X_{j \to i}$$

$$a_j^{n} = (1 - \gamma) A \lambda^{n}_{j \to i} \Delta t / \Delta X_{j \to i}$$

$$a_i^{k} = [\rho_0 V(c_0 + c_v u_v) + c_l m_l - \sum a_j^{k}, \text{ and}$$

m_v : moisture mass flow rate [kgv/s]

In equation (A.32), the heat flux term due to moisture transfer, $h_s m_v$, is treated as source term. This is because of the difficulties associated with its dependence on the moisture flow direction. For most cases the future self-coupling term, $[\rho_0 \xi_i V/(P_s)]$, is relatively small. From a numerical standpoint, increasing the self-coupling coefficient reduces the

differences between the values of the present and future dependent variables. The coupled moisture/energy equations for a given system are then given by

$$
\begin{bmatrix} \mathbf{E} \\ \mathbf{M} \end{bmatrix} \times \begin{bmatrix} \mathbf{T} \\ \mathbf{P} \end{bmatrix} = \begin{bmatrix} \mathbf{B}_e \\ \mathbf{B}_m \end{bmatrix}
\tag{5.1}
$$

where $\mathbf{E}$ and $\mathbf{M}$ are the energy and moisture coefficient matrices respectively, $\mathbf{T}$, $\mathbf{P}$ the temperature and water vapour pressure vectors, and $\mathbf{B}_e$, $\mathbf{B}_m$ the energy and moisture boundary conditions. The solution approach enables each equation set to be integrated at different frequences depending on the system's characteristics (Clarke 2001). An alternative solution technique via a two-nested iteration loop system is presented in the next sub-section.

Solution technique for 1-dimensional HAM model

To solve the HAM model equations, an iterative procedure of two nested iteration steps is followed. In the first step, the temperatures in the solid domain are computed. This yields estimated surface temperatures to be used in the second step to solve the heat and moisture balance equations for the internal space. From these equations, the temperatures and humidities are computed. The heat fluxes at the surface elements are also computed and used as boundary conditions for the iteration step. The process is repeated until the desired accuracy is attained.

APPENDIX B   AN OVERVIEW OF IEA ANNEX XIV HAM CODE

CLASSIFICATIONS

An overview of the 9 classified HAM codes as presented in Chapter 2 are described as follows.

Type 1: is the steady-state Glaser scheme of heat conduction and vapour diffusion with constant material properties. There is a thermal-hygric link and the p_{sat} (T) equation of state is used.

Type 2: is the steady-state Glaser scheme of heat conduction and vapour diffusion corrected for capillary moisture transfer. Constant material properties are assumed and a thermal-hygric link and the p_{sat} (T) equation of state are used.

Type 3: is a non-steady state heat and vapour transfer code. Material properties are considered as a function of the moisture ratio. There is a thermal–hygric link and consideration of the p_{sat} (T) equation of state and latent heat.

Type 4: is a non-steady state heat, vapour and liquid transfer code. Material properties are regarded as being a function of the moisture ratio and temperature. There is a thermal - hygric link and the p_{sat} (T) equation of state and latent heat are considered,

Type 5: is a steady and non-steady state heat and air transport code. Constant material properties are assumed and there is a thermal-air link. Enthalpy transfer and stack-effect are considered.

Type 6: is a steady state uncoupled heat, vapour and air transport code with assumption of constant material properties. It has a heat-mass link with a consideration of the p_{sat} (T) equation of state, latent heat, enthalpy transfer and stack effect.

Type 7: is a steady state heat and air transfer and non-steady state vapour transfer code with constant material properties. It has a link between heat and mass transfer, the p_{sat} (T) equation of state, latent heat, enthalpy transfer and stack effects.

Type 8: is a transient state heat, vapour and air transfer code. Material properties are considered as a function of moisture ratio and temperature. There is a link between heat and mass transfer; the p_{sat} (T) equation of state, latent heat, enthalpy transfer and stack effects are included,

Type 9: is a non-steady state heat, vapour, liquid and air transfer code. Material properties are considered as a function of moisture ratio (and temperature). There is a link between heat and mass transfer; the p_{sat} (T) equation of state, latent heat, enthalpy transfer and stack effects are included.

It became evident after the classification that:

- most codes belong to Type 4. This type is seen as the ultimate development when hygric behaviour of envelope parts, composed of capillary porous materials, is the major objective; and

- heat + air + moisture transfer in its overall complexity appears more intensively analysed and modelled in countries with a wood frame building tradition such as Canada, Finland and Sweden, than in countries with a stone wall tradition.

APPENDIX C   THE SEQUENTIAL SOLUTION PROCEDURE

For incompressible flows, the density is by definition not linked to the pressure. Coupling between pressure and velocity introduces a constraint on the solution of the flow field. By adopting an iterative solution strategy, namely the SIMPLE algorithm (Patankar and Spalding 1974), problems associated with the non-linearities in the equation set and the pressure-velocity linkage are resolved. The convective fluxes per unit mass, F, through the respective cell faces are determined from guessed velocity components using this algorithm. Within the algorithm, a guessed pressure field is used to solve the momentum equations. The pressure correction equations, determined from the continuity equation is solved to obtain a pressure correction field, which is in turn used to update the velocity and pressure fields. Estimates of the velocity field , defined as u^*, v^*, and w^* for the respective coordinate directions are then obtained. Due to anticipated inaccuracies contained in the guessed pressure field a pressure-correction term (p') is introduced. It is given by the difference between the correct pressure, whose solution is required (p) and the guessed pressure p^*. The pressure-correction (p') and the velocity-correction (u') terms (Malalasekera 1995) are defined as

$$p' = p - p^* \qquad (C.1)$$

and

$$u' = u - u^* . \qquad (C.2)$$

At the next step the x-momentum equations expressed in guessed quantities (p^*, u^*, etc.) are subtracted from the x-momentum equations expressed in correct quantities (p, u, etc.). A relation between the velocity and pressure corrections results in the u-velocity correction equation of the SIMPLE algorithm.

$$u' = \frac{A(p'_w - p'_e)}{a_P - \Sigma a_{nb}} \qquad (C.3)$$

where u' is the velocity-correction term and p' the pressure-correction term at the faces, east

and west respectively. Substitution of the velocity-pressure correction relations (Eq. C.3 and those for v' and w') into the continuity equation (Eq.3.2 , Ch. 3) eliminates the velocity variables, and leads to a balance between adjacent p' points. The discretised algebraic relations for the p' balance is given as

$$a_P p'_P = \Sigma \, a_{nb} \, p'_{nb} + b' \; .$$ (C.4)

The p' coefficients are obtained from the coefficients of the momentum equations and thus establishes a tight linkage between velocity and pressure. Through replacement of the velocity form of the continuity equation with equation C.4, pressure is provided with its own equation. The resultant velocity-pressure linkage requires a sequential solution approach. Within this process, a pressure field is guessed and the momentum equations are solved. Using equation C.4 the pressure-correction terms, p', is calculated. Similarly, the velocity and pressure estimates are updated using equations (C.1) and (C.2). The energy equation is then solved to complete the iteration loop. The entire process is repeated, using the corrected pressures and velocities from the previous iteration as the current iteration's guesses until convergence is obtained. Figure C1.1 illustrates the sequential and iterative solution process. Within the sequential solution process, the tri-diagonal matrix algorithm (TDMA), developed by Thomas (1949) is applied. TDMA is a direct method for one-dimensional situations that can be applied iteratively in a line-by-line fashion to solve multi-dimensional problems (Malalasekera 1995).
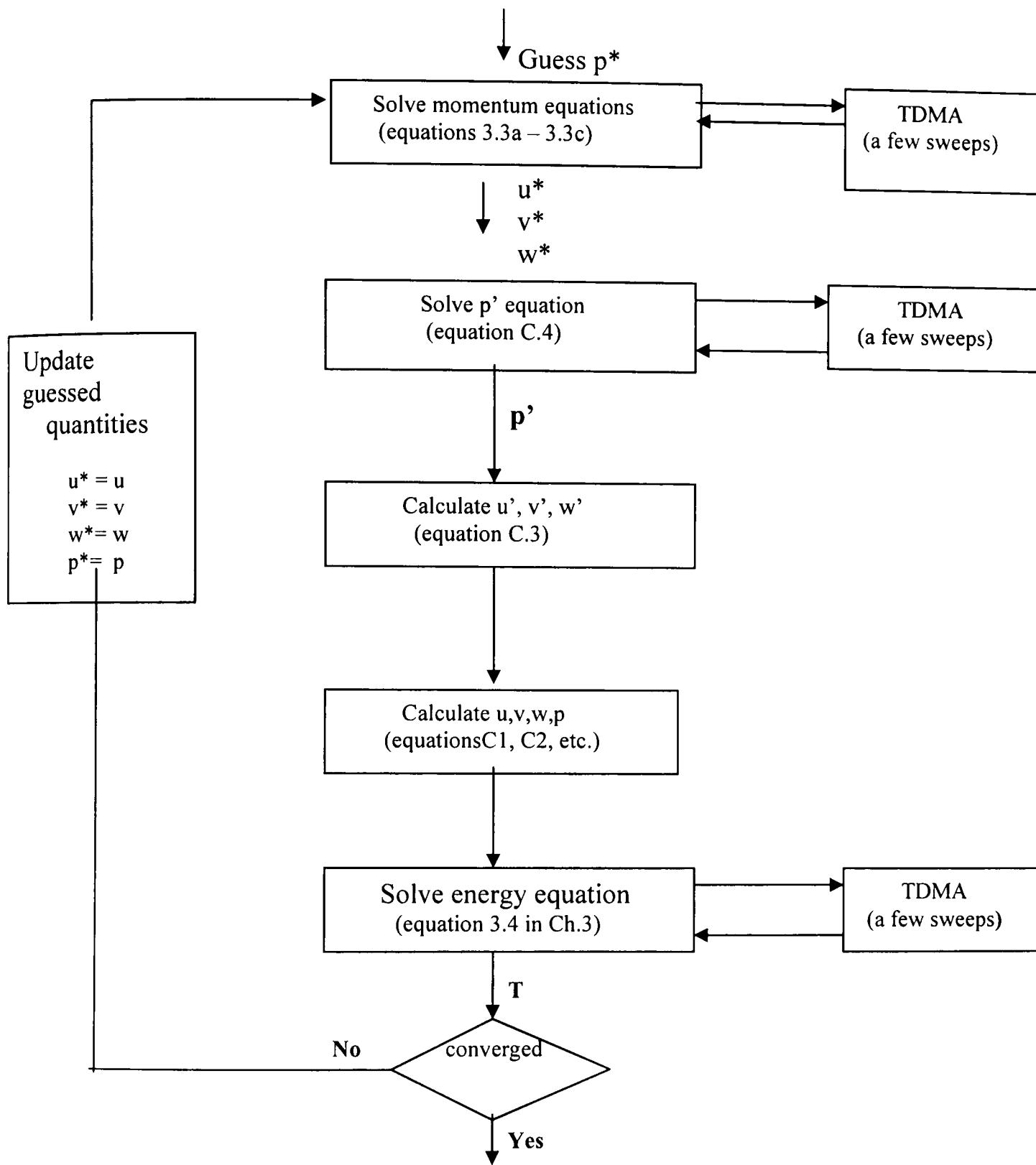
Figure C1.1: Sequential and iterative solution process.

High Reynolds Number modelling with k-ε model

At high Reynolds Number, the standard k-ε model (Launder and Spalding 1974) avoids the need to integrate the model equation right to the wall by making use of the universal behaviour of near-wall flows. If y is the coordinate direction normal to a solid wall, the mean velocity at a point y_p with $30 < y^+_p < 500$ satisfies the log-law (equation 3.79) and measurements of turbulent kinetic energy budgets showed that the rate of turbulence production equaled the rate of dissipation. Based on these assumptions and the eddy viscosity formula (3.70), the following wall function is developed:

$$u^+ = \frac{U}{u_\tau} = \frac{1}{k} \ln(Ey^+_p) \; ; \; k = \frac{u^2_\tau}{\sqrt{C_\mu}}; \; \varepsilon = \frac{u^3_\tau}{\kappa y} \qquad (D.1)$$

Von Karman's constant, κ, equals 0.41 and the wall roughness parameter, E, equals 9.8 for smooth walls (Schlictung 1979). For heat transfer application, the universal near-wall temperature distribution, valid at high Reynolds Number is used (Launder and Spalding 1974):

$$T^+ \equiv - \frac{(T_p - T_w) \, C_p \rho u_\tau}{q_w} = \sigma_{T,t} \left[u^+ + \left\{ P\frac{\sigma_{T,l}}{\sigma_{T,t}} \right\} \right] \qquad (D.2)$$

where T_P is the temperature at near wall point y_P, T_w the wall temperature, q_w the wall heat flux, $\sigma_{T,t}$ the turbulent Prandtl Number, $\sigma_{T,l} = \mu C_p/\Gamma_T$ the Prandtl Number (laminar), Γ_T the thermal conductivity, C_p the fluid specific heat at constant pressure and P the 'pee-function', a correction function dependent on the ratio of laminar to turbulent Prandtl Numbers (Launder and Spalding 1974). The associated wall function formulae (D.1 and D.2) are used to determine the shear stress, heat flux and other variables within the log-law region. Table D.1 gives the optimum near-wall relationships as given by (Launder and Spalding 1974).

Table D1: Near wall relationships for the standard k-ε model

- *Momentum equation tangential to wall*

wall shear stress $\tau_w = \rho C_\mu^{1/4} k_p^{1/2} u_p/u^+$ (D.3)

wall force $F_s = -\tau_w A_{cell} = -(\rho C_\mu^{1/4} k_p^{1/2} u_p/u^+) A_{cell}$ (D.4)

- *Momentum equation normal to wall*

normal velocity $= 0$

- *Turbulent kinetic energy equation*

net k-source per unit volume $= \left(\tau_w u_p - \rho C_\mu^{3/4} k_p^{3/2} u^+ \right) \Delta V/\Delta y_p$ (D.5)

- *Dissipation rate equation*

set nodal value $\varepsilon_p = C_\mu^{3/4} k_p^{3/2}/(\kappa \Delta y_p)$ (D.6)

- *Temperature (or energy) equation*

wall heat flux $q_w = -\rho C_p C_\mu^{1/4} k_p^{1/2} (T_p - T_w)/T^+$ (D.7)

These relationships are used in conjunction with the universal velocity and temperature

distributions for near-wall turbulent flows in (D.1 and D.2). The 'pee-function' given by the

expression $P(\sigma_{T,l}/\sigma_{T,t})$ is evaluated using the following expression derived by Jayatilleke

(1969):

$$P\left(\sigma_{T,l}/\sigma_{T,t} \right) = 9.2 \left[(\sigma_{T,l}/\sigma_{T,t})^{0.75} - 1 \right] \times \left[1 + 0.28 \exp\{-0.007 \, (\sigma_{T,l}/\sigma_{T,t}) \right. \quad \text{(D.8)}$$

In order of their appearance in Table D1, variables are treated as follows in their

discretised equation.

- u velocity component parallel to the wall: the link with the wall (south) is suppressed

by setting $a_s = 0$ and the wall force, F_s, from (Eq. D.2) is introduced into the discretised

u-equation as a source term, thus

$$S_p = \frac{-\rho C_\mu^{1/4} k^{1/2}}{u^+} A_{cell} . \quad \text{(D.9)}$$

- k-equation: the link at the boundary is suppressed and a_s is set equal to zero. In the

volume source (Eq. D.5), the second term contains $k^{3/2}$. This is linearised as $k_p^{*1/2}.k_p$.

where $k*$ is the k-value at the end of the previous iteration, which yields the source terms S_p and S_u in the discretised k-equation:

$$S_p = - \rho C_\mu^{3/4} \frac{k_P^{*1/2} u^+}{\Delta y_P} \Delta V \quad \text{and} \quad S_u = \frac{\tau_w u_P \Delta V}{\Delta y_P} . \qquad (D.10)$$

- ε- equation: in the discretised ε- equation, the near-wall node is fixed to the value given by Eq. (D.6).by setting the source terms S_p and S_u (Malalasekera and Versteeg 1995) :

$$S_p = - 10^{30} \quad \text{and} \quad S_u = \frac{C_\mu^{3/4} k_P^{3/2}}{\kappa \Delta y_P} \times 10^{30} . \qquad (D.11)$$

A fixed heat flux enters the source terms directly by means of the normal source term linearisation:

$$q_s = S_u + S_p T_p \qquad (D.12)$$

where,for an adiabatic wall, $S_u = S_p = 0$ as before.

APPENDIX E   BOUNDARY LAYER THEORY

Significant dimensionless parameters

The boundary layer equations are normalized by first defining dimensionless independent variables of the form

$$x^* \equiv \frac{x}{L} \quad \text{and} \quad y^* \equiv \frac{y}{L} \tag{E.1}$$

where L is some characteristic length for the surface of interest (e.g, the length of a flat plate). Dependent variables are also defined as

$$u^* \equiv \frac{u}{V} \quad \text{and} \quad v^* \equiv \frac{v}{V} \tag{E.2}$$

where V is the velocity upstream of the surface.

Similarly,

$$T^* \equiv \frac{T - T_s}{T_\infty - T_s} \quad \text{and} \quad C_A^* \equiv \frac{C_A - C_{A,s}}{C_{A,\infty} - C_{A,s}} \quad . \tag{E.3}$$

From the transfer equations for the velocity, thermal and concentration boundary layers the dimensionless groups presented below are relevant. These parameters facilitate the application of results obtained for a surface experiencing one set of conditions to geometrically similar surfaces experiencing entirely different conditions. These conditions may vary with the nature of the fluid, the fluid velocity and/or with the size of the surface (as determined by L).

Reynolds Number, Re_L, is interpreted as the ratio of inertia to viscous forces in the velocity boundary layer. For large values of Re inertia forces dominate, whereas for small values of Re viscous forces take over. The Re determines the existence of laminar (Re ≤ 2300) or turbulent flow (Re ≥ 2300).

Prandtl number, Pr, is interpreted as the ratio of the momentum diffusivity, ν, to the thermal diffusivity, α, and provides a measure of the relative effectiveness of momentum and energy transport by diffusion in the velocity and thermal boundary layers respectively. Pr strongly influences the relative growth of the velocity and thermal boundary layers as a

result of which the following relation is relevant.

$$\delta / \delta_t = Pr^n \qquad (E.4)$$

where n is a positive exponent. For a gas $\delta_t \approx \delta$, for a liquid metal $\delta_t \gg \delta$ and for an oil $\delta_t \ll \delta$.

Schmidt number, Sc, provides a measure of the relative effectiveness of momentum and mass transport by diffusion in the velocity and concentration boundary layers respectively. For convection mass transfer in laminar flows, δ_c determines the relative velocity and concentration boundary layer thicknesses. They are related through the expression

$$\delta / \delta_c = Sc^n \qquad (E.5)$$

Lewis number, Le is relevant to situations involving simultaneous heat and mass transfer by convection and is given as

$$Le = \frac{\alpha}{D_{AB}} = \frac{Sc}{Pr} \qquad (E.6)$$

where D_{AB} is the mass diffusivity of species A in B, for example, water vapour in air.

The complete set of boundary layer equations becomes

$$\frac{\partial u^*}{\partial x^*} + \frac{\partial v^*}{\partial y} = 0 \qquad (E.7)$$

$$u^* \frac{\partial u^*}{\partial x^*} + v^* \frac{\partial u^*}{\partial y^*} = -\frac{dp^*}{dx^*} + \frac{1}{Re_L} \frac{\partial^2 u^*}{\partial y^{*2}} \qquad (E.8)$$

$$u^* \frac{\partial T^*}{\partial x^*} + v^* \frac{\partial T^*}{\partial y^*} = \frac{1}{Re_L Pr} \frac{\partial^2 T^*}{\partial y^{*2}} \qquad (E.9)$$

$$u^* \frac{\partial C^*_A}{\partial x^*} + v^* \frac{\partial C^*_A}{\partial y^*} = \frac{1}{Re_L Sc} \frac{\partial^2 C^*_A}{\partial y^{*2}} \; . \qquad (E.10)$$

Intuitively, it is anticipated that h depends on the fluid properties (k, C_p, ρ, μ), the fluid velocity, V, and the length scale, L, and the surface geometry. From the definition of the convection coefficient and the dimensionless variables, the heat transfer coefficient, h, is expressed as

$$h = -\frac{k_f}{L} \frac{(T_\infty - T_s)}{(T_s - T_\infty)} \left.\frac{\partial T^*}{\partial y^*}\right|_{y^*=0} = +\frac{k_f}{L} \left.\frac{\partial T^*}{\partial y^*}\right|_{y^*=0} \qquad (E.11)$$

174

Similarly, *Nusselt number*, Nu_L is equal to the dimensionless temperature gradient at the surface, and provides a measure of the convection heat transfer occurring at the surface. It is given as

$$Nu_L \equiv \frac{hL}{k_f} = + \frac{\partial T^*}{\partial y^*} \Big|_{y^*=0} \qquad (E.12)$$

where k_f is the thermal conductivity of the fluid. It follows that for a prescribed geometry:

$$Nu_L = f_4 (x^*, Re_L, Pr) . \qquad (E.13)$$

Equation (E.13) implies that, for a given geometry, the Nusselt number must be some universal function of x^*, Re_L and Pr. It is observed that Nu_L is to the thermal boundary layer as the friction is to the velocity boundary layer. For the case of mass transfer in a gas or air flow over an evaporating liquid or a sublimating solid, the convection mass transfer coefficient, h_m, depends on the properties D_{AB}, ρ, μ, velocity V, and the characteristic length, L. By definition of the convection coefficient and the dimensionless variables, h_m is expressed as

$$h_m = - \frac{D_{AB}}{L} \frac{(C_{A,\infty} - C_{A,s})}{(C_{A,s} - C_{A,\infty})} \frac{\partial C_A^*}{\partial y^*} \Big|_{y^*=0} = + \frac{D_{AB}}{L} \frac{\partial C_A^*}{\partial y^*} \Big|_{y^*=0} \qquad (E.14)$$

A dependent parameter, the *Sherwood Number*, Sh is given as

$$Sh = \frac{h_m L}{D_{AB}} = + \frac{\partial C_A^*}{\partial y^*} \Big|_{y^*=0} . \qquad (E.15)$$

This parameter is equal to the dimensionless concentration gradient at the surface and provides a measure of the convection mass transfer occurring there. For a prescribed geometry:

$$Sh = f_6 (x^*. Re_L, Sc) . \qquad (E.16)$$

Thus, the Sherwood number is to the concentration boundary layer what the Nusselt number is to the thermal boundary layer. Equation (E.16) implies that Sh is a universal function of x^*. Re_L and Sc. Lewis number, Le, is given as

$$\frac{\delta_t}{\delta_c} \approx Le^n \qquad\qquad\qquad (E.17)$$

Le is therefore a measure of the relative thermal and concentration boundary layer thicknesses. For most applications, it is reasonable to assume that n = 1/3 in equation E.17 (Incropera and DeWitt 2002).

Appendix F Characterisation of the energy transfer mechanisms by ESP-r

Energy balance for surface nodes

Figure F1.1(a) shows the energy transfer mechanisms in a surface node. The finite volume heat balance method is utilised to characterise the regions encountered within buildings. For each region or node type, the derivation of energy conservation equation to link the region with other regions that are in thermodynamic contact by conduction, convection (heat and mass transfer), radiation and fluid flow is derived.
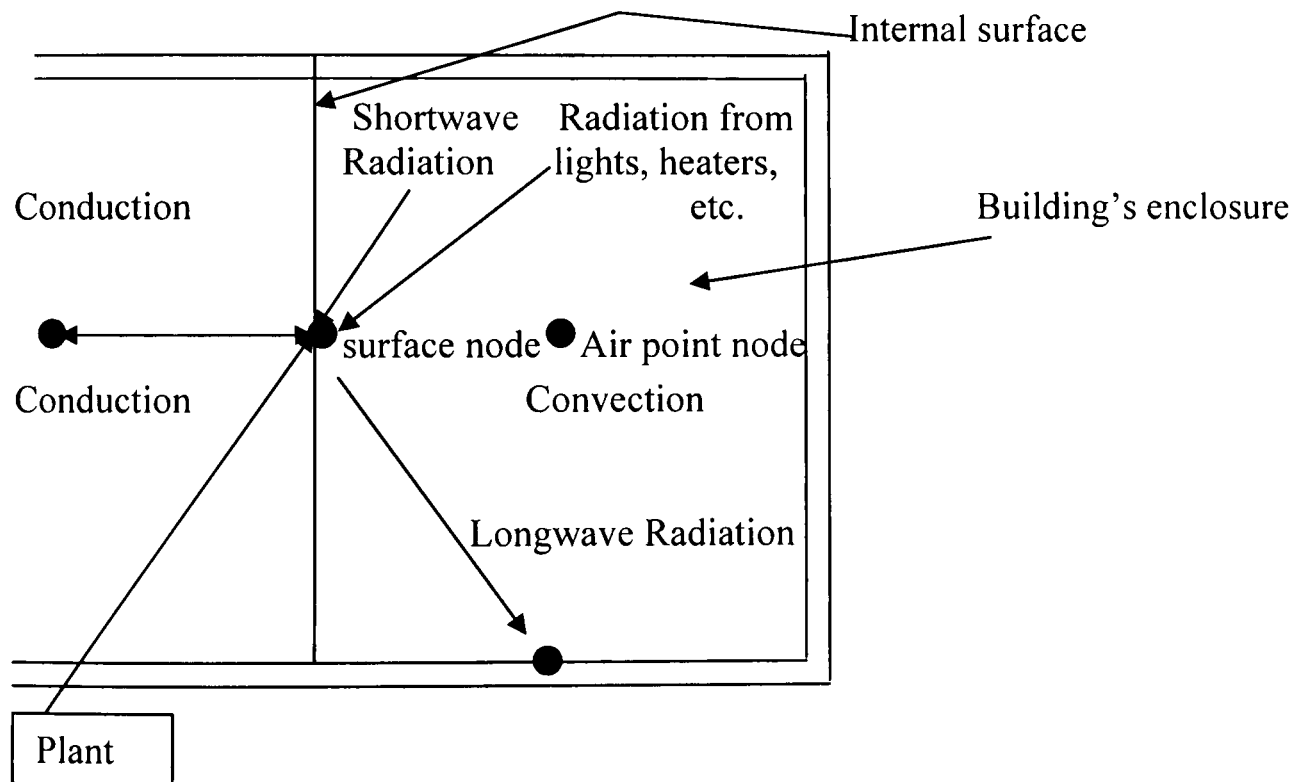

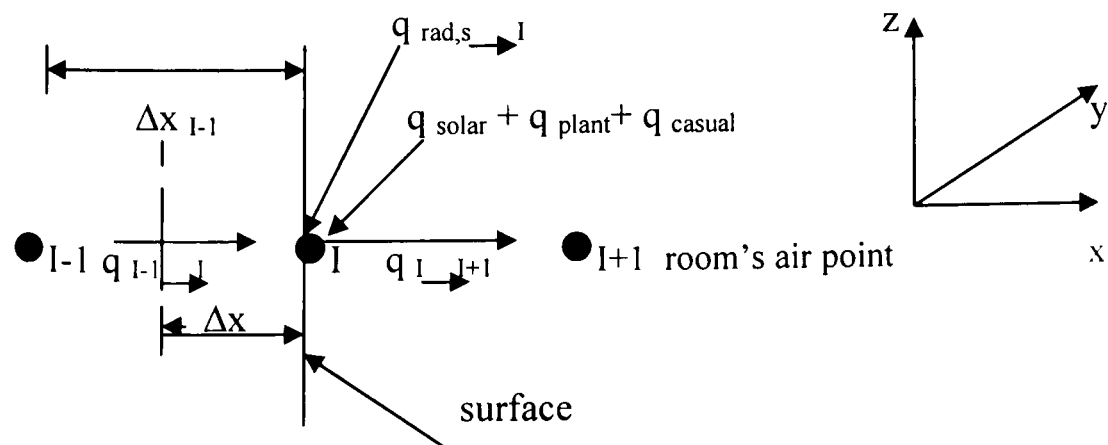Figure F1.1(a): Energy transfer mechanism associated with a surface node.

Figure F1.1(b) Energy balance on surface node I.

with reference to Figure F1.1(b), node I represents the exposed surface of the construction, where surface convection operates, node I+1 represents the adjacent room (fluid type node) and node I-1 represents the solid node embedded within the multi-layered construction. Heat transfer through node I-1 towards the exposed surface is by conduction whilst heat transfer at the surface node I is by surface convection. For the fluid type node I+1, there exist two possibilities for energy transfer: fluid-to fluid energy exchange due to pressure (for example,. vapour pressure), temperature (for example, inside surface temperature. indoor air temperature), and other heat or mass transfer plant; and fluid-to-surface energy exchange due to convective effects. The energy balance for node I is given by

$$\left(\begin{array}{l}\text{Heat stored} \\ \text{in volume}\end{array}\right) = \left(\begin{array}{l}\text{Net heat} \\ \text{conducted} \\ \text{into volume}\end{array}\right) + \left(\begin{array}{l}\text{Heat generated} \\ \text{within volume}\end{array}\right) + \left(\begin{array}{l}\text{Net heat radiated} \\ \text{into volume by} \\ \text{longwave radiation}\end{array}\right) + \left(\begin{array}{l}\text{Net heat} \\ \text{convected into} \\ \text{into volume}\end{array}\right).$$

$$(F.1)$$

Net heat conduction into the control volume only occurs at the boundary with the next-to-surface node (I-1). The discretised explicit form of the conduction term is thus given by

$$\left\{\text{Net heat conduction into volume}\right\} = \frac{k_{I-1} \Delta y \Delta z}{\Delta x_{I-1}} (T^t_{I-1} - T^t_I). \qquad (F.2)$$

Heat generated as source terms within the control volume includes solar gains and longwave radiation from sources of heat within the room in addition to heat flux injections from plant. The explicit form of which is given by

$$\left\{\text{Heat generated within control volume}\right\} = q^t_{solar,I} + q^t_{cas\text{-}rad,\ I} + q_{tplant,I} \qquad (F.3)$$

where $q^t_{solar,I}$ is the solar radiation absorbed at node I at the present time, $q^t_{cas\text{-}rad,I}$ the radial energy absorbed from casual gains (for example,occupants, lights, etc.) and $q^t_{plant,I}$ radiant plant input to node I (for example, from heat radiator installed in the room).

The net heat exchange of node I with surrounding surfaces that are in longwave contact with other internal surfaces of the rooms is represented by the longwave radiation term.

The discretised explicit form is expressed as

$$\left\{ \text{net longwave radiation into the control volume} \right\} = \sum_{I=1}^{N} h_{r,s \rightarrow I}^{t} \, \Delta y \Delta z \, (T_s^t - T_I^t) \qquad (F.4)$$

where N is the number of surrounding surfaces in longwave contact and $h_{r,s \rightarrow I}^{t}$ a linearised radiation heat transfer coefficient (W/m²K). Such coefficients are recalculated at each time step on a surface-by-surface fashion. Heat exchange between the room air and the solid surface node, I is represented through the convection term based on the assumption that the room air is considered uniform. Evidently, the temperature at node I+1 (room air point) represents conditions within the room. In discretised explicit form the convection term is given by

$$\left\{ \text{Net heat convected into volume} \right\} = h_{c,I}^{t} \, \Delta y \Delta z \, (T_{I+1}^t - T_I^t) \qquad (F.5)$$

where $h_{c,I}^{t}$ represents the convection heat transfer coefficient (W/m²K) between the surface at node I and the room's air point, evaluated at the present time-row. Substitution of equations (F.2) through (F.5) into (F.1) and representing the storage term with a backward difference scheme gives the explicit form of the energy balance. Similarly, evaluation of convection and radiation heat transfer coefficients as well as the conduction, convection, radiation, and the source terms with future values yields the implicit form of the energy balance. Simplification through division by the volume and grouping future time row terms on the left-hand side and the present time-row terms on the right-hand side results in the generalised form of the equation for an internal surface stated in equation F.6. This is the basic equation employed by ESP-r to characterise the energy balance for internal surface nodes.equation. With reference to Eq.F.6, the bracketed term in front of the nodal temperature $T_i^{t+\Delta t}$ is the self-coupling coefficient, it is the coefficient of the state variable to which the equation applies (the target). It is the self coupling coefficient that modifies the present and future temperatures of the node under consideration. With reference to Eq. F.6.

the self coupling coefficient is given by

$$\left\{2\,(\rho C_p)_I/\Delta t + k_{I-1}/\Delta x \Delta x_{\,I-1} + h_{c,I}{}^{t+\Delta t} + \sum_{s=1}^{N} h_{r,s\to I}{}^{t+\Delta t}\,/\Delta x\right\}\ .$$

The terms in front of the other future time step nodal temperatures are the cross coupling

coefficients. These provide the link to the other nodes which exchange energy with node I.

$$\left[\frac{2\,(\rho C_p)_I}{\Delta t} + \frac{k_{I-1}}{\Delta x \Delta x_{\,I-1}} + \frac{h_{c,I}{}^{t+\Delta t} + \sum_{s=1}^{N} h_{r,s\to I}{}^{t+\Delta t}}{\Delta x}\right] T_I{}^{t+\Delta t} - \left[\frac{k_{I-1}}{\Delta x \Delta x_{\,I-1}}\right] T_{I-1}{}^{t+\Delta t} - \left[\frac{h_{c,I}{}^{t+\Delta t}}{\Delta x}\right] T_{I+1}{}^{t+\Delta t}$$

$$- \left[\frac{\sum_{s=1}^{N} h_{r,s\to I}{}^{t+\Delta}\, T_s{}^{t+\Delta t}}{\Delta x}\right] - \left[\frac{q_{solar,I}{}^{t+\Delta}}{\Delta x \Delta y \Delta z}\right] - \left[\frac{q_{cas-rad,I}{}^{t+\Delta t}}{\Delta x \Delta y \Delta z}\right] - \left[\frac{q_{plant,I}{}^{t+\Delta t}}{\Delta x \Delta y \Delta z}\right]$$

$$= \left[\frac{2\,(\rho C_p)_I}{\Delta t} - \frac{k_{I-1}}{\Delta x \Delta x_{\,I-1}} - \frac{h_{c,I}{}^{t} - \sum_{s=1}^{N} h_{r,s\to I}{}^{t}}{\Delta x}\right] T_I{}^{t} + \left[\frac{k_{I-1}}{\Delta x \Delta x_{\,I-1}}\right] T_{I-1}{}^{t}$$

$$+ \left[\frac{h_{c,I}{}^{t}}{\Delta x}\right] T_{I+1}{}^{t} + \left[\frac{\sum_{s=1}^{N} h_{r,s\to I} T_s{}^{t}}{\Delta x}\right] + \left[\frac{q_{solar,I}{}^{t}}{\Delta x \Delta y \Delta z}\right] + \left[\frac{q_{cas-rad,I}{}^{t}}{\Delta x \Delta y \Delta z}\right] + \left[\frac{q_{plant,I}{}^{t}}{\Delta x \Delta y \Delta z}\right]\ . \qquad (5.6)$$

The characteristic equation F.6 gives equal weighting to the implicit and explicit terms

(Crank- Nicholson scheme). It can also be inferred from Eq.F.6 that each heat balance

expresses the thermal interaction between a node and its neighbours and the resultant

equation set (Eq.F.6) links all inter-node heat flows over time and space (Clarke 2001).

Energy balance for air point node

Considering the energy transfer mechanism in a fluid node which serves also as the air point

for the room as shown in Figure F1.2, node I represents the air point while nodes S, the

surface nodes of bounding internal fabric surfaces. Node L as denoted in the diagram

represent the air point of another room with node Q representing the outdoor air. The air

within the room is assumed to be uniform and therefore node I represents the conditions

throughout the volume. The air point serves alternatively as the handshaking point for the

conflation of the two models. The energy for the air point node takes into consideration bulk

air flow from adjacent rooms and outdoors, surface convection transfer at the internal bounding surfaces, and convective sources of heat, for example from casual sources (such as occupants, lights, etc.) convective plants, e.g. convective heaters located in the room.
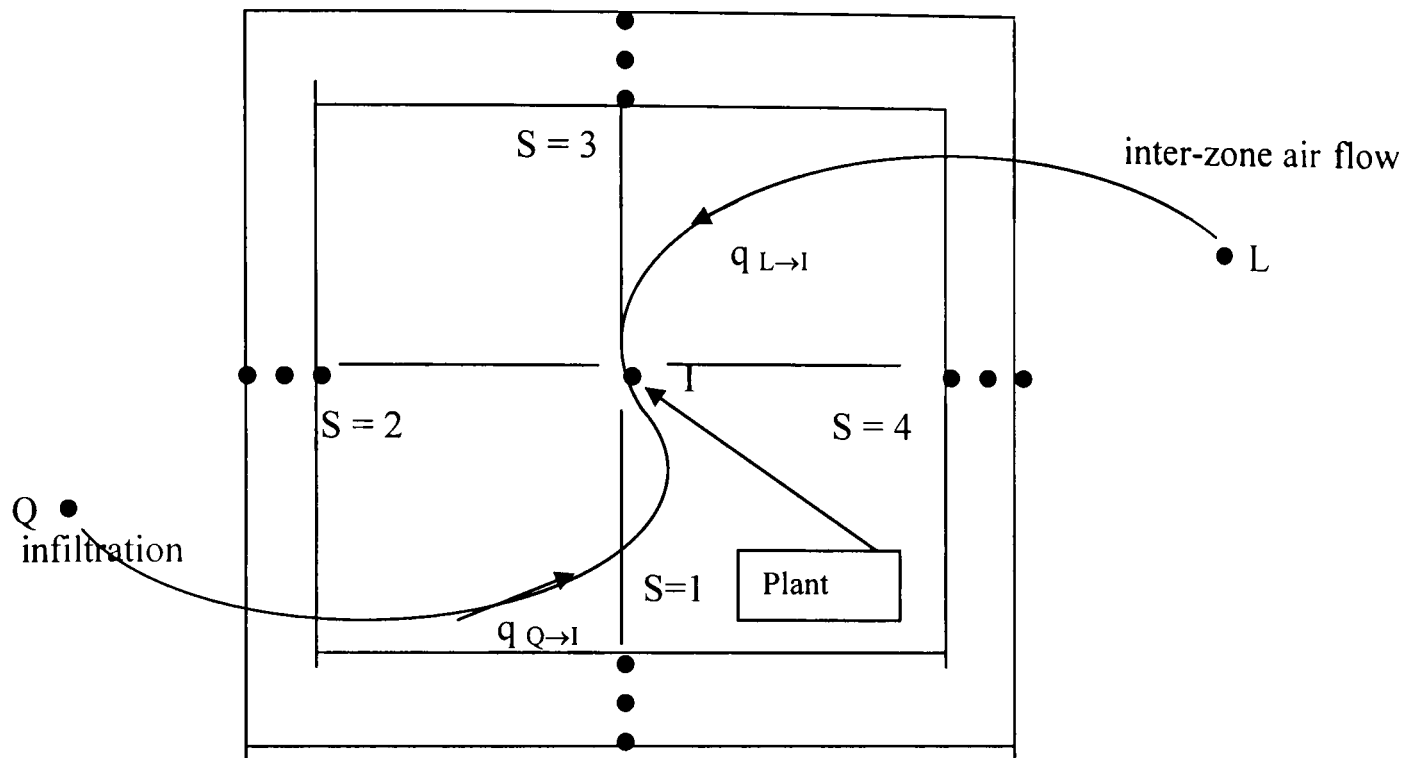

Figure F1.2: Energy balance on an air point node.

The energy balance for the air point node I is given as

$$
\left\{ \begin{array}{c} \text{Storage of} \\ \text{heat in control} \\ \text{volume} \end{array} \right\} = \left\{ \begin{array}{c} \text{net convection} \\ \text{into control} \\ \text{volume} \end{array} \right\} + \left\{ \begin{array}{c} \text{advection into} \\ \text{control volume} \\ \text{by inter-zonal} \\ \text{air flow} \end{array} \right\} + \left\{ \begin{array}{c} \text{advection into} \\ \text{control volume} \\ \text{by infiltration} \end{array} \right\} + \left\{ \begin{array}{c} \text{source of heat} \\ \text{within control} \\ \text{volume} \end{array} \right\} \tag{F.7}
$$

In discretised explicit form, the convection term, which represents the total heat transfer from all bounsing surfaces (e.g. walls, roof, windows, floor, etc) to the room air is given as

$$
\left\{ \begin{array}{c} \text{net convection into control} \\ \text{volume} \end{array} \right\} = \sum_{s=1}^{N} h^{t}_{c,s} A_s (T^{t}_{s} - T^{t}_{I}) \tag{F.8}
$$

where A_s is the area (m^2), N the number of bounding fabric faces, $h^{t}_{c,s}$ the present time-row

convective heat transfer coefficient, for surface, s. The internal surface nodes and the convective transfer coefficients are evaluated in the same manner. Similarly, the advection terms represent the thermal energy carried by air flowing into the control volume from the outdoor environment or from other zones. In discretised explicit form these terms are given by

$$\left\{ \begin{array}{l} \text{advection into control volume} \\ \text{by inter-zonal air flow} \end{array} \right\} = \sum_{L=1}^{M} m^t_{L \to I} \, C_p \, (T^t_L - T^t_I) \tag{F.9}$$

$$\left\{ \begin{array}{l} \text{advection into control volume} \\ \text{by infiltration from outdoor} \end{array} \right\} = m^t_{Q \to I} \, C_p (T^t_Q - T^t_I) \tag{F.10}$$

where $m^t_{L \to I}$ is the air flow from zone L to zone I (kg/s) at the present time-row, $m^t_{Q \to I}$ the infiltration rate (kg/s) from outdoors for the present time-row and M the number of zones within the neighbourhood supplying air to the control volume. T^t_L and T^t_Q are the present time-row temperatures of the air point in zone L and the outdoor air. The source term is given in discretised explicit form as

$$\left\{ \begin{array}{l} \text{source of heat within} \\ \text{control volume} \end{array} \right\} = q^t_{\text{cas-conv,I}} + q^t_{\text{plant,I}} \tag{F.11}$$

With the addition of the present time-row (fully explicit form) and that obtained using future time-row (fully implicit form) and dividing through by the volume of the room and subsequently re-arranging the future time-row terms on the left hand side and the present time-row terms gathered on the right hand side, the following relation is obtained

$$\left[\frac{2(\rho C_p)_I}{\Delta t} + \frac{\sum\limits_{s=1}^{N} h_{c,s}^{t+\Delta t} A_s}{V_{room}} + \frac{\sum\limits_{L=1}^{M} m_{L \to I}^{t+\Delta t} C_p}{V_{room}} + \frac{m_{Q \to I}^{t+\Delta t} C_p}{V_{room}} \right] T_I^{t+\Delta t}$$

$$- \left[\frac{\sum\limits_{s=1}^{N} h_{c,s}^{t+\Delta t} A_s T_s^{t+\Delta t}}{V_{room}} \right] - \left[\frac{\sum\limits_{L=1}^{M} m_{Q \to I}^{t+\Delta t} C_p T_Q^{t+\Delta t}}{V_{room}} \right] - \left[\frac{q_{\text{cas-conv,I}}^{t+\Delta t}}{V_{room}} \right] - \left[\frac{q_{\text{plant,I}}^{t+\Delta t}}{V_{room}} \right]$$

$$= \left[\frac{2(\rho C_p)_I}{\Delta t} - \frac{\sum\limits_{s=1}^{N} h_{c,s} A_s}{V_{room}} - \frac{\sum\limits_{L=1}^{M} m_{L \to I}^t C_p}{V_{room}} + \frac{m_{Q \to I}^t C_p}{V_{room}} \right] T_I^t + \left[\frac{q_{\text{cas-conv,I}}^t}{V_{room}} \right] + \left[\frac{q_{\text{plant,I}}^t}{V_{room}} \right]$$

$$\tag{F.12}$$

This is the basic equation used by ESP-r in the calculation of a fluid volume's temperature. As before, the bracketed term in front of the nodal temperature, $T_I^{t+\Delta t}$ is the self-coupling coefficient. The terms in front of the other future time step nodal temperatures are the cross coupling coefficients. These provide the link to the other nodes which exchange energy with node I (for example nodes L and Q in Figure 1.2). Similar expressions for the present and future time-row of the nodal temperatures for the moisture/energy coupling are provided in Appendix A.

References

Chapter 1

ASHRAE Standard 62 - 1989, 'Ventilation for acceptable indoor air quality', Atlanta.

Commission of the European Countries, 1992, 'Indoor Air Quality and its impact on man', Report No. 11, Office for Publication of the European. Countries, Luxembuorg.

Environmental Health Directorate, 1989, 'Exposure Guidelines for Residential Indoor Air Quality'.

European Concerted Action (COST 613). 1969, ' Indoor Pollution by NO2 in European Countries', Report No. 3, Commission of the European Communities, Luxembourg.

Fanger, P. O., 1988, 'Introduction to the olf and the decipol units to quantify air pollution perceived byhumans – indoors and outdoors'. Energy and Building 12: 1-6.

Healthy Buildings 2000 Workshop, Finland, August 6 – 10, 2000, 'The effect of wood-based material on Indoor Air Quality and climate'.

Oldengarm, J, Pernot C and De Witt, M,1990, IEA Annex XIV, 'Condensation and Energy' , 'Modelling: combined heat, air and moisture transport' , Leuven.

Spengler, J. D., Divali, K.M. and Samet, J., 1993, 'Lesson 26, Volume II – Indoor air Pollution'.

Straube, J.F. and Acahrya, V., 1995, 'Indoor Air Quality, Healthy Buildings, and Breathing Walls'

White, Frank M., 1998, 'Heat and Mass Transfer' 5th edition, Addison Wesley Publishing Co. Inc. USA.

World Health Organisation Regional Office for Europe, 1967, ' Air Quality Guidelines for Europe', Copenhagen.

Chapter 2

Bomberg, M., 1974, 'Moisture flow through porous building materials', Report 52, Division of Building Technology, Lund Institute of Technology, Sweden.

Bomberg, M.T. and W.C. Brown, 1993,'Building Envelope and Environmental

Carsten R. Pederson, 190, ' A Transport Model for Analysing the Hygrothermal Behaviour of Building Construction', Thermal Insulation Laboratory, Technical University of Denmark, Lyngby, Denmark.

Control : Part 1- Heat, Air and Moisture Interactions, 'Construction and Canada' Vol.35(1),1993, p15-18.

Chen, Q., 1988, 'Indoor air flow, air quality and energy consumption of building'. Ph D Thesis, Delft University of Technology, The Netherlands.

De Vries, D.A., 1987, 'The theory of heat and moisture transfer in porous media revisited', Int. J. Heat Mass Transfer, Vol. 30, No. 7, pp 1343 – 1350.

ESRU (2000), 'The ESP-r system for Building Energy Simulation' User Guide Version 9 Series, University of Strathclyde, Glasgow.

Galbraith, G.H., 1992, 'Heat and mass transfer within porous building materials', PhD Thesis, University of Strathclyde, Glasgow.

Hedenblad, G, 1993, 'Moisture permeability of concrete, mature cement mortar and cement paste', Report TVBM-1014, Div. Of building Materials, Lund Institute of Technology, Lund, Sweden.

Hens, H.,1986, 'Heat and moisture transfer in insulated enveloped parts', International Energy Agency, Annex 24. Volume 1.

Karagiozis, N.A. and Salonvaara, M. , 'Influence of material properties of the Hygrothermal Performance of a high-rise residential wall', ASHRAE Transactions, CH-95-3-5, ASHRAE, USA.

Karl Grau and Carsten Rode, 2000, 'Simulation of Whole-Building Hygrothermal Conditions', Danish Building and Urban Research, Denmark.

Kerestecioglu, A.and Gu, L.,1990,'Theoretical and computational investigation of simultaneous heat and moisture transfer in buildings: 'Evaporation and Condensation' theory, ASHRAE Transaction Volume 96, Pt.1, ASHRAE, USA.

Kusuda,T ,1983, 'Indoor humidity calculations' ASHRAE Transactions, V.89, Part 2, ASHRAE, USA.

Marit Stoere Valen, 1998 ' Moisture Transfer in Organic Coatings on Porous Materials', Doctoral Thesis, Nowegian University of Science and Technology, Trondheim, Norway.

Nakhi, A.E.,1995, 'Adaptive Construction Modelling within whole Building Dynamic Simulation' PhD Thesis, University of Strathclyde, Glasgow.

Philip, J. R. and de Vries, D. A. 1957, 'Moisture movement in porous materials under temperature gradients', Transactions of the American Geophysical Union.v.38,n.2.

Thomas, WC and Burch, DM, 1990, ' Experimental Validation of a Model for Predicting Water Vapour Sorption at Interior Building Surfaces.Virginia Polytechnic Institute, Blacksburg, USA

Wong, S.P.W. and Wang, S.K. , 1990, 'Fundamentals of Simultaneous Heat and Moisture Transfer between the Building Envelope and the Conditioned Space Air', ASHRAE Transactions, Vol.96, Part 2, ASHRAE, USA.

Chapter 3

Beausoleil-Morrison, I., 2000, 'The Adaptive Coupling of Heat and Air flow Modelling within Dynamic Whole-Building Simulation', PhD Thesis, University of Strathclyde, Glasgow.

Chen, Q., 1988, 'Indoor air flow, air quality and energy consumption of building'. Ph D Thesis, Delft University of Technology, The Netherlands.

Clarke, J.A.,1985,'Energy simulation in building design' , Butterworth-Heinemann.

ESRU (2000), 'The ESP-r system for Building Energy Simulation' User Guide Version 9 Series, University of Strathclyde, Glasgow.

Ferziger J.H. and Peric, M 1996, 'Computational Methods for Fluid Dynamics', Springer-Verlag, Berlin, Germany.

FLUENT 5. User's Guide Volume 2, 1998, Fluent Inc., Lebanon, USA

Hens, H.,1986, 'Heat and moisture transfer in insulated enveloped parts', International Energy Agency, Annex 24. Volume 1.

Launder, B.E. and Spalding, D.B. , 1974, 'The Numerical Computation of Turbulent Flows', Vol. 3.Page 269

Malalasekera,W.and Versteeg, H.K,1995, 'An introduction to Computational Fluid Dynamics – The Finite Volume Method', Longman Publishers..

Negrão, C.O.R. , 1995, 'Conflation of Computational Fluid Dynamics and Building Thermal Simulation', PhD Thesis, University of Strathclyde, Glasgow.

Patankar, S.V.,1980, 'Numerical Heat Transfer and Fluid Flow', Hemisphere Publishing Corporation.

Chapter 4

CIBSE Guide A, 1999, 'Environmental Design' The Chartered Institution of Building and Services Engineers, London.

Eastop, T.D. and Watson, W.E. , 1992, 'Mechanical Services for Buildings, 1st edition.

Fisher, D.E. and Pederson, C.O., 1997, 'Convection Heat Transfer in Building Energy and Thermal Load Calculations', ASHRAE Transactions, Vol.103 (2), Pg. 137-148.

Galbraith, G.H. , 1992,'Heat and Mass Transfer within Porous Building Materials', PhD Thesis, University of Strathclyde, Glasgow.

Incropera, Frank M. and DeWitt, David P. , 2002, 'Fundamentals of Heat and Mass Transfer', 5th edition, John Wiley and Sons.

.

White, Frank M. , 1988, 'Heat and Mass Transfer', 5th edition, Addison Wesley Publishing Co. Inc. USA.

Chapter 5

Beausoleil-Morrison, I. 2000, ' The Adaptive Coupling of Heat and Air flow Modelling within Dynamic-Whole Building Simulation' PhD Thesis, University of Strthclyde, Glasgow.

Clarke, J A, 2001, 'Energy Simulation in Building Design', 2nd Edition, Butterworth-Heinemann Publishers, Oxford, United Kingdom.

Gibelling, H, Mahaffy, J, 1992, 'Benchmarking simulations with CFD to 1-D coupling', Penn State University, Applied Research Laboratory, State College, PA, USA.

Loehner, R., Chi Yang, Cebral Juan, 1995, 'Fliud-Structure Interaction Using a Loose Coupling Algorithm and Adaptive Unstructured Grids, George Mason University, Fairfax, VA, USA.

Maliska, C.R. 2001, 'Issues on the Integration of CFD to Building Simulation Tools', Computational Fluid Dynamics Laboratory – SINMEC, Federal University of Santa Catarina, Brazil.

Mehta, U.B., 1998, 'Creidble Computational Fluid Dynamics Simulations', A.I.A.A. Journal, Vol. 136, No. 5, 1998, pg 665-667.

Musy, M, Wurtz, E and Sergent, A. 2001, 'Buildings Air-Flow Simulation: Automatically-Generated Zonal Model', Seventh International IBPSA Conference, August 13 – 15, 2001, Rio de Janeiro, Brazil.

Rode, C. and Grau, K. 2001, 'Simulation of Whole-Building Hygrothermal Conditions' Danish Building and Urban Research, Denmark.

Srebric, J. and Novoselac, A. 2002, 'Design of Low-Energy Cooling Systems by using Coupled Energy Simulation and Computational Fluid Dynamics' 8th Int. Conference on Air Distribution in Rooms, Sept. 2002, Copenhagen, Denmark.

To W.M. Humphrey, J.A.C, 1986, 'Numerical simulation of turbulent buoyancy, flow –

free convection along a heated, vertical, flat plate'. Int.J. Heat and Mass transfer.

Zhiqiang Zhah and Quingyan Chen, 2001, 'Strategies for Coupling Energy Simulation

and Computational Fluid Dynamics Programmes' Seventh International IBPSA. Brazil.

Chapter 6

Ferziger J.H. and Peric, M 1996, 'Computational Methods for Fluid Dynamics', Springer-

Verlag, Berlin, Germany.

Healthy Buildings 2000 Workshop, Finland, August 6 – 10, 2000, 'The effect of

wood-based material on Indoor Air Quality and climate'.

Hens, H.,1986, 'Heat and moisture transfer in insulated enveloped parts',

International Energy Agency, Annex 24. Volume 1.

Incropera, Frank M. and DeWitt, David P. , 2002, 'Fundamentals of Heat and Mass

Transfer', 5th edition, John Wiley and Sons.

Karl Grau and Carsten Rode, 2000, 'Simulation of Whole-Building Hygrothermal

Conditions', Danish Building and Urban Research, Denmark.

Malalasekera,W.and Versteeg, H.K,1995, 'An introduction to Computational

Fluid Dynamics – The Finite Volume Method', Longman Publishers..

Nathan Mendes and G. H. dos Santos, 2001, 'Dynamic Analysis of Building Hygrothermal

Behaviour', Seventh International IBPSA Conference, August 13-15,2001, Rio de Janeiro,

Brazil.

Negráo, C.O.R. , 1995, 'Conflation of Computational Fluid Dynamics and Building

Thermal Simulation', PhD Thesis, University of Strathclyde, Glasgow.

Appendix A

Galbraith, G.H., 1992, 'Heat and mass transfer within porous building materials'. PhD Thesis, University of Strathclyde, Glasgow.

Nakhi, A.E.,1995, 'Adaptive Construction Modelling within whole Building Dynamic Simulation' PhD Thesis, University of Strathclyde, Glasgow.

Wong, S.P.W. and Wang, S.K. , 1990, 'Fundamentals of Simultaneous Heat and Moisture Transfer between the Building Envelope and the Conditioned Space Air', ASHRAE Transactions, Vol.96, Part 2, ASHRAE, USA.

Appendix B

Hens, H.,1986, 'Heat and moisture transfer in insulated enveloped parts', International Energy Agency, Annex 24. Volume 1.

Appendix C

Malalasekera,W.and Versteeg, H.K,1995, 'An introduction to Computational Fluid Dynamics – The Finite Volume Method', Longman Publishers..

Negrảo, C.O.R. , 1995, 'Conflation of Computational Fluid Dynamics and Building Thermal Simulation', PhD Thesis, University of Strathclyde, Glasgow.

Appendix D

Malalasekera,W.and Versteeg, H.K,1995, 'An introduction to Computational Fluid Dynamics – The Finite Volume Method', Longman Publishers..

Appendix E

Incropera, Frank M. and DeWitt, David P. , 2002, 'Fundamentals of Heat and Mass Transfer', 5th edition, John Wiley and Sons.

Appendix F

Clarke, J A, 2001, 'Energy Simulation in Building Design', 2nd Edition, Butterworth-

Heinemann Publishers, Oxford, United Kingdom